

JUSTUS-LIEBIG-UNIVERSITÄT GIESSEN
INSTITUT FÜR ANORGANISCHE UND ANALYTISCHE CHEMIE



**INVESTIGATIONS OF THE REACTION BEHAVIOR OF COPPER AND
NICKEL COMPLEXES WITH N-DONOR OR OLEFIN LIGANDS**

Inaugural-Dissertation

zur Erlangung des Doktorgrades der Naturwissenschaften im Fachbereich Biologie
und Chemie der Justus-Liebig-Universität Gießen

vorgelegt von

Anja Henß

aus

Jena

Erstgutachter:	Prof. Dr. S. Schindler
Zweitgutachter:	Prof. Dr. R. Göttlich
Abgabe der Dissertation im Prüfungsamt:	13.10.2008
Tag der mündlichen Prüfung:	29.10.2008

For my family

Acknowledgements

The work described in this doctoral thesis has been carried out between September 2005 and September 2008 at the Institute of Inorganic and Analytical Chemistry at the Justus-Liebig-University of Gießen under the supervision of Prof. Dr. Siegfried Schindler.

At this place I would like to thank my supervisor Prof. Dr. Siegfried Schindler for his support, his patience and guidance during these years.

Furthermore I wish to thank my colleagues and labmates Dr. Sabrina Turba, Sandra Kisslinger, Jenny Friebe, Alexander Beitat, Jörg Müller, Thomas Nebe, Christian Würtele, Tobias Hoppe, Dr. Jing-Yuan Xu, Dr. Ildikó Kerezi, Dr. Jörg Astner, Janine Will, Sabrina Schäfer, Janine Cappell, Jonathan Becker and Sabine Löw for their friendship and encouragement.

I would like to express my gratitude to Dipl. Chem. A. Beitat, Dipl. Chem. J. Müller, Dipl. Chem. C. Würtele, Dr. O. Walter and Dr. M. Serafin for their friendly support with the X-Ray Crystallography studies.

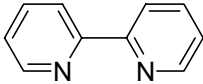
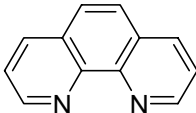
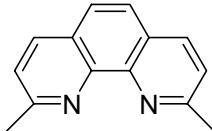
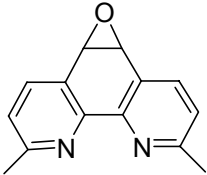
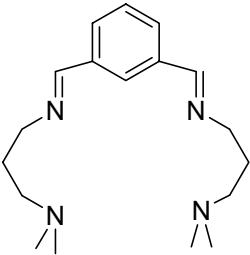
Furthermore I would like to thank the people of the Institute of Inorganic and Analytical Chemistry and the people of the Institute of Organic Chemistry at the Justus-Liebig-University in Gießen for their support of my work.

My warmest thanks belong to my friends and colleagues in our research group. You made the laboratory more than just a working place.

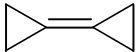
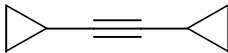
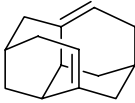
Surely I would like to thank Stefan and my family for their support during all these years.

LIGANDS USED

Ligands used

Name	Abbreviation	Structure and Formula	Molar Mass [g/mol]
2,2'-bipyridine	bipy	 $C_{10}H_8N_2$	156,2
1,10-phenanthroline	phen	 $C_{12}H_8N_2$	180,2
2,9-dimethyl-1,10-phenanthroline	dmp	 $C_{14}H_{12}N_2$	208,3
2,9-dimethyl-1,10-phenanthroline-5,6-epoxide	dmpe	 $C_{14}H_{12}N_2O$	224,3
1,3-bis-[(3-(N-dimethyl)propyl)imino methyl]benzene	dapa	 $C_{18}H_{30}N_4$	302,2

LIGANDS USED

bicyclopropylidene	bcp	 C_6H_8	80,1
dicyclopropyl- acetylene	dcpa	 C_8H_{10}	106,1
tetracyclo [7.3.1.1 ^{4,12} .0 ^{2,7}] tetradeca-6,11-diene	tctd	 $C_{14}H_{18}$	186,0

Abbreviations

d	Doublet (NMR)
δ	chemical shift in ppm (NMR)
THF	Tetrahydrofuran
e. g.	for example (Latin: <i>exempli gratia</i>)
IR	Infrared
m	Multiplet
MeOH	Methanol
CH ₂ Cl ₂	Dichlormethane
NMR	Nuclear Magnetic Resonance
Ph	Phenyl
RT	Room temperature
s	Singlet (NMR)
t	Triplet (NMR)
UV-vis	Ultraviolet-visible

Table of contents

Acknowledgements	I
Ligands used	II
Abbreviations.....	IV
Table of contents	V
Table of Figures.....	IX
Tables.....	XII
Chapter 1 - Introduction	1
1.1 Motivation	1
1.2 Background.....	2
1.2.1 Copper.....	2
1.2.2 Oxygen	3
1.2.3 Copper proteins	4
1.2.4 Model complexes for copper proteins	6
1.2.5 Mechanisms of dioxygen binding.....	9
1.3 Copper(I) complexes with Schiff base ligands	10
1.4 Copper(I) complexes with phenanthroline and bipyridine as ligands	11
1.4.1 Copper oxo species with phenanthroline as ligand.....	12
1.4.2 Copper olefin complexes	13
1.5 Nickel complexes.....	14
1.5.1 The element nickel and some of its compounds	14
1.5.2 Nickel(0) olefin complexes.....	15
1.5.3 Dioxygen activation at monovalent nickel	17
1.6 Projects.....	19
1.6.1 Copper complexes with Schiff base ligands	19
1.6.2 Copper complexes with phenanthroline and bipyridine as ligands	19
1.6.2.1 Copper-oxo-species.....	20
1.6.3 Copper(I) olefin complexes.....	20

TABLE OF CONTENTS

1.6.4 Nickel(0) olefin complexes	20
Chapter 2 - Theoretical part	21
2.1 Chemical Kinetics	21
2.2 Reaction rate	21
2.3 First order dependence	22
2.4 Second order dependence	23
2.5 Equilibrium reactions	24
2.6 Consecutive Reactions	24
2.7 Determination of enthalpy, entropy and volume of activation: ΔH^\ddagger , ΔS^\ddagger , ΔV^\ddagger	26
Chapter 3 - Aromatic Hydroxylation in a Copper Bis(imine) Complex Mediated by a μ-η^2:η^2 Peroxo Dicopper Core: A Mechanistic Scenario	28
3.1 Abstract	28
3.2 Introduction	28
3.3 Experimental and Computational Details	31
3.3.1 Materials and Techniques	31
3.3.2 Tetrakis(acetonitrile)copper(I) perchlorate	32
3.3.3 DAPA (1,3-bis-[(3-(N-dimethyl)propyl)iminomethyl]benzene)	32
3.3.4 Cu(I) ₂ -DAPA (Ia, Ib, Ic)	32
3.3.5 Cu(II) ₂ -DAPA-OH (II), perchlorate salt	33
3.3.6 Isophthalaldehyde-d ₆	33
3.3.7 Cu(I) ₂ -DAPA-d ₆ , perchlorate salt (I ^D)	34
3.3.8 Cu(II) ₂ -DAPA-d ₆ -OH, perchlorate salt (II ^D)	34
3.3.9 Single crystal structure analysis	35
3.3.10 Computational Methods	35
3.4 X-ray Structure Analysis	38
3.4.1 Cu(I) complex (Ia)	38
3.4.2 Cu(II) complex (II)	40
3.5 Spectroscopic Investigations	43
3.5.1 UV-Vis spectroscopy	43
3.5.2 Vibrational spectroscopy	45

TABLE OF CONTENTS

3.6	Kinetic Investigations	49
3.7	Quantum Chemical Investigations on Reaction Pathways.....	53
3.8	Summary and Discussion	60
3.9	Unpublished Material	65
3.9.1	Kinetic Investigations	65
Chapter 4- Copper complexes with phenanthroline and bipyridine as ligands		69
4.1	A Copper(I) complex with an adamantane derivative as ligand	69
4.1.1	Introduction	69
4.1.2	Results.....	70
4.2	Copper(I) complexes with bicyclopropylidene and dicyclopropylacetylene as ligands	73
4.2.1	Introduction	73
4.2.2	Results.....	74
4.2.2.1	[Cu(bipy)(bcp)]PF ₆	74
4.2.2.2	[Cu(bipy)dcpa]PF ₆	75
4.2.2.3	Reactivity towards dioxygen.....	76
4.3	Copper(I) complexes with phenanthroline and derivatives as ligands.....	81
4.3.1	Introduction	81
4.3.2	Results.....	82
4.3.2.1	[Cu(dmpe) ₂]PF ₆ x 1/2 CH ₃ CONH ₂	82
4.4	Efforts to synthesize a copper-oxo-species	86
4.4.1	Introduction	86
4.4.2	Results.....	87
4.4.2.1	Reactivity of [Cu(bipy)COD] ⁺ towards dioxygen.....	87
4.4.2.2	[Cu(phen)COD]PF ₆	88
4.4.2.3	Efforts to synthesize a [Cu(dmp)COD] ⁺ complex	89
4.4.2.4	Oxidation with dioxygen	92
4.4.2.5	Ozonolysis	94
4.5	Experimental Section	98
4.5.1	Materials and Reagents.....	98
4.5.2	Physical Measurements.....	98

TABLE OF CONTENTS

4.5.3	Kinetic Measurements	98
4.5.4	X-ray Crystallography	99
4.5.5	Synthesis of the complexes	99
4.5.5.1	[Cu ₂ (bipy) ₂ (tctd)](PF ₆) ₂	99
4.5.5.2	[Cu(bipy)bcp]PF ₆	100
4.5.5.3	[Cu(bipy)dcpa]PF ₆	100
4.5.5.4	[Cu ₂ (bipy) ₂ (OH) ₂] ²⁺	100
4.5.5.5	[Cu(phen)COD]PF ₆	101
4.5.5.6	[Cu(dmp) ₂]CF ₃ SO ₃	101
4.5.5.7	[Cu ₄ (2-methoxy-9-methyl-phenanthroline) ₄] ⁴⁺	101
4.5.6	Ozonolysis	102
Chapter 5-	Nickel-olefin complexes	103
5.1	Introduction	103
5.3	Results	106
5.3.1	[Ni(bipy)dcpa].....	106
5.3.2	Mechanistic studies of the reaction of [Ni(bipy)COD] with dcpa	106
5.4	Experimental Section	111
5.4.1	Materials and Reagents	111
5.4.2	Kinetic Measurements	111
5.4.3	X-ray Crystallography	111
5.4.4	Synthesis of the complexes	112
5.4.4.1	[Ni(bipy)(dcpa)]	112
6	Summary.....	113
7	Zusammenfassung.....	117
8	Publication and Presentations.....	121
9	Curriculum Vitae.....	122
10	Bibliography	124

Table of Figures

Figure 1-1: Selected copper enzymes and proteins that activate O ₂	3
Figure 1-2: O ₂ -binding site in hemocyanin.....	5
Figure 1-3: Conversion of tyrosine to melanin catalysed by tyrosinase	5
Figure 1-4: Catechol oxidase activity	6
Figure 1-5: Synthetic analogue to metalloprotein active sites.....	7
Figure 1-6: The ligand tris[2-pyridyl)methyl]amine (tmpa)	7
Figure 1-7: The formation of the copper-peroxo complex.....	8
Figure 1-8: Intramolecular ligand hydroxylation during the reaction of [Cu ₂ (R-XYL-H)] ²⁺ with dioxygen.....	8
Figure 1-9: Characterized examples of copper "oxygen adduct" complexes	9
Figure 1-10: Hydroxylation of a Schiff base ligand	10
Figure 1-11: Reaction of [Cu ₂ L ¹ (CH ₃ CN) ₂](ClO ₄) ₂ with dioxygen.....	11
Figure 1-12: 1,10-phenanthroline and 2,2'-bipyridine	11
Figure 1-13: Structure of the orange copper(I) phenanthroline complex cation	12
Figure 1-14: Calculated copper oxide cation (phen)CuO ⁺	13
Figure 1-15a: Structure of the cation [Cu(COD) ₂] ⁺	14
Figure 1-15b: Structure of the cation [Cu(bipy)(COD)] ⁺	14
Figure 1-16: Oligomerization of alkynes	16
Figure 1-17: Postulated mechanism for the synthesis of COD	17
Figure 1-18: Nickel dioxygen adduct complexes	18
Figure 1-19: Hydroxylation of [Cu ₂ (DAPA)] ²⁺	19
Figure 1-20: Bicyclopropylidene (a) and dicyclopropylacetylene (b).....	20
Figure 3-1: Hydroxylation of [Cu(DAPA)] I leading to the product.....	30
Figure 3-2: Molecular structure of the cation of I	39
Figure 3-3: Molecular structure of the cation of II	41
Figure 3-4: UV-Vis spectra of Ib (black line, 8 x 10 ⁻⁵ mol/l) in acetonitrile.....	44
Figure 3-5: UV-vis showing the oxygenation of Ib to II (red) by O ₂	44
Figure 3-6: IR-spectra of Ib (black) and II (red).....	45
Figure 3-7: Experimental (bottom) and calculated (top) IR-spectra of II (black)	46
Figure 3-8: FT-Raman-spectra of Ib (black) and II (red)	47
Figure 3-9: FT-Raman-spectra of II (black) and ¹⁸ O-II (red)	48
Figure 3-10: Eigenvectors of the most important vibrations	48

TABLE OF FIGURES

Figure 3-11: Spectral changes during reaction of I with dioxygen in MeOH	50
Figure 3-12: Absorbance during oxygenation of Ia at 353 nm in MeOH.....	52
Figure 3-13: Absorbance at 358 nm for the DAPA- and DAPA-d ₆ -complex	52
Figure 3-14: Reaction pathways identified for the hydroxylation reaction.....	54
Figure 3-15: Dienone 4•ClO ₄ and transition structure TS9•ClO ₄	58
Figure 3-16a: Geometries in the transition states leading to the σ-complex.....	64
Figure 3-16b: Geometries in the transition states leading to the σ-complex.....	64
Figure 3-17: Dependence of the reaction constants k _{obs} 1 and k _{obs} 2 in MeOH.....	66
Figure 3-18: Several complex species existing in solution	66
Figure 3-19: Dependence of the reaction constants k _{obs} 1 and k _{obs} 2 in CH ₂ Cl ₂	68
Figure 4-1: Adamantane and derivatives.....	69
Figure 4-2: Tetracyclo[7.3.1.1 ^{4,12} . 0 ^{2,7}] tetradeca-6,11-diene (tctd).....	70
Figure 4-3: ORTEP plot of [Cu ₂ (bipy) ₂ (tctd)] ²⁺	71
Figure 4-4: Bicyclopropylidene bcp and dicyclopropylacetylene dcpa	73
Figure 4-5: ORTEP plot of [Cu(bipy)bcp] ⁺	74
Figure 4-6: ORTEP plot of [Cu(bipy)dcpa] ⁺	75
Figure 4-7: ORTEP plot [Cu ₂ (bipy) ₂ (OH) ₂] ²⁺	77
Figure 4-8: Ligand templates.....	81
Figure 4-9: Phenanthroline derivatives used as ligands	82
Figure 4-10: ORTEP plot of [Cu(dmpe) ₂] ⁺	83
Figure 4-11: ORTEP ellipsoide plot of a part of [Cu(dmpe) ₂] ⁺ x 1/2 CH ₃ CONH ₂	83
Figure 4-12: ORTEP plot of [Cu(dmp) ₂] ⁺	86
Figure 4-13: Spectral changes during reaction of [Cu(bipy)COD] ⁺ with O ₂	88
Figure 4-14: ORTEP plot of [Cu(phen)COD] ⁺	89
Figure 4-15: ORTEP plot of [Cu(dmp)CH ₃ CN] ⁺	90
Figure 4-16: ORTEP plot of [Cu ₄ (2-methoxy-9-methyl-phenanthroline) ₄] ⁴⁺	93
Figure 4-17: [Cu(dmp) ₂] ⁺ + O ₂	94
Figure 4-18: Generation of an iron(IV)oxo species by oxidizing with O ₃	95
Figure 4-19: [Cu(dmp) ₂] ⁺ + O ₃	95
Figure 4-20: Spectral changes during reaction of [Cu(dmp) ₂] ⁺ with O ₃ in acetone ..	96
Figure 5-1: Right: ORTEP plot of nickel(0) cyclopropene complex.....	103
Left: Molecular structure of 2,2-bipyridyl (η ² - diphenylacetylene)nickel	103
Figure 5-3: Bicyclopropylidene and dicyclopropylacetylene	104
Figure 5-4: ORTEP plot of [Ni(bipy)bcp]	105

TABLE OF FIGURES

Figure 5-5: Proposed mechanism for [Ni(bipy)COD] with bcp	105
Figure 5-6: ORTEP plot of [Ni(bipy)dcpa]	106
Figure 5-7: Spectral changes during reaction of [Ni(bipy)COD] with dcpa in THF ..	107
Figure 5-8: Plot of observed rate constants k_{obs} vs dcpa concentration at different temperatures	109

Tables

Table 3-1: Crystal data and Structure Refinement for I and II.....	42
Table 3-2: Selected Bond Distances and Angles for I (Å, °)	42
Table 3-3: Selected Bond Distances and Angles for II (Å, °)	43
Table 3-4: Computed energy contributions (in atomic units)	59
Table 3-5: Measured reaction rates of the reaction of Ia with O ₂ in MeOH	66
Table 3-6: Measured reaction rates of the reaction of Ia with O ₂ in CH ₂ Cl ₂	67
Table 4-1: Crystal data and structure refinement for [Cu ₂ (bipy) ₂ (tctd)] ²⁺	71
Table 4-2: Selected bond lengths and angles (Å, °) for [Cu ₂ (bipy) ₂ (tctd)] ²⁺	72
Table 4-4: Selected bond lengths and angles (Å, °) for [Cu(bipy)bcp]PF ₆	78
Table 4-5: Crystal data and structure refinement for [Cu(bipy)dcpa]PF ₆	78
Table 4-6: Selected bond lengths and angles (Å, °) for [Cu(bipy)dcpa]PF ₆	79
Table 4-7: Crystal data and structure refinement for [Cu ₂ (bipy) ₂ (OH) ₂](PF ₆) ₂	79
Table 4-8: Selected bond lengths and angles (Å, °) for [Cu ₂ (bipy) ₂ (OH) ₂](PF ₆) ₂	80
Table 4-9: Crystallographic data for [Cu(dmpe) ₂]PF ₆ x 1/2 CH ₃ CONH ₂	85
Table 4-10: Selected bond lengths (Å) and bond angles (°) for [Cu(dmpe) ₂]PF ₆ x 1/2 CH ₃ CONH ₂	85
Table 4-11: Crystallographic data for [Cu(phen)COD] ⁺	91
Tab. 4-12: Selected bond lengths (Å) and bond angles (°) for [Cu(phen)COD] ⁺	91
Tab. 4-13: Crystallographic data for [Cu(dmp) ₂]CF ₃ SO ₃	92
Tab. 4-14: Selected bond lengths (Å) and bond angles (°) for [Cu(dmp) ₂]CF ₃ SO ₃ ...	92
Tab. 4-15: Crystallographic data for	97
[Cu ₄ (2-methoxy-9-methyl-phenanthroline) ₄](CF ₃ SO ₃) ₄	97
Tab. 4-16: Selected bond lengths (Å) and bond angles (°) for [Cu ₄ (2-methoxy-9-methyl-phenanthroline) ₄](CF ₃ SO ₃) ₄	97
Table 5-1: Measured reaction rates of the reaction of [Ni(bipy)COD] with dcpa	108
Table 5-2: Crystallographic data for [Ni(bipy)dcpa].....	109
Table 5-3: Selected bond length (Å) and bond angles (°) for [Ni(bipy)dcpa].....	110

Introduction

1.1 Motivation

Bioinorganic chemistry is a combination of inorganic chemistry and biology in which mainly molecules are investigated that contain metal ions and which are furthermore related to biological systems. An important study object are metalloenzymes, a subclass of metalloproteins, that are responsible for many different essential processes in biology such as dioxygen uptake and oxidation of organic substrates.^[1, 2] Binding and activation of small molecules such as dioxygen or carbon dioxide takes place at the so called active site of the enzyme. Responsible for this are, in about half of the known proteins, the metal cations bound in the active site which are coordinated through donor atoms of the amino acid chains. In order to understand such processes and their implications on binding and activation of substrate molecules, there have been numerous attempts to mimic the active sites of these enzymes and their catalytic reactions using low molecular weight complexes.^[2-4] Studies of coordination behavior and kinetic investigations of low molecular weight metal complexes contribute to the better understanding of the structural and functional properties of these metalloproteins. Investigations of model complexes can offer a less complicated approach compared with the biological molecules and also may allow the development of so called artificial enzymes. Especially it is interesting to model the reactivity of the metalloenzymes in regard to find new catalysts for selective reactions under mild conditions. For example if selective oxidation reactions could be performed in water using a simple metal complex and air. This would mean a significant progress towards “greener” chemistry. Due to the fact that such oxidation reactions are extremely important there is high interest in the investigation of the uptake, transport, activation and transfer of oxygen by iron and copper proteins as well as their according model complexes.^[2-4] Furthermore, it is important to point out that the molecular structure and the functionality of the active centers of metalloproteins as well as of the model compounds are determined by the coordinated side-chain donor groups and by the properties of the coordinated ligands respectively.

1.2 Background

1.2.1 Copper

Copper is already known to mankind for thousands of years. During the Roman Empire copper was gained out of mines on Cyprus, hence the origin of the name “cyprium”, which was later shortened to cuprum. Copper is an essential trace element and its compounds are important for plants and animals. It is found in the bloodstream of humans and animals, in various enzymes as a co-factor and in copper-based pigments.^[5]

The properties of copper in coordination chemistry are due to the almost noble metal character, the intermediate stability, the reactivity of the d^{10} electron configuration in Cu(I) and the relative small radius of the Cu(II) ion, which contributes to the high energy of hydration and thus to the higher stability of Cu(II) (aq) over Cu(I) (aq).^[1, 6-8] Cu(I) ions need to be stabilized by chelating ligands. The preferred coordination geometries of such complexes are four-coordinated tetrahedral or trigonal pyramidal structures, but also three- and two coordinated complexes have been reported. Furthermore, five coordinated Cu(I) complexes are well known adopting either a square pyramidal or a trigonal bipyramidal geometry.^[5, 6]

Comparison of the Cu(II)/Cu(I) redox potentials with those of the Fe(III)/Fe(II) potentials in the enzymes with similar biological functions usually show higher potentials for the copper systems. Due to the high potential necessary for oxidation of the less soluble Cu(I) to Cu(II), copper only became bioavailable to a larger extent, once an oxidizing environment was present due to photosynthesis. In contrast Fe(II) became less bio-available because it then was easily oxidized to Fe(III) and special mechanisms needed to be developed for iron uptake of an organism. However, due to this redox activity copper and iron containing enzymes are well suited to participate in reactions involving dioxygen such as transport or transfer to substrates by oxidases and oxygenases. Furthermore, they are important for the decomposition of toxic side products in the O_2 metabolism such as superoxide anion.^[2-4, 9-11] An overview of some of the known copper enzymes and the great variety of their reactions with dioxygen is presented in Figure 1-1.^[4]

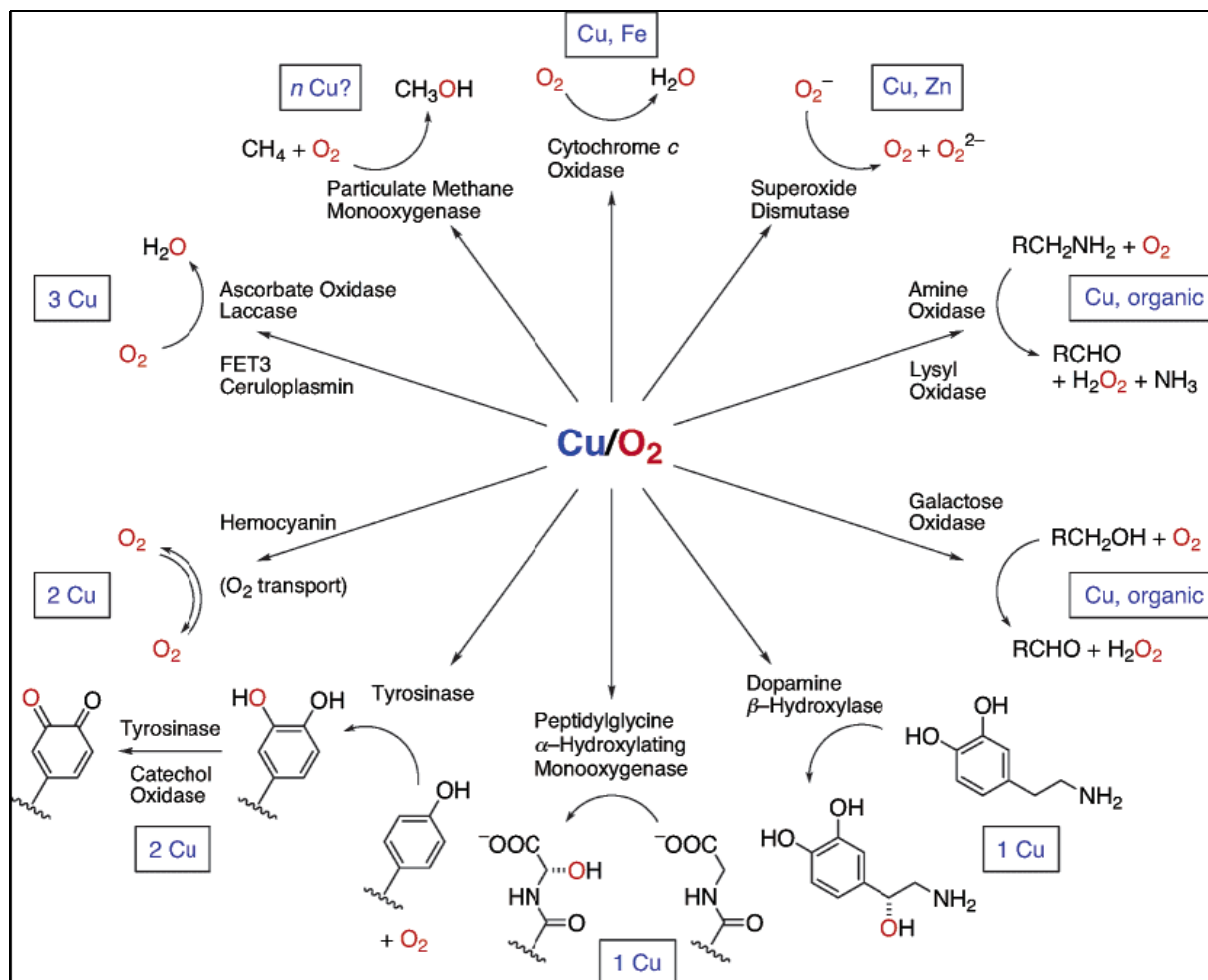


Figure 1-1: Selected copper enzymes and proteins that activate O₂

1.2.2 Oxygen

Dioxygen is a colorless, odorless, tasteless gas with a spin triplet electron configuration (ground state). Molecular dioxygen is essential for most animals and plants because of generating energy by photosynthesis and cellular respiration in all aerobic organisms. Oxygen is the most abundant chemical element in our biosphere.

Dioxygen was almost not existent until photosynthetic processes of archaea and bacteria developed. Today green algae and cyanobacteria in marine environments provide about 70% of the free oxygen produced on earth. The rest is produced by terrestrial plants. The present atmosphere consists of 21% O₂.

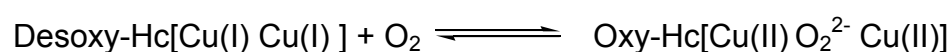
Dioxygen is a very strong oxidant with the second highest electronegativity of all elements. However, usually reactions between O₂ and metal complexes proceed irreversibly by cleavage of oxygen-oxygen bond leading to oxides, hydroxides or

water. With appropriate ligand configurations the reversible binding of dioxygen with transition metal complexes is possible.^[12]

1.2.3 Copper proteins

As described above many metalloproteins and metalloenzymes contain copper ions, ranging from active sites with one up to four copper ions which bind and/or activate dioxygen and perform a variety of important biological reactions. Copper containing enzymes such as laccase, tyrosinase, galactose oxidase, cytochrome c oxidase and superoxide dismutase, are involved in the selective oxidation of organic substrates, e. g. by transferring one (monooxygenases) or two (dioxygenases) oxygen atoms to the substrate molecule. Thus galactose oxidase catalyses the aerobic oxidation of primary alcohols to aldehydes while superoxide dismutase is involved in the degradation of superoxide anion as a side product of the aerobic metabolism (Figure 1-1).^[2-4, 9-11, 13]

An exceptionally important copper containing metalloprotein is the respiratory protein hemocyanin (Hc) in arthropods and mollusks.^[2] Hemocyanins are colourless in the reduced deoxygenated state and blue when exposed to air / oxygen dissolved in the blood. In the active site a binuclear copper centre is coordinated to the protein by the amino acid histidine, so a tris(imidazole) ligation is found at each copper centre.^[3, 4] The binding site of dioxygen in Hc is shown in Figure 1-2. Hemocyanin has the ability to bind and release dioxygen reversible by formation of a $\mu\text{-}\eta^2\text{:}\eta^2\text{-peroxo-dicopper(II,II)}$ unit:



Related to the binuclear Cu protein hemocyanin are the binuclear Cu enzymes tyrosinase (TY) and catechol oxidase (CO) that also can bind O_2 reversibly in the same way. Both enzymes have been crystallographically characterized and possess a very similar structure compared with hemocyanin.^[13-15]

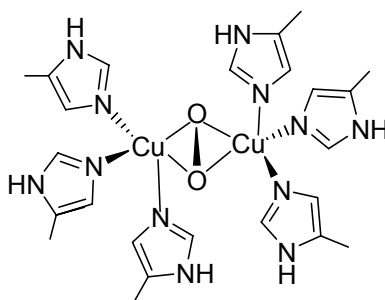


Figure 1-2: O₂-binding site in hemocyanin

Tyrosinase, a monooxygenase is involved in the composition of insect's exoskeleton (cuticula) and in browning reactions of vegetables and fruit such as the blackening of a peeled or sliced potato when exposed to air. Tyrosinase mediates the hydroxylation of monophenols to *o*-diphenols and the subsequent two-electron oxidation to *o*-quinones.^[16] Thus the pigment melanin (browning reaction) is formed by polymerization and is responsible for the colour of our skin and hair. The reaction of tyrosine to melanin is shown in Figure 1-3.^[10]

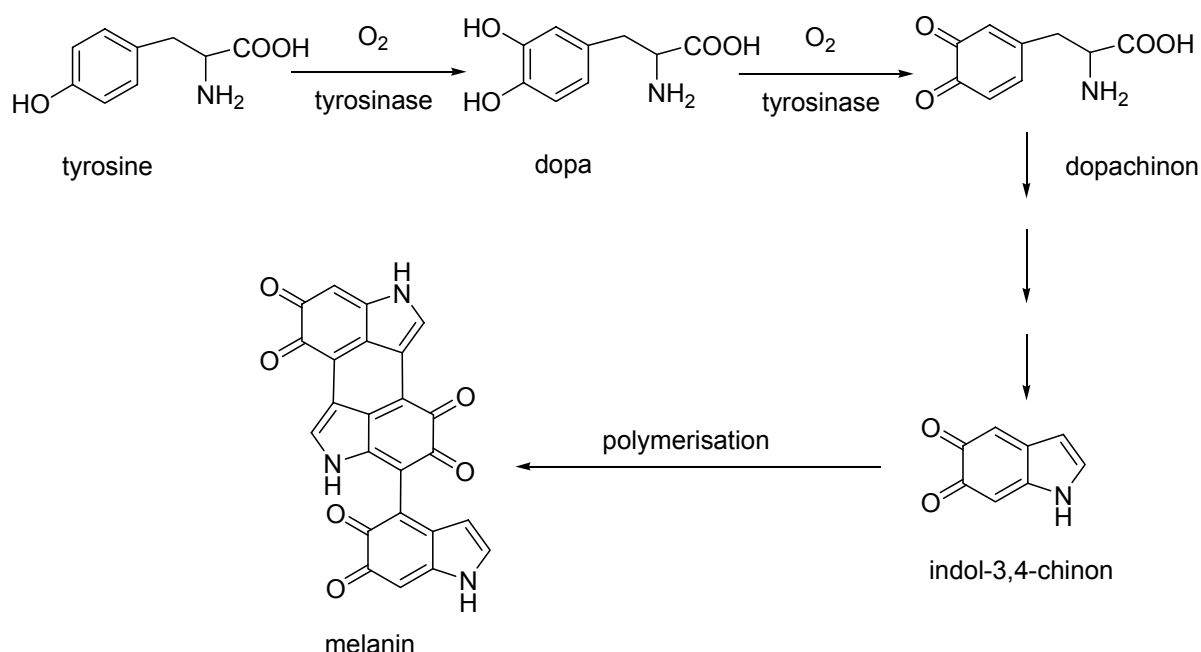


Figure 1-3: Conversion of tyrosine to melanin catalysed by tyrosinase

As a further member of such type III copper proteins, the catechol oxidase (CO = 1,2-benzenediol/oxygen oxidoreductase) catalyzes exclusively the oxidation of catechols (i.e., *o*-diphenols) to the corresponding quinones (Figure 1-4) and is believed to be responsible for the disease resistance in higher plants. Quinones are reactive

compounds, which undergo autopolymerization to produce melanin as already described above. COs are generally found in plant tissues, in some insects and crustaceans, whereas TYs can be obtained from a variety of plants, fungi, bacteria, mammals and insects.^[11, 17, 18] The functional differences between CO and TY should not be overemphasized because some plant COs also exhibit weak monooxygenase activity.

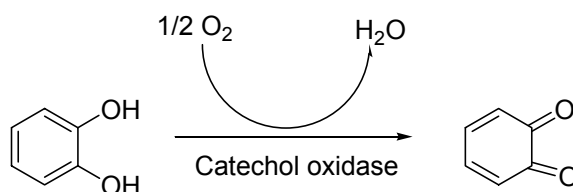


Figure 1-4: Catechol oxidase activity

1.2.4 Model complexes for copper proteins

As described above, low molecular weight copper complexes can be quite important for the better understanding of copper proteins and might be interesting in regard to their potential use as catalysts in selective oxidation reactions. Several excellent review articles describe these investigations in great detail.^[3, 4, 19] The development of biomimetic copper complexes, which react with dioxygen in the same way as their natural analogues has attracted much interest during the past decades.^[3, 4, 20-22] The general approach is shown in Figure 1-5.

Efforts to functionally model the copper protein hemocyanin and different copper enzymes led to the development of a series of mononuclear and binuclear copper model complexes.^[7, 23, 24] The applied ligand system plays a crucial role. Nitrogen donor ligands such as pyrole, imidazole, pyridine and derivatives have been used successfully in experimental studies to model dioxygen “activation” chemistry with copper complexes.^[3, 4, 21]

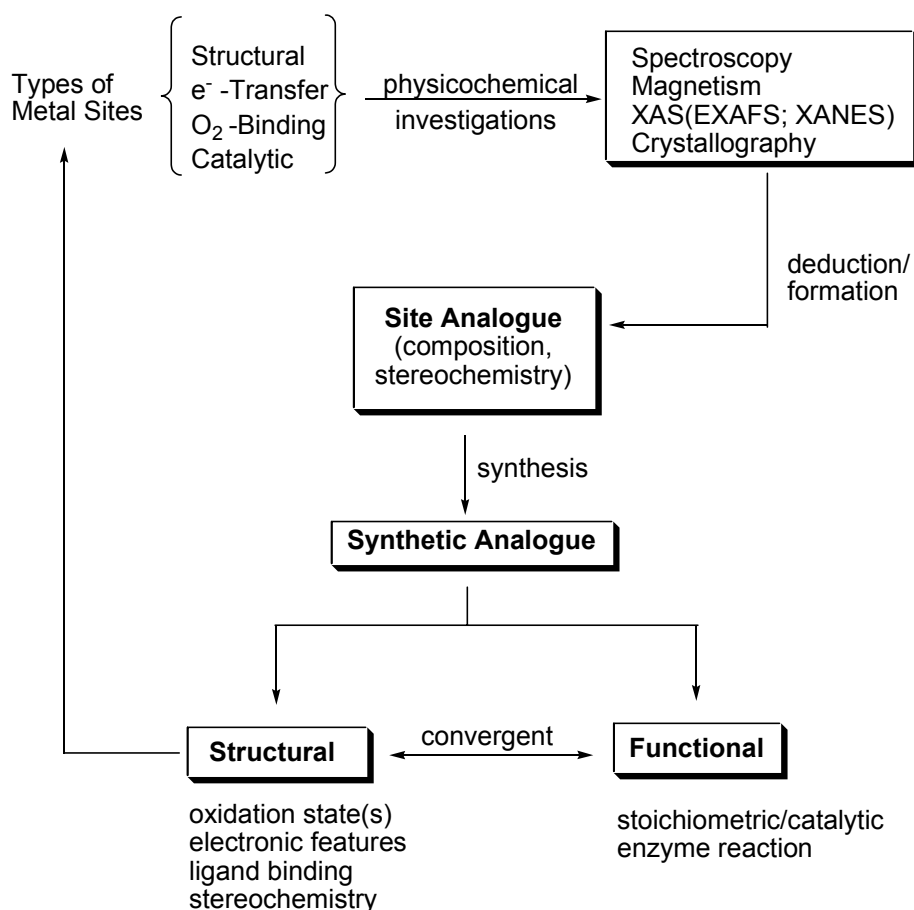


Figure 1-5: Synthetic analogue to metallobiomolecule active sites^[25]

Especially pyridine based ligands proved to be quite useful in that regard and Karlin and co-workers were able to model the reversible dioxygen binding of a copper(I) complex at low temperatures using tris(2-pyridylmethyl)amine (tmpa, Figure 1-6) as a ligand.^[26-28]

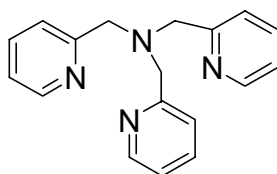


Figure 1-6: The ligand tris[2-pyridyl]methylamine (tmpa)

The reaction of dioxygen with two of the Cu(I) complexes led to the formation of a purple binuclear copper peroxo complex (Figure 1-7). Karlin and co-workers also succeeded for the first time to crystallize and to structurally characterize this copper peroxo complex, $[\text{Cu}_2(\text{tmpa})_2(\text{O}_2)]^{2+}$, at low temperatures.

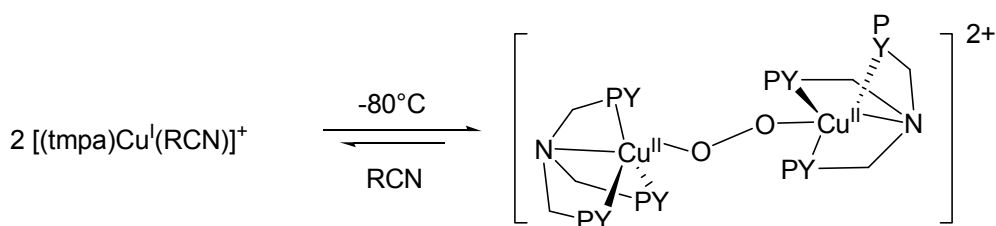


Figure 1-7: The formation of the copper-peroxo complex
 $[\text{Cu}_2(\text{tmpa})_2(\text{O}_2)]^{2+}$

Tyrosinase activity was first modeled successfully by Karlin and co-workers as well, who observed, that an intramolecular ligand hydroxylation occurred during the reaction of dioxygen with the binuclear copper(I) complex $[\text{Cu}_2(\text{R-XYL})]^{2+}$ wherein a *m*-xylyl group links two bis[2-(2-pyridyl)ethyl]amine units (Figure 1-8).^[28-33]

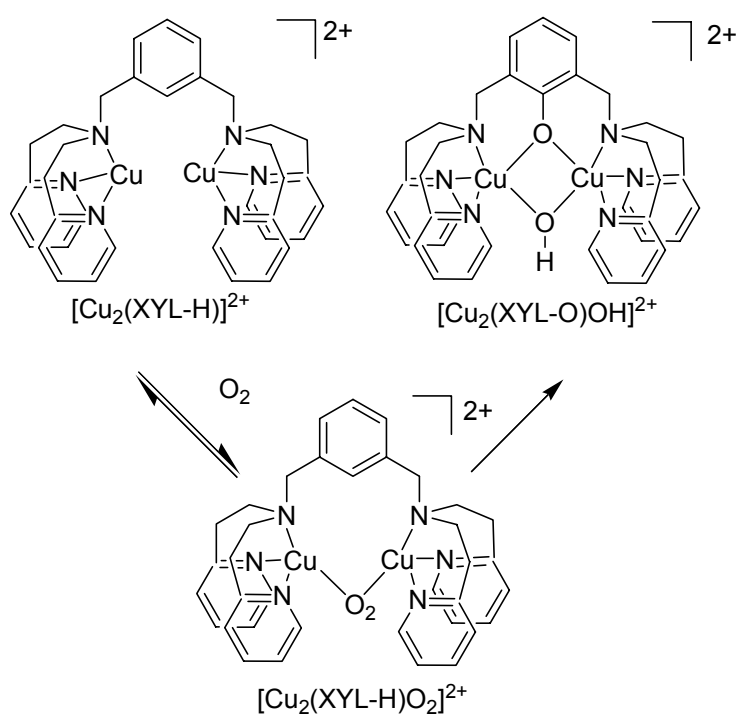
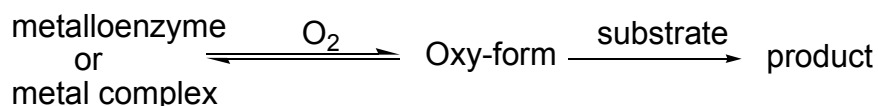


Figure 1-8: Intramolecular ligand hydroxylation during the reaction of $[\text{Cu}_2(\text{R-XYL-H})]^{2+}$ with dioxygen

The occurrence of an $\mu\text{-}\eta^2\text{:}\eta^2$ -peroxo bridged dicopper(II) species as an intermediate during this reaction was observed spectroscopically in a detailed stopped-flow kinetics study and in a resonance raman study. However, further investigations have shown that bis- μ -oxo copper units are also capable to perform ligand hydroxylation reactions.^[34]

1.2.5 Mechanisms of dioxygen binding

The oxidation of copper(I) complexes with dioxygen leads in a first reaction step to the formation of Cu/O₂ adduct complexes. During this process dioxygen is activated and thus consecutive reaction, the oxidation of a substrate according to the following general equation can follow:



Molecular dioxygen can react in different ways with the copper ions of enzymes or model compounds. Several of these "oxygen adduct" complexes could be fully characterized in recent works and some selected examples of the different binding modes are presented in Figure 1-9.^[3, 4, 19, 21, 35, 36] As discussed above dioxygen in hemocyanin is coordinated as a side-on μ - $\eta^2:\eta^2$ peroxide in contrast to the trans- μ -1,2-peroxo coordination in [Cu₂(tmpa)₂(O₂)]²⁺.^[37, 38] In methane monooxygenase it is most likely that a bis- μ -oxo unit represents the active species.

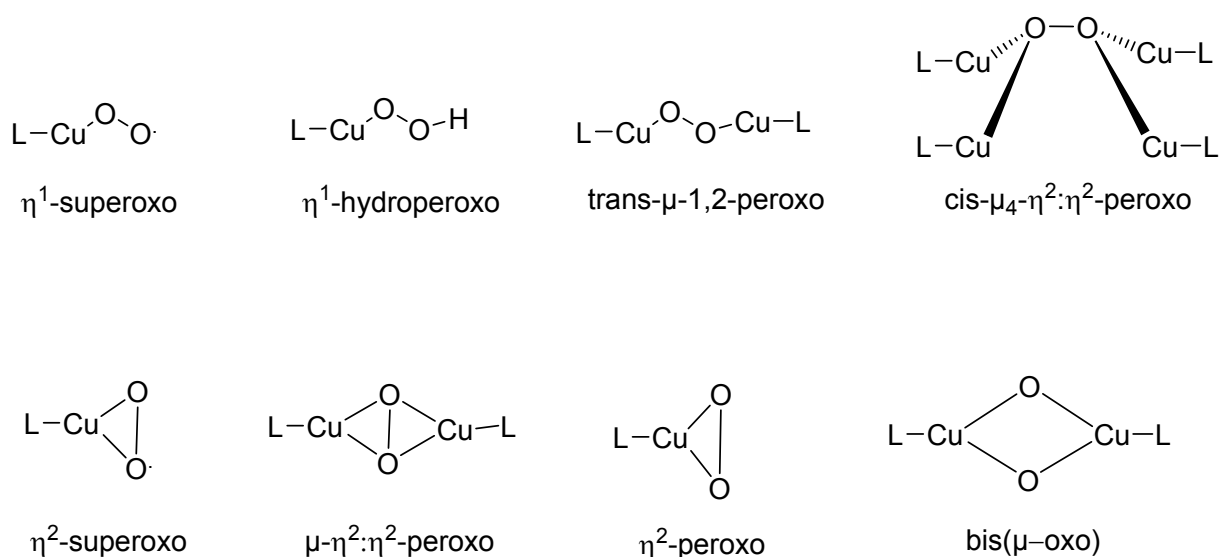


Figure 1-9: Characterized examples of copper "oxygen adduct" complexes

So far, most of the Cu/O₂ adduct complexes described are thermally unstable and very reactive. There have been many efforts to stabilize and characterize these dioxygen adduct complexes formed during the oxidation of Cu(I) complexes. The stability and reactivity of the "dioxygen adduct complexes" can be influenced by

changing the ligand system of the model. Systematic variation of the sterical and electronic properties of the ligands is an accessible way to generate Cu/O₂ adducts that could be well characterized.^[3, 4, 19, 35] This success is also attributed to modern spectroscopic tools and to a better appreciation of appropriate reaction conditions as low temperature, aprotic solvents and weakly coordinating anions.

1.3 Copper(I) complexes with Schiff base ligands

As described above modeling the tyrosinase activity was first successfully demonstrated by Karlin and co-workers who observed an intramolecular ligand hydroxylation using the binuclear copper(I) complex [Cu₂(R-XYL)]²⁺. In the following it turned out, that the nature of the N-donor atoms is very important for this reaction. Substitution of the pyridine groups in [Cu₂(R-XYL)]²⁺ with pyrazole or benzimidazole donors surprisingly completely suppressed the intramolecular ligand hydroxylation reaction described above. In contrast if two triazacyclononane units, bridged by the xylol group, were used, the intramolecular hydroxylation reaction was observed. So far, a clear detailed explanation for these observations is still missing.^[21, 34, 39-46]

Furthermore, for a series of similar and structurally related binuclear copper(I) imine complexes (so called Schiff base complexes) intramolecular ligand hydroxylation was observed as well, if the complexes were exposed to dioxygen (Figure 1-10). Interestingly, in these cases the intramolecular hydroxylation reaction is much less sensitive towards ligand modifications.^[42, 47-56]

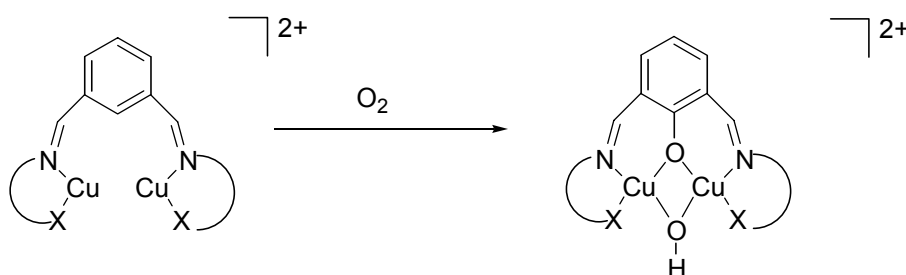


Figure 1-10: Hydroxylation of a Schiff base ligand

Again, detailed information on the reaction mechanisms is missing. To gain further insight into the reaction behavior of such imine systems, several Schiff base ligands and their copper complexes have been synthesized and investigated previously by Schindler and co-workers. For example, it was observed that the macrocyclic

binuclear copper(I) complex $[\text{Cu}_2\text{mac}(\text{CH}_3\text{CN})_2](\text{ClO}_4)_2$ (mac = 3,6,9,17,20,23-Hexaaza-tricyclo[23.3.1.1]trianta-1(29),2,9,11(30),12(13),14,16,23,25,27-decaene) as well undergoes an intramolecular ligand hydroxylation when exposed to dioxygen (Figure 1-11). However, a dioxygen adduct complex, most likely a copper(II) peroxo species, could not be detected by a stopped flow analysis under different conditions.^[31, 48] Furthermore, these findings are related to kinetic studies performed with the complex $[\text{Cu}_2(\text{HBPB-H})(\text{CH}_3\text{CN})_2](\text{BF}_4)_2$ (HBPB = 1,3-bis[N-(2-pyridylethyl)formimidoyl]benzene).^[49]

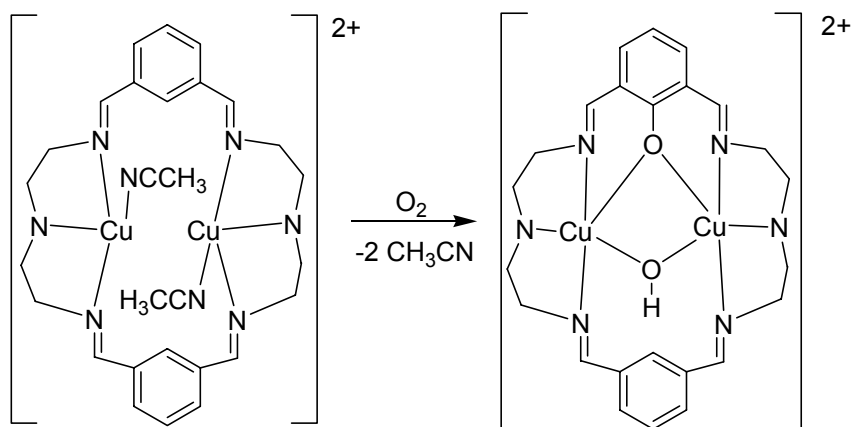


Figure 1-11: Reaction of $[\text{Cu}_2\text{L}^1(\text{CH}_3\text{CN})_2](\text{ClO}_4)_2$ with dioxygen

1.4 Copper(I) complexes with phenanthroline and bipyridine as ligands

It is well known that phenanthroline and bipyridine (Figure 1-12) as well as derivatives are excellent ligands for complexation of copper(I) ions.

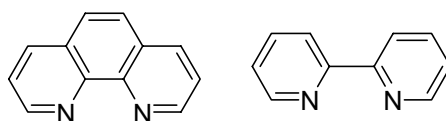


Figure 1-12: 1,10-phenanthroline and 2,2'-bipyridine

Already in the 1960ties 2,9-dimethyl-1,10-phenanthroline was successfully applied as an analytical reagent because of the stability and the special photo physical properties of its copper(I) complexes.^[57]

In Figure 1-13 the copper(I) complex cation is shown. This complex is characterized by its intensive orange color which allows the exact analysis of copper(I) ions with a

low detection limit.^[58] The ligand 2,9-dimethyl-1,10-phenanthroline is commercially available under the name “neocuproine”.

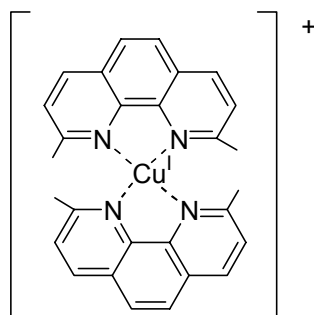


Figure 1-13: Structure of the orange copper(I) phenanthroline complex cation

1.4.1 Copper oxo species with phenanthroline as ligand

Due to the fact that transition metal oxides are capable to activate hydrocarbons, these processes are important for catalytic reactions and attract continuous interest. Furthermore it is well known, that transition metal oxides such as FeO^+ , NiO^+ and PtO^+ , are even capable to oxidize quite inactive alkanes such as methane.^[59] To perform a selective oxidation of methane to methanol in chemical industry is currently one of the big challenges in research. In contrast this oxidation is a facile reaction in nature, catalyzed by the enzyme methane monooxygenase, with either iron or copper ions in its active site.

However, it is expected that simple transition metal complexes should have similar catalytic properties. So it is assumed that an Fe(IV)=O intermediate generated through dioxygen activation could perform the oxidation and functionalization of aliphatic C-H bonds. Recently Que Jr. and co-workers were able to synthesize several iron(IV) oxo complexes that can be used to oxidize C-H bonds of alkanes at room temperature.^[60, 61] Furthermore, such an iron(IV) oxo species could be fully characterized recently.^[62]

It is also believed that the analogous copper-oxo-species unit should be an important reactive intermediate in the oxidation processes in copper chemistry. However so far such a species could not be characterized. Recently Schröder, Holthausen and Schwarz postulated the generation of a Cu=O^+ cation with phenanthroline as a stabilizing ligand.^[63] This ligated copper oxide ion $(\text{phen})\text{CuO}^+$ (the calculated structure is shown in Figure 1-14) is accessible by ESI of a copper nitrate solution containing equimolar amounts of phenanthroline. It could be demonstrated that this

species is able to oxidize simple hydrocarbons such as propane and n-butane. However, it has to be kept in mind, that ions generated by ESI undergo rearrangement and cannot be described as a single structure.

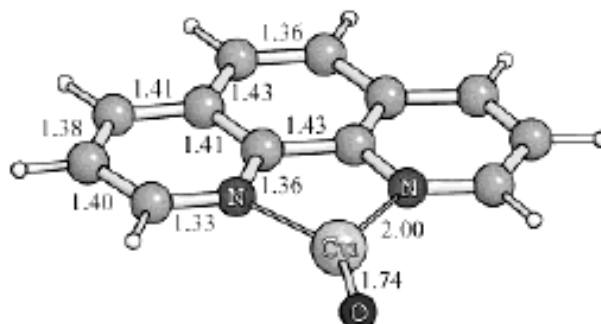


Figure 1-14: Calculated copper oxide cation (phen)CuO⁺

1.4.2 Copper olefin complexes

As described above, copper complexes can activate dioxygen and therefore they play an essential role not only in nature. Thus it is also interesting to investigate the reaction behavior of these copper complexes towards olefins. Furthermore, organo copper(I) complexes are often used for different applications in organic synthesis.^[64-67] In this regard, especially the simple unsaturated hydrocarbon ethylene plays an important role. Ethylene is produced in chemical industry as the largest amount of an organic compound. However, it is also a plant hormone that causes seeds to sprout, flowers to bloom and fruit to ripen and fall off. This effect can be observed as well with carbon monoxide, acetylene and other olefins with a terminal C=C bond. These findings and the requirement of dioxygen for biological processes suggest that a metal ion is present at the ethylene receptor site. On this account several copper(I) complexes with phenanthroline, bipyridine and derivatives and ethylene as ligated olefin were investigated in detail some years ago. It could be shown that the copper(I) ion (as expected) only has a very weak π -back bonding ability in comparison with related Ni(0) or Pt(0) compounds.

Other unsaturated hydrocarbons have been used as ligands for copper(I) ions and the corresponding complexes have been fully characterized.^[65] In this regard Munakata et al. could successfully synthesize the first binary copper(I) complex with the cyclic olefin cyclooctadiene (COD) where the copper centre is ligated only by olefins (Figure 1-15a).^[68] In comparison with the isoelectronic [Ni(COD)₂] it was

observed that both complexes have a very similar molecular structure. $[\text{Ni}(\text{COD})_2]$ plays an important role for the synthesis of several nickel(0) containing compounds used in organometallic chemistry. Furthermore, $[\text{Cu}(\text{bipy})\text{COD}]\text{ClO}_4$ also could be structurally characterized by Munakata et al. (Figure 1-15b). The molecular structure is again quite similar to $[\text{Ni}(\text{bipy})\text{COD}]$.

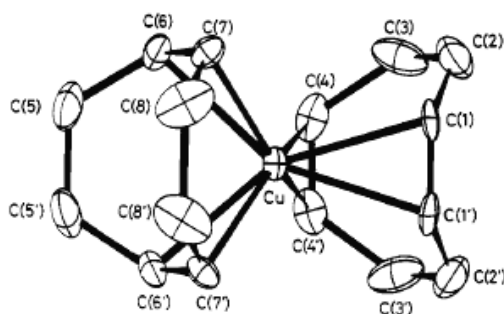


Figure 1-15a: Structure of the cation $[\text{Cu}(\text{COD})_2]^+$ [68]

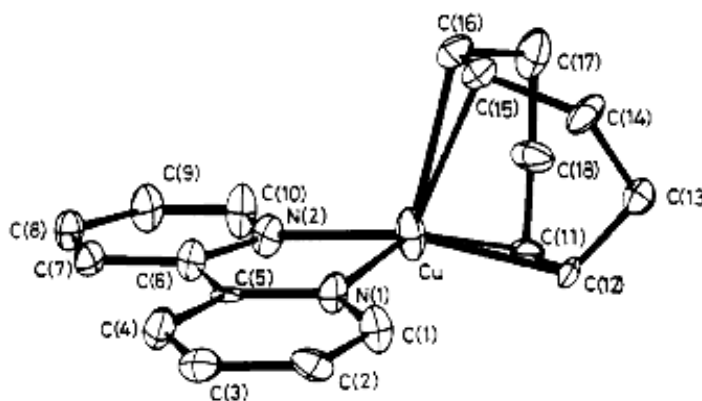


Figure 1-15b: Structure of the cation $[\text{Cu}(\text{bipy})(\text{COD})]^+$ [68]

Important in that regard is that copper(I) complexes containing cyclooctadiene (COD) as ligand are characterized by only weak copper-olefin bonds. This offers the possibility to use these complexes for reactions where the olefin easily can be replaced by other substituents such as dioxygen.

1.5 Nickel complexes

1.5.1 The element nickel and some of its compounds

Because of its silvery appearance nickel was mistaken for other ores for a long time and therefore not known as a pure metal. However, the use of nickel is ancient:

Since 1000 b.C. it has been used by the Chinese within a copper-nickel alloy to manufacture articles for their daily use.

Also in the ancient Greece coins were made of a copper-nickel alloy. Later on in the middle ages nickel salts were of value for coloring glasses green. The mineral used for coloring glass was called "Kupfernickel" (false copper).

Finally nickel was discovered by the Swedish chemist Axel Frederik Cronstedt in the mineral niccolite in 1751. Apparently, he had expected to extract copper from this mineral but obtained none of it. Instead he discovered a white colored metal that he named nickel after the mineral from which it was extracted. Later on the pure nickel metal could be isolated by Torben Bergmann.

Today, most of nickel is obtained from the mineral pentlandite ($\text{NiS} \times 2\text{FeS}$). Most of the world's supply of nickel is found in mines in the Sudbury region of Ontario, Canada. It is believed that this large deposit of nickel ore is a result of an ancient meteor impact.

Nickel is a hard, corrosion resistant metal. It can be electroplated onto other metals to form a protective coating. Finely divided nickel is used as a catalyst for hydrogenations.

In 1888 the isolation of tetracarbonylnickel was the beginning of nickel organic chemistry. $\text{Ni}(\text{CO})_4$ was discovered by Ludwig Mond and can be synthesized by the direct reaction of finely distributed nickel metal with CO at 80°C . Mond recognized the thermal instability of $\text{Ni}(\text{CO})_4$ at 180°C and this is used even today to obtain nickel metal with a purity of 99,9%.

The discovery of the Reppe-catalyst in 1940 and of the nickelocene in 1953 triggered finally the enormous commercial and industrial interest in the organometallic chemistry of nickel.^[69]

1.5.2 Nickel(0) olefin complexes

Complexes containing Ni(0) as metal centre have become quite important for organic synthesis.^[69, 70] The current state of chemical technology allows the successful handling of these complexes that are very sensitive towards dioxygen. In the

following, Ni(0) complexes and their catalytic properties concerning cycloOligomerization of alkenes, alkynes and dienes will be described briefly.^[69, 71]

Nickel catalyzed selective cyclooligomerizations of alkynes by W. Reppe and co-workers in the 1940s and the analogous cyclooligomerizations of 1,3-alkadiens by G. Wilke and co-workers were important discoveries in transition metal mediated organic synthesis. Reppe postulated that acetylene is principally cyclotrimerized into benzene by nickel(0) catalysts, such as $(\text{Ph}_3\text{P})(\text{CO})_2\text{Ni}$. But findings that acetylene is cyclotetramerized by catalysts like $\text{Ni}(\text{CN})_2$ or by Ni(0) complex having labile ligands such as $[\text{Ni}(\text{COD})_2]$, were difficult to understand. Subsequent detailed mechanistic studies of these Oligomerization by Eisch and co-workers have led to a clearer picture. The following mechanism was postulated (Figure 1-16): the reactive nickelacyclopropene (**1**) and nickelacyclopentadiene (**2**) rings are crucial intermediates in both cyclooligomerizations. Trimerization to **3** or tetramerization to **4** depends on whether **2** reacts with a third alkyne (path a) or undergoes autodimerization (path b).^[72-79]

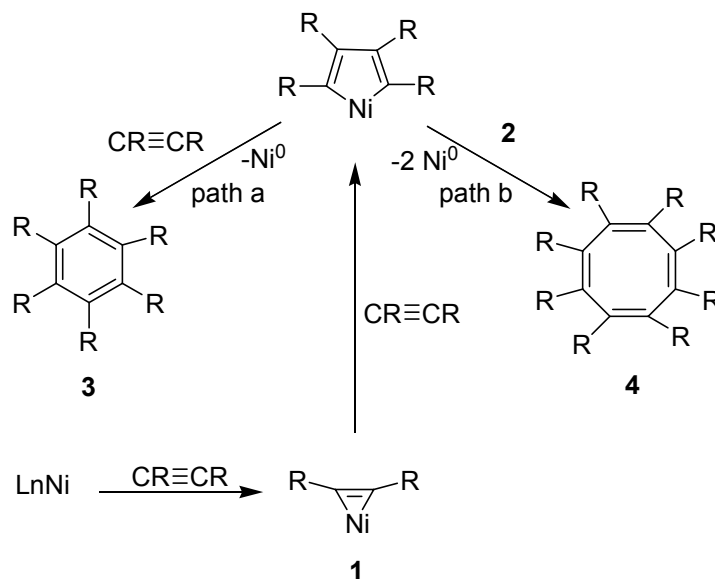


Figure 1-16: Oligomerization of alkynes^[79]

Today the catalytic dimerization of 1,3-butadiene (C_4H_6) to 1,5-cyclooctadiene (COD) using Ni(0) phosphane complexes as catalysts is performed in industry.^[80] Wilke and co-workers discovered this reaction, while investigating a new Ziegler Natta catalyst for polymerization of 1,3-butadiene. After detailed and careful work a mechanism for

the dimerization and trimerization could be postulated. Figure 1-17 shows only the reactions leading to COD.^[75, 81-85]

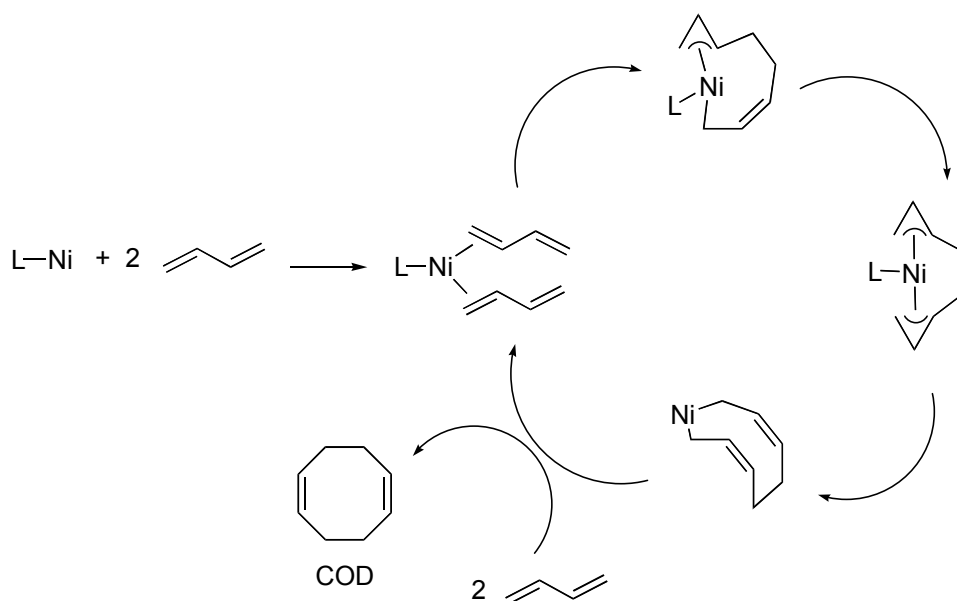


Figure 1-17: Postulated mechanism for the synthesis of COD

Today this mechanism is well accepted and has been supported and enhanced more recently by theoretical calculations performed on this system.^[86] Although such nickel catalyzed C-C coupling reactions are now well established, they are still of high interest because they offer the opportunity to possibly replace more expensive noble metal catalysts.

1.5.3 Dioxygen activation at monovalent nickel

It is well known and already described herein that dioxygen activation is important requirement for many chemical reactions of life. Therefore copper and iron containing enzymes constitute an important class of biologically active compounds which received a widespread attention from both inorganic chemists and biochemists. Because the biological functions of iron and copper enzymes range from oxygen transport, superoxide dismutation to oxidation or oxygenation of organic substrates including electron transfer processes, investigations focused on these systems for the last two decades.

Beside copper and iron enzymes, more recently nickel has received a growing amount of interest. The monovalent oxidation state of nickel is suggested to have a

catalytic role in a number of metalloprotein-mediated transformations. For example nickel enzymes are responsible for reactions involving transformations of one-carbon substrates such as CO or CO₂ and methyl equivalents, most essential for early life.^[87] Nickel proteins found in anaerobic organisms are the acetyl coenzyme A synthase, carbon monoxide dehydrogenase and the methyl coenzyme M reductase. All these proteins catalyze reactions required for autotrophic growth.^[87]

Inspired by the rich biomimetic studies of copper complexes (described in chapter 1.2.4) and inspired by the discovery of two nickel-dependent enzymes which utilize dioxygen (a nickel superoxide dismutase and a nickel dioxygenase)^[88-93], there is a recent intent on investigations of nickel dioxygen chemistry. Corresponding to copper chemistry, very labile nickel dioxygen adduct complexes have been synthesized using ligands which can stabilize nickel (I) towards disproportionation reaction. Therefore monomeric side-on and end-on superoxo and trans- μ -1,2-peroxodinickel intermediates could be characterized spectroscopically (Figure 1-18). Therefore this could become an attractive research area in regard to use such complexes and intermediates as stoichiometric and catalytic oxidants in organic chemistry.

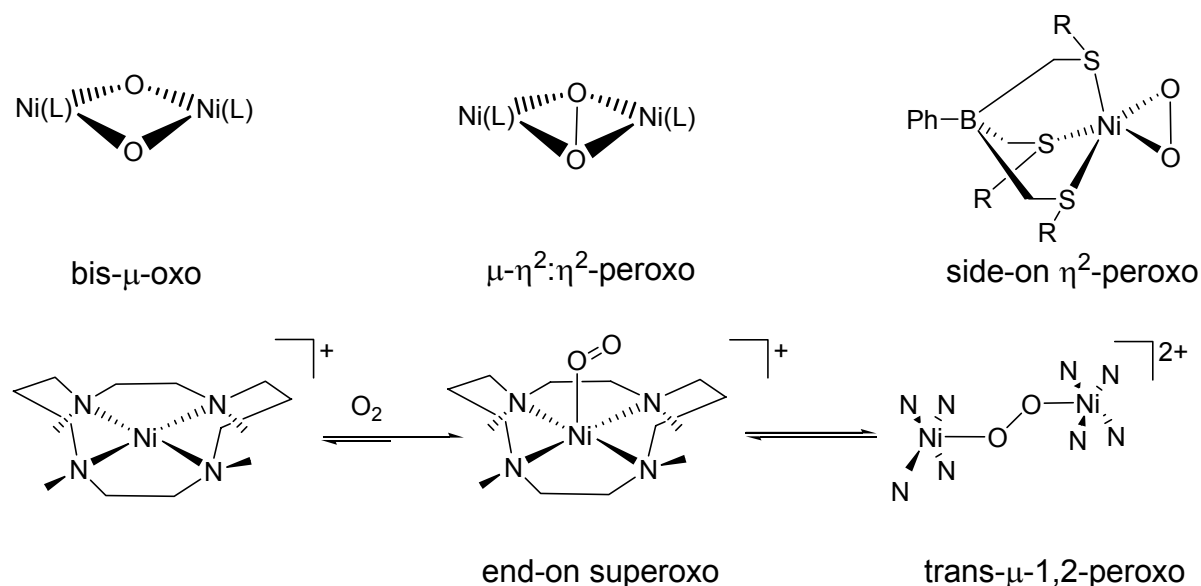


Figure 1-18: Nickel dioxygen adduct complexes

1.6 Projects

As discussed above copper and nickel complexes can play an important role in organic synthesis. Therefore, the topic of this thesis is a detailed study on reactions of these complexes. Investigations on the following projects were performed and are described in this work:

1.6.1 Copper complexes with Schiff base ligands

As described in the introduction there is high interest to model tyrosinase activity using small molecule model systems for a better understanding of the detailed mechanism of intra- and intermolecular hydroxylation reactions. So far there is only limited knowledge on the mechanisms of these reactions. As mentioned in paragraph 1.3 Schiff base ligands are well suited to support the according copper complexes to model tyrosinase activity. To gain further insight into the reaction behavior of these complexes the ligand hydroxylation reaction of the Cu_2 bis(imine) complex $[\text{Cu}_2(\text{DAPA})]^{2+}$ (DAPA = 1,3-bis-[(3-(N-dimethyl)propyl)iminomethyl]benzene (fig 1-19) was investigated.

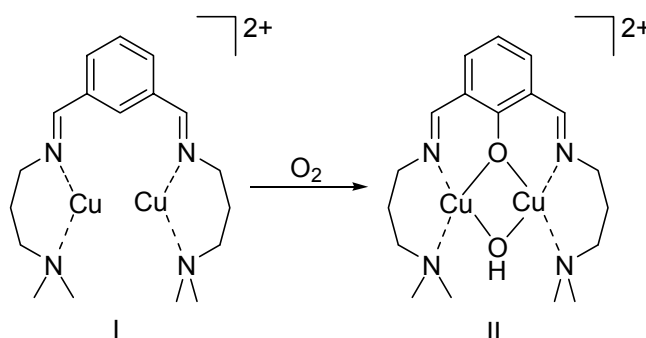


Figure 1-19: Hydroxylation of $[\text{Cu}_2(\text{DAPA})]^{2+}$

1.6.2 Copper complexes with phenanthroline and bipyridine as ligands

As described in chapter 1.4 it is well known, that bidentate chelate ligands with nitrogen donor atoms such as bipyridine and phenanthroline are suitable for preparation of copper(I) complexes. Together with these chelate ligands it is possible to synthesize complexes containing either saturated or unsaturated hydrocarbons as further ligands. There is a great interest in such transition metal complexes because of their possible application as catalysts in organic chemistry. Furthermore, most of these complexes with only weakly coordinated olefin ligands are suitable for

substitution processes and can easily react with dioxygen. Thus it should be possible to observe the formation of "dioxygen adduct" complexes (that might be difficult to prepare otherwise) and/or oxidation of the olefin. Reactions of this type were studied in detail.

1.6.2.1 Copper-oxo-species

In contrast to the according iron complexes, (see 1. 4) so far it was not possible to synthesize and fully characterize a copper oxo species. Because such complexes seem to play an important role as reactive intermediates in oxidation processes it was tried to synthesize such a species. Based on the results of Schröder, Holthausen and Schwarz who suggested the formation of such a species from ESI measurements and theoretical calculations phenanthroline and derivatives were used as ligands in these studies.

1.6.3 Copper(I) olefin complexes

The binding of unsaturated hydrocarbons to transition metals such as copper plays an essential role not only in nature but also in organometallic chemistry. So organo copper(I) complexes are often used for applications in organic synthesis. Characterization and investigation of these complexes and their behavior are important aspects in organometallic chemistry. Therefore copper complexes with several olefin ligands were synthesized, characterized and investigated kinetically.

1.6.4 Nickel(0) olefin complexes

As described above transition metal complexes such as Ni(0) complexes are essential catalysts in numerous organic synthesis and therefore important materials in industry and laboratories. Therefore it is important to synthesize and investigate Ni(0) complexes with unsaturated substrates as ligands and their reaction behavior in detail. Especially in cooperation with the research group of Prof. A. de Meijere (University of Göttingen) several Nickel(0) bipyridine complexes with quite special olefin ligands such as bicyclopropylidene **bcp** (a) and dicyclopropylacetylene **dcpa** (b) were synthesized, characterized and investigated.

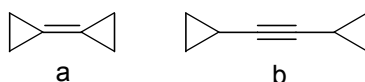


Figure 1-20: Bicyclopropylidene (a) and dicyclopropylacetylene (b)

Theoretical part

2.1 Chemical Kinetics

Chemical kinetics or reaction kinetics deals with the measurement and study of rates of chemical reactions and the analysis of experimental data to gain as much information as possible about a chemical reaction. The final goal is the postulation of a reaction mechanism and to obtain information on the transition state. Kinetic investigations include different experimental conditions like different concentrations, temperature, pressure or different solvents and how these can influence the rate and the course of a chemical reaction. In the following description the most important terms and mathematic relations of reaction kinetics concerning this work will be summarized. A complete and detailed summary on this topic is described in detail in several textbooks.^[94-97]

2.2 Reaction rate

The rate of change in the concentrations of the reactants and products can be used to characterize the rate of a chemical reaction. In the correct form a reaction can be described as the differential change of n_i :

$$dn_i = \nu_i \cdot d\zeta \quad [2.1]$$

with

ζ = extent of the reaction

n_i = mol

ν_i = stoichiometric coefficient.

Under constant volume conditions, a reaction can be determined as:

$$\frac{dn_i}{V} = \nu_i \cdot \frac{d\zeta}{V} = \nu_i \cdot d\chi \quad [2.2]$$

χ = volume based extent of the reaction

The reaction rate v_R for a chemical reaction occurring in a closed system under constant-volume conditions is defined as:

$$v_R = \frac{d\chi}{dt} = \frac{1}{\nu_i} \cdot \frac{dc_i}{dt} \quad [2.3]$$

For a common reaction (eq. 2.4) , the reaction rate is determined as follows (eq. 2.5):



$$v_R = -\frac{1}{a} \frac{d[A]}{dt} = -\frac{1}{b} \frac{d[B]}{dt} = \frac{1}{c} \frac{d[C]}{dt} \quad [2.5]$$

If the rate of the reaction depends only on the concentrations of A and B, the proportionality factor k in the rate law is usually termed the rate constant (eq. 2.6):

$$v_R = -\frac{d[A]}{dt} = k[A]^x[B]^y \quad [2.6]$$

The terms x and y in equation [2.6] determine the order of the reaction. If $x = 1$, the reaction order is termed first order in A, if $y = 2$ the reaction rate is second order in B. The overall order for the reaction is $x + y$.

2.3 First order dependence

First order reactions are extremely common chemical reactions. The reaction rate depends only on the concentration of one reactant.

For a reaction such as $A \rightarrow B$, the decrease in concentration of **A** over time can be written as shown in equation [2.7] It is a *first order rate law* because the rate is proportional to the *first power* of [A].

$$-\frac{d[A]}{dt} = \frac{d[B]}{dt} = k[A] \quad [2.7]$$

The differential form leads to an equivalent integrated expression:

$$\int_{A_0}^A \frac{d[A]}{[A]} = -k \int_0^t dt \Rightarrow \ln \frac{[A]}{[A_0]} = -kt \Rightarrow \ln[A] = \ln[A_0] - kt \quad [2.8]$$

To establish if a reaction follows first order kinetics it is common to plot the measured concentration versus the time. Therefore properties which are proportional to the concentration of the reactant such as absorbance or conductivity have to be measured. A plot of $\ln[A]$ versus time is a straight line with slope $m = -k$. Alternatively, a plot of rate versus $[A]$ is a straight line with a slope of $-k$. From experimental data the rate constant can be calculated from the slope of the appropriate plot. Today linearization is not the most accurate method to determine the reaction rate but computer programs such as Origin or Igor can be used to fit the measured data directly to exponential functions.

2.4 Second order dependence

Second order kinetics play an important role in the reactions of complex ions. In a general reaction between two molecules A and B (equation 2.4), the reaction order is termed 1 in A and B but overall it is a *second order rate law* because the rate is proportional to the product of two concentrations. The reaction law in this case is given by:

$$-\frac{d[A]}{dt} = -\frac{d[B]}{dt} = \frac{d[C]}{dt} = k[A][B] \quad [2.9]$$

Integration of the differential equation leads to:

$$\frac{1}{[A]_0 - [B]_0} \cdot \ln \frac{[B]_0 \cdot [A]}{[A]_0 \cdot [B]} = kt \quad [2.10]$$

These reactions usually are studied under pseudo first order conditions because this is a much easier procedure. Pseudo first order conditions mean that one of the reactants is provided in excess in respect to the other one of at least a concentration ratio of 10 : 1. Thus the concentration of the reactant in excess can be regarded as constant and can be included into the rate constant, obtaining a pseudo first order constant. That allows to determine a pseudo first order rate constant from a second order rate equation. This makes the treatment to obtain an integrated rate equation much easier. If B is the reactant whose concentration is constant ($[B] \gg [A]$ and $[B] \approx [B]_0 \approx \text{const}$) the rate law can be derived to:

$$-\frac{d[A]}{dt} = k_{obs}[A] \quad [2.11]$$

This leads to the following expression of the rate constant:

$$k_{obs} = k[B]_0 \quad [2.12]$$

The rate constant k can be obtained by a plot of k_{obs} versus $[B]_0$.

2.5 Equilibrium reactions

Many chemical reactions such like ligand exchange processes of metal complexes are equilibrium reactions, defined by a forward and back reaction.

For example MX and Y react to MY and X:



(M = metal complex ; X, Y = ligands)

To obtain pseudo first order conditions concerning k_+ and k_- the ligand concentration of X and Y is kept in great excess in respect to the concentration of the metal complex. Therefore the reaction rate expression for the above reaction can be expressed as

$$-\frac{d[M - X]}{dt} = \frac{d[Y]}{dt} = k_+[M - X][Y] - k_-[M - Y][X] \quad [2.14]$$

with

$$k_{obs} = k_+[Y] - k_-[X] \quad [2.15]$$

The rate constant k_{obs} can be determined as the sum of k_+ and k_- . These rate constants can be obtained by plots of k_{obs} versus $[X]$ or $[Y]$.

2.6 Consecutive Reactions

Most chemical reactions consist of several reaction steps. Therefore educts, products as well as intermediates can influence the reaction kinetics. Several different possible reaction pathways are observed. The most simple case includes one intermediate I formed in a reversible reaction step. To determine the according rate law is becoming more difficult, if more than one reversible reaction step has to be considered as shown for example in the first reaction step of equation 2.16.



(A, B = educts; I = intermediate; P = product)

The mathematical description of such reactions becomes more and more difficult and is quite complex. Therefore it is common to use approximations to simplify such terms.

One approach is to assume that the first reversible reaction step is much more rapid than the second step and so k_1 and k_{-1} are much larger than k_2 . Therefore the intermediate I will be in equilibrium with A and B throughout the reaction

$$\frac{[I]}{[A][B]} = \frac{k_1}{k_{-1}} = K \quad [2.17]$$

and will be continually maintained.

Insertion of equation 2.17 in 2.16 offers a mathematical term for k_{obs} , which is considered to be the solution of the reaction law.

The steady-state approximation is an alternative method to simplify such complex reactions. It is assumed that the intermediate is quite reactive and therefore the concentration of I will be very low throughout the reaction. This means that the rate of the concentration change of this reaction intermediate is very close to zero:

$$[I] \ll [A], [B] \quad \frac{d[I]}{dt} \approx 0 \quad [2.18]$$

and therefore:

$$k_1[A][B] - k_{-1}[I] - k_2[I] = 0 \quad [2.19]$$

Now it is possible to determine a mathematical term for k_{obs} without knowing the exact concentration of the reaction intermediate I. The steady state approximation facilitates the solution of the differential equation that arises from most reaction laws, which lack of analytical solutions. For example this method is applied in Michaelis Menten kinetics.

2.7 Determination of enthalpy, entropy and volume of activation: ΔH^\ddagger , ΔS^\ddagger , ΔV^\ddagger

The Eyring equation also known as Eyring and Polany equation concerns the theory of the transition state and the activated complex. It is also the basis for the determination of the activation parameters ΔH^\ddagger , ΔS^\ddagger and ΔV^\ddagger . This equation describes the dependence of the reaction rate from temperature and pressure, following the transition state theory and the basic thermodynamic concepts.

$$k = \frac{k_B T}{h} \cdot e^{\left(-\frac{\Delta H^\ddagger}{RT} + \frac{\Delta S^\ddagger}{R} \right)} \quad [2.20]$$

with ΔH^\ddagger = enthalpy of activation, ΔS^\ddagger = entropy of activation.

It can also be written in a linear form:

$$\ln\left(\frac{k}{T}\right) = \ln\left(\frac{k_B}{h}\right) - \frac{\Delta H^\ddagger}{RT} + \frac{\Delta S^\ddagger}{R} \quad [2.21]$$

If the reaction is performed at different temperatures, the reaction rate can be determined.

The plot of $\ln\left(\frac{k}{T}\right)$ versus $\frac{1}{T}$ gives a straight line with a slope of $-\frac{\Delta H^\ddagger}{R}$ from which the enthalpy of activation can be derived. From the intercept $\ln\left(\frac{k_B}{h}\right) + \frac{\Delta S^\ddagger}{R}$ the entropy of activation can be derived.

The study of the temperature dependence provides values of ΔS^\ddagger that contain important information about the transition state complex. A large negative value of ΔS^\ddagger (unfavourable) indicates a more ordered transition state complex. This is the case if degrees of freedom (translation, rotation, vibration) are reduced in the transition state compared with the initial state. A negative value of ΔS^\ddagger may indicate an associative mechanism, while a positive ΔS^\ddagger supports a dissociative mechanism.

The determination of ΔS^\ddagger through linearization and extrapolation ($T \rightarrow \infty$), usually leads to large errors. In contrast activation volumes can be obtained during high

pressure measurements without including such a large error. If possible these measurements should be made to obtain more reliable data for a mechanistic discussion. The volume of activation is derived from the pressure dependence of the rate constant of a reaction (mainly used for reactions in solution), defined by the following equation:

$$\left(\frac{\partial G}{\partial p}\right)_T = V \quad \Rightarrow \quad \Delta V^\ddagger = \left(\frac{\partial(\Delta G^\ddagger)}{\partial p}\right)_T \quad [2.22]$$

$$\Delta V^\ddagger = -RT \left(\frac{\partial(\ln k)}{\partial p}\right)_T \quad [2.23]$$

According to the transition state theory ΔV^\ddagger is interpreted as the difference between the partial molar volumes of the transition state and the sum of the partial volumes of the reactants. ΔV^\ddagger can be determined from the slope, if $\ln k$ is plotted versus pressure p .

Aromatic Hydroxylation in a Copper Bis(imine) Complex Mediated by a $\mu\text{-}\eta^2\text{:}\eta^2$ Peroxo Dicopper Core: A Mechanistic Scenario

This work has been published in Chemistry, A European Journal

Sander, O.; Henß, A.; Näther, C.; Würtele, C.; Holthausen, M. C.; Schindler, S.; Tuczek, F.; Aromatic Hydroxylation in a Copper Bis(imine) Complex Mediated by a $\mu\text{-}\eta^2\text{:}\eta^2$ Peroxo Dicopper Core: A Mechanistic Scenario *Chem. Eur. J.*, **2008**, in press.

3.1 Abstract

Detailed mechanistic studies of the ligand hydroxylation reaction mediated by a Cu bis(imine) complex are presented. Starting from a structural analysis of the Cu(I) complex and the Cu(II) product exhibiting a hydroxylated ligand the optical absorption and vibrational spectra of the educt and the product are analyzed. The kinetic analysis of the ligand hydroxylation reaction shows that O₂-binding is the rate-limiting step in the hydroxylation reaction. The reaction is found to proceed much faster in methanol than in acetonitrile. Moreover, an inverse kinetic isotope effect is evidenced for the reaction in acetonitrile which is attributed to a sterically congested transition state leading to the peroxo adduct. In methanol, however, no KIE is observed. A DFT analysis of the oxygenation reaction mediated by the $\mu\text{-}\eta^2\text{:}\eta^2$ peroxo core demonstrates that the major barrier after O₂-binding is represented by the electrophilic attack on the arene ring. The relevant orbital interaction occurs between the σ^* orbital of the Cu₂O₂ unit and the HOMO of the ligand. On the basis of the activation energy for the rate limiting step (18.3 kcal/mol) this reaction is thermally allowed, in agreement with the experimental observation. The calculations also predict the presence of a stable dienone intermediate which, however, escaped experimental detection so far. Reasons for these findings are considered. The implications of the results with respect to the mechanism of tyrosinase are discussed.

3.2 Introduction

Recent publication of the first crystal structure determination of a tyrosinase has opened a new perspective to understand the chemical reactivity of this class of enzymes at a molecular level.^[13, 14] Tyrosinases (Ty) are ubiquitous copper enzymes

mediating the hydroxylation of monophenols to *o*-diphenols and the subsequent two-electron oxidation to *o*-quinones.^[11] Specifically, tyrosine is converted to dopaquinone, the first step of melanine synthesis.^[98] Two-electron oxidation of *o*-diphenols (catechols) to *o*-quinones is also catalyzed by the related enzyme catechol oxidase (CO) which, however, lacks monooxygenase activity.^[99, 100] The active sites of Ty and CO exhibit two copper atoms both of which are coordinated by three histidines (type3 copper). The third group of proteins with type3 copper active sites is that of hemocyanins (Hc) which serve as oxygen carriers in some arthropods and mollusks, exhibiting highly cooperative oxygen binding characteristics.^[101, 102]

There have been numerous attempts to reproduce and understand the chemical reactivity of tyrosinase with small-molecule model systems, both on the basis of the hydroxylation or oxidation of *external substrates* and on hydroxylations of the *ligand*.^[3, 103-105] In the latter case a part of the ligand coordinating one or both copper centers is hydroxylated after exposure of the Cu(I) complex to dioxygen. The relevance of these reactions to tyrosinase has intensively been discussed, and a molecular mechanism of the tyrosinase function has been suggested based on DFT calculations.^[3, 103-107] It has further been established that both aliphatic and aromatic parts of the ligand can be hydroxylated this way (*aliphatic* and *aromatic* ligand hydroxylation).^[3, 108] The latter reactivity has been discovered by Karlin and co-workers in their study of the [Cu₂(XYL)] complex (XYL=tetrakis(2-(pyridin-2-yl)ethyl)benzene-1,3-diamine).^[29, 30] Reaction of the Cu(I)₂ precursor with O₂ was found to lead to hydroxylation of the bridging xylylene spacer in 2-position. It was later shown that the Cu(I)₂ species binds O₂ in a side-on bridging fashion and that most probably the Cu₂ μ-η²:η²-peroxo unit mediates an electrophilic attack on the aromatic ring, leading to O-O cleavage and hydroxylation.^[109] A mechanistic alternative to this scenario is the full or partial conversion of the Cu(II)₂ μ-η²:η² peroxo to the Cu(III)₂ bis(μ-oxo) form which then mediates the aromatic hydroxylation reaction.^[110-112] For the Cu₂(XYL) complex, this pathway has been excluded. For other systems, however, an aromatic ligand hydroxylation mediated by a Cu₂ bis(μ-oxo) species is well established.^[34]

A simplified version of the Karlin system is provided by Cu(II) bis(imine) complexes which also mediate a hydroxylation of the bridging ligand upon reaction with O₂. This

reaction has been intensively studied as well^[48, 54, 113, 114] and the relevance to the tyrosinase reaction has been stressed.^[49, 51] The binucleating ligand contains a bridging phenylene group carrying two arms which provide two nitrogen donors (one imine and one terminal amine) each. Upon exposure of the Cu(I) precursor to dioxygen, the central phenylene spacer is hydroxylated, in analogy to the XYL complex (Figure 3-1). With respect to the latter system, however, the bis(imine) complex enforces an almost planar molecular geometry which highly restricts the configuration space involved in the ligand hydroxylation reaction. Although it has been speculated that in this reaction a peroxo or bis(μ -oxo) intermediate is involved, no such intermediate has ever been detected. Correspondingly, key features of the reaction course applying to this important class of tyrosinase model systems have remained unclear to date.

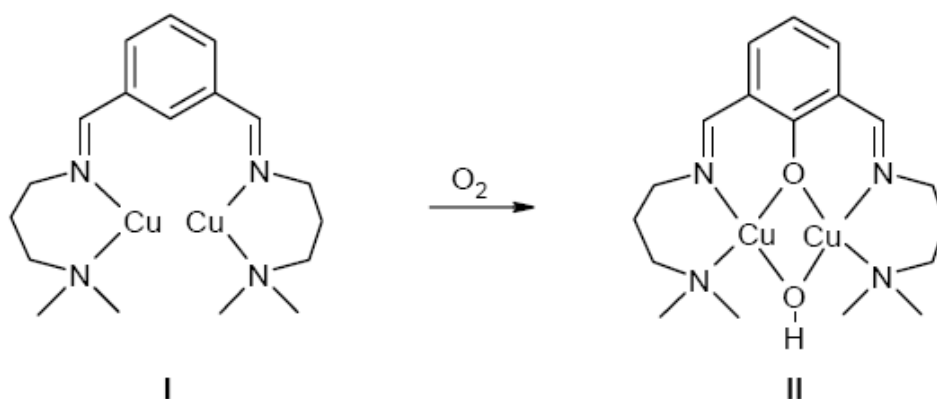


Figure 3-1: Hydroxylation of [Cu(DAPA)] I leading to the product

Herein we present spectroscopic, kinetic and theoretical investigations on the Cu₂ bis(imine) complex [Cu₂(DAPA)]²⁺ (I; DAPA = 1,3-bis-[(3-(N-dimethyl)propyl)iminomethyl]benzene; Figure 3-1) with the goal of developing a mechanistic scenario for the ligand hydroxylation reaction occurring in this system. To this end the kinetics of the reaction is studied in different solvents and at different temperatures, also employing a deuterium substituted ligand. In order to monitor the time course of the hydroxylation spectroscopically the UV/Vis spectra of the Cu(I) precursor I and the hydroxylated Cu(II) product II are analyzed and compared with each other. Moreover the vibrational spectroscopic properties of the reactant and the product are determined. In particular, the infrared and Raman spectra of the Cu(II) complex II are analyzed with the help of ¹⁸O substitution and quantum chemical

calculations. The reactant **I** and the product **II** are further characterized by X-ray crystallography. Density functional theory is employed to identify potential reaction pathways leading from the initially formed $\mu\text{-}\eta^2\text{:}\eta^2$ peroxo dicopper intermediate to the hydroxylated product **II**. The quantum chemical results are discussed in light of the experimental findings and implications for the reactivity of tyrosinase are discussed.

3.3 Experimental and Computational Details

3.3.1 Materials and Techniques.

The reagents isophthalaldehyde and 3-dimethylaminopropylamine were used as received from Aldrich Chemical Co. Tetrakis(acetonitrile)copper(I) hexafluorophosphate was either obtained commercially from Aldrich or synthesized from copper(I) oxide according to a method described in the literature.^[115] Solvents used were all reagent grade and have been further purified by refluxing over drying agents and distilling under argon. Methanol was distilled from $\text{Mg}(\text{OCH}_3)_2$; diethylether was distilled from LiAlH_4 ; acetonitrile was distilled from CaH_2 . The NMR spectra were recorded at 300 K on a Bruker Avance 400 Pulse Fourier Transform spectrometer operating at a ^1H frequency of 400.13 MHz and ^{13}C frequency of 100.62 MHz. Referencing was carried out using TMS as the substitutive standard. The elemental analysis was performed using a Euro Vector CHNS-O-element analyzer (Euro EA 3000). Samples were burned in sealed tin containers by a stream of oxygen. FT-IR spectra were recorded in KBr pellets on a Mattson Genesis Type I spectrometer. Optical absorption spectra of solutions were recorded on a Cary 5 UV-Vis-NIR spectrometer equipped with a CTI cryocooler. Raman spectra were recorded on a Bruker IFS 66 FT spectrometer equipped with a Raman assembly.

Variable temperature stopped-flow measurements allowed the collection of time-resolved UV-vis spectra for the fast reaction of **I** with dioxygen in methanol. Solutions of the complexes were prepared in a glovebox (MBraun, Garching, Germany) and transferred using syringes to the low-temperature stopped-flow instrument. A dioxygen saturated solution was prepared by bubbling dioxygen through methanol in a syringe (solubility of dioxygen at 25 °C in MeOH: 8.5 mM).^[116] Lower dioxygen concentrations were obtained by mixing these solutions with argon saturated solvents. The reaction was studied under pseudo-first-order conditions ($[\text{complex}] \ll$

[O₂]), and time-resolved UV-vis spectra of the reactions of dioxygen with copper(I) complexes were recorded with a modified Hi-Tech SF-3L low-temperature stopped-flow unit (Salisbury, U.K.) equipped with a J&M TIDAS 16-500 photodiode array spectrophotometer (J&M, Aalen, Germany). Data fitting was performed using the integrated J&M software Kinspec. Details on such studies have been described previously.^[117]

3.3.2 Tetrakis(acetonitrile)copper(I) perchlorate

CuCO₃ was added to 10 mL of perchloric acid until the solution was saturated. The remaining precipitate was filtered off and the solution was concentrated *in vacuo*. After cooling the solution over night, blue crystals precipitated which were filtered off and dissolved in acetonitrile. The blue solution was refluxed with copper turnings under argon till the colour disappeared. After cooling of the colourless solution colourless crystals precipitated which were filtered off and dried. Anal. Calcd. for CuC₈H₁₂N₄ClO₄: C, 29.37; H, 3.7; N, 17.12; Cl, 10.84. Found: C, 29.2; H, 3.66; N, 17.4; Cl, 10.81.

3.3.3 DAPA (1,3-bis-[(3-(N-dimethyl)propyl)iminomethyl]benzene)

400 mg (2.98 mmol) isophthalaldehyde and 610 mg (5.96 mmol) 3-dimethylaminopropylamine were dissolved in 40 mL methanol and refluxed for 1h. The solvent was rotary-evaporated and the remaining yellow oil was dried *in vacuo*. The product was purified by chromatography on silica gel with methanol as eluant (R_f = 0.4). Anal. Calcd for C₁₈H₃₀N₄: C, 71.48; H, 10.0; N, 18.52. Found: C, 70.93; H, 10.35; N, 18.53; ¹H-NMR (400 MHz, CD₂Cl₂/TMS) δ 8.3 (s, 2H, *imin*-H), 8.03 (s, 1H, Ar-H), 7.76 (dd, 2H, Ar-H), 7.44 (t, 1H, Ar-H), 3.61 (dt, 4H, =N-CH₂), 2.3 (t, 4H, -CH₂-N), 2.18 (s, 12H, -CH₃), 1.81 (q, 4H, -CH₂-); ¹³C-NMR (100.6 MHz, CD₂Cl₂/TMS) δ 160.2, 137.0, 129.6, 128.7, 127.5, 59.4, 57.4, 42.2, 29.0; MS (EI, 70 eV): m/z (%) = 303.4 (100) [M⁺]; calcd: 303.46.

3.3.4 Cu(I)₂-DAPA (**la**, **lb**, **lc**)

The synthesis was performed under argon atmosphere. The complex was either prepared according to the published procedure as the PF₆ salt (**la**)^[56] or as the ClO₄ salt (**lb**) by using the following modified procedure: 230 mg (0.76 mmol) DAPA were dissolved in 20 mL dry and degassed methanol. 296 mg (1.52 mmol)

tetrakis(acetonitrile)copper(I) perchlorate were added. The resulting yellow solution was heated for 1h. After concentrating the solution to 10 mL a yellow solid precipitated which was filtered off and washed two times with 5 mL of degassed methanol. $^1\text{H-NMR}$ (400 MHz, $\text{CD}_3\text{CN/TMS}$) δ 8.37 (s, 2H, imin-H), 8.25 (s, 1H, Ar-H), 7.93 (d, 2H, Ar-H), 7.55 (t, 1H, Ar-H), 3.72 (t, 4H, =N-CH₂), 2.51 (t, 4H, -CH₂-N), 2.23 (s, 12H, -CH₃), 1.81 (q, 4H, -CH₂-); $^{13}\text{C-NMR}$ (100.6 MHz, $\text{CD}_3\text{CN/TMS}$) δ 163.2, 137.0, 131.8, 130.0, 129.1, 62.7, 60.7, 47.2, 29.3. Crystals suitable for diffraction studies were obtained by diffusion of diethyl ether into a solution of $[\text{Cu}(\text{I})_2(\text{DAPA})](\text{PF}_6)_2$ (**la**) in acetonitrile.

For synthesis of the tetraphenylborate salt of Cu(I)-DAPA (**lc**) 200 mg (0.32 mmol) Cu(I)-DAPA perchlorate (**lb**) were dissolved in 10 mL of dry, degassed acetonitrile. 228 mg (0.64 mmol) potassium tetraphenylborate dissolved in 15 mL of acetonitrile were added. After concentrating the yellow solution to 10 mL a colourless solid precipitated and was filtered off. The solution was evaporated to dryness and the yellow residue was used without further purification. The conversion of the perchlorate to the tetraphenylborate salt was checked for completeness by IR spectroscopy. The perchlorate bands were absent in the product.

3.3.5 $\text{Cu}(\text{II})_2\text{-DAPA-OH}$ (**II**), perchlorate salt

60 mg $\text{Cu}(\text{I})_2\text{-DAPA}$ (**lb**) were dissolved in 40 mL of dry dichloromethane. Dioxygen was bubbled through the solution for 5 minutes. The colour changed from yellow to green. The solution was concentrated to 5 mL. By adding 20 mL of diethylether a green solid precipitated which was filtered off. The product was recrystallized from dichloromethane by diffusing diethylether into the solution. Green crystals were obtained. Anal. Calcd for $\text{C}_{18}\text{H}_{30}\text{N}_4\text{Cu}_2\text{O}_2(\text{ClO}_4)_2(\text{CH}_2\text{Cl}_2)$: C, 30.6; H, 4.33; N, 7.52. Found: C, 31.1; H, 4.78; N, 7.63; UV-VIS (CH_3CN) λ_{max} nm (ϵ , $\text{M}^{-1}\text{cm}^{-1}$) 255 (35753), 357 (9135), 628 (253). The ^{18}O isotopomer of **II** was prepared analogously, employing $^{18}\text{O}_2$ instead of $^{16}\text{O}_2$.

3.3.6 Isophthalaldehyde- d_6

2.5g (21.55 mmol) *m*-xylene- d_{10} were dissolved in 250 mL of CCl_4 . 22.55g (126.7 mmol) NBS and 1 drop of bromine was added. The reaction was started with little amounts of AIBN and the mixture was heated for 15h under reflux. The succinimide

was filtered off and after removal of the solvent the product was used without further purification. The reddish product was dissolved in 30 mL of H₂SO₄ at 110°C. After the formation of bromine the solution was hydrolyzed with 100 mL ice and extracted with methyl-*tert*-butyl-ether (MTBE). The combined organic phases were neutralized with NaHCO₃-solution and the aqueous phase was again extracted with MTBE. The combined organic phases were dried over MgSO₄ and after removal of the solvent the product was purified chromatographically on silica gel with dichloromethane as eluant ($r_f = 0.35$). ¹H-NMR shows no signals; ¹³C-NMR (100.6 MHz, CD₂Cl₂/TMS) δ 190.7 (deutero-t), 136.9 (s), 134.1 (deutero-t), 130.2 (deutero-t), 129.4 (deutero-t); MS (EI, 70 eV): m/z (%) = 141.1 (100) [M⁺]; calcd: 141.2.

3.3.7 Cu(I)₂-DAPA-d₆, perchlorate salt (I^D)

0.4 g (2.82 mmol) isophthalaldehyde-d₆ was dissolved in 40 mL of dry methanol. 0.75 mL (5.9 mmol) 3-dimethylaminopropylamine was added and refluxed for 1h. After cooling 1.1 g (5.9 mmol) tetrakis(acetonitrile)copper(I) perchlorate were added to the orange solution and stirred for 1h. After concentrating the solution to 10 mL a yellow solid precipitated which was filtered off and washed two times with 5 mL of degassed methanol. ¹H-NMR (400 MHz, CD₃CN/TMS) δ 3.74 (t, 4H, =N-CH₂), 2.53 (t, 4H, -CH₂-N), 2.24 (s, 12H, CH₃), 1.82 (q, 4H, -CH₂-); ²H-NMR (61.4 MHz, CD₃CN/TMS) between 7.4 and 8.4ppm 4 Peaks with integration ratio 2:2:1:1 are observed; ¹³C-NMR (100.6 MHz, CD₃CN/TMS) δ 61.8, 59.8, 46.2, 28.2.

3.3.8 Cu(II)₂-DAPA-d₆-OH, perchlorate salt (II^D)

60 mg Cu(I)₂-DAPA (I^D) were dissolved in 40 mL of dry dichloromethane. Dioxygen was bubbled through the solution for 5 minutes. The colour changed from orange to green. The solution was concentrated to 5 mL. By adding 20 mL of diethylether a green solid precipitated which was filtered off and recrystallized from dichloromethane. Anal. Calcd for C₁₈H₁₂D₆N₄Cu₂O₂(ClO₄)₂: C, 32.44; H, 5.44; N, 8.41. Found: C, 32.92; H, 5.28; N, 8.20;

Caution! Although the compounds reported in this paper seem to be stable to shock and heat, extreme care should be used in handling them for the potential explosive nature of perchlorate salts.

3.3.9 Single crystal structure analysis

The X-ray crystallographic data for complex **I** were collected on a STOE IPDS-diffractometer at 173 K equipped with a low temperature system (Karlsruher Glastechnisches Werk). Mo-K α radiation ($\lambda = 0.71069 \text{ \AA}$) and a graphite monochromator was used. Cell parameters were refined by using up to 5000 reflections. No absorption corrections were applied. The structure was solved by Direct Methods in SHELXS97, and refined as a racemic twin by using full-matrix least squares in SHELXL97(BASF-Parameter:0.542). It was attempted to solve and refine the structure also in the centrosymmetric space group P2 $_1$ /m which was not successful. The hydrogen atoms were positioned geometrically and all non-hydrogen atoms were refined anisotropically, if not mentioned otherwise. Details of the structure determination are given in Table 3-1.

Data collection on complex **II** was performed with an Imaging Plate Diffraction System (IPDS-1) from STOE & CIE. Structure solutions was done using SHELXS-97 and structure refinements was performed against F^2 using SHELXL-97. All non-hydrogen atoms were refined with anisotropic displacement parameters. All C-H hydrogen atoms were positioned with idealized geometry and were refined isotropically using a riding model. The O-H H atom was located in the difference map, its bond length was set to ideal values and afterwards it was refined using a riding model. Crystallographic data (excluding structure factors) for the two structures reported in this paper have been deposited with the Cambridge Crystallographic Data Centre as supplementary publication no. CCDC-686492 (**I**) and CCDC-686493 (**II**). Copies of the data can be obtained, free of charge, on application to CCDC, 12 Union Road, Cambridge CB2 1 EZ, UK. (fax: +44-(0)1223-336033 or email: deposit@ccdc.ca.ac.uk).

3.3.10 Computational Methods

Quantum chemical calculations on reaction pathways have been performed at the density functional theory (DFT) level employing the three parameter hybrid functional B3LYP/G^[118-121] as implemented in the ORCA program.^[122] Geometry optimizations and harmonic frequency calculations were performed employing the SVP basis set of Ahlrichs and co-workers^[123] for all atoms. In all calculations we used the *TighSCF*,

NoFinalGrid, and *Grid4* options/cutoffs, and the RIJONX approach^[124, 125] was used together with the SV/J auxiliary basis set^[126, 127] for enhanced numerical efficiency via the RI approximation.^[128] Solvation effects have been included in these calculations employing the COSMO continuum model (solvent acetonitrile, dielectric constant at room temperature $\epsilon = 36.6$; the following radii have been used for the construction of the cavity: H: 1.300 Å, C: 2.000 Å, N: 1.830 Å, O: 1.720 Å, Cu: 2.223 Å, solvent: 1.300 Å).^[129, 130] The nature of stationary points localized (minima or transition structures) were identified by Hessian calculations based on numerical evaluation of energies and analytical gradients, which were also used to obtain zero point vibrational energy (ZPVE) and thermal contributions to Gibbs free energies at 298.15 K. We verified the connections between minima and transition structures implied in Figure 3-14 below by intrinsic reaction coordinate (IRC) following calculations. For transition state searches, IRC calculations, and numerical Hessian calculations we used the Gaussian03^[131] external driver facility in combination with a *Gau_External* module that we developed to extract energies and gradients from ORCA calculations, which were then fed into geometry optimization driver routines of the Gaussian03 program.^[132] Improved final energies were obtained by single point calculations employing the B3LYP/G functional in combination with the TZVP basis of Ahlrichs and co-workers and the COSMO continuum solvent model (together with the TZV/J auxiliary basis sets, with all other program parameters and options as described above).

In several instances frequency analyses of stationary points obtained for the full molecular model showed spurious imaginary modes related to rotations of the methyl groups at the *tert*-amine N-donor atoms, which seriously deteriorates the use of computed ZPVE and thermal contributions to obtain Gibbs free energies. In view of the unjustifiably large numerical effort necessary for repeated reoptimizations of geometries and numerical frequency calculations, we decided to perform investigations on reaction pathways based on a simpler molecular model, in which we replaced the methyl groups by hydrogen atoms.

In all species studied here (but **TS8** with its closed shell singlet ground state wave function, cf. Figure 3-14 and Table 3-4), the presence of two coupled Cu^{II} ions with their formal d⁹ electronic configuration gives rise to spin-spin coupling phenomena;

i.e., the two unpaired electrons can couple to yield either singlet or triplet states. While the treatment of the triplet states is straightforward within the spin-unrestricted Kohn-Sham framework, a description of the corresponding singlet states by spin-restricted Kohn-Sham calculations can be highly problematic, depending on the strength of the spin-spin coupling. The broken-symmetry (bs) approach has been identified as an efficient means to include the dynamic as well as static correlation effects underlying these magnetic interactions to a large extent and it has been applied to related bioinorganic problems with considerable success.^[133] Following Noodleman's suggestion^[134-138] we applied spin-unrestricted broken-symmetry calculations for the antiferromagnetically coupled singlet states. The overlap integrals $\langle\alpha|\beta\rangle$ of the magnetic orbitals obtained for the BS wave functions vary significantly (Table 3-4), which indicates strongly varying coupling strengths between the spin centers involved. We therefore applied the formalism of Yamaguchi^[139, 140] to obtain the Heisenberg coupling parameter J relating to the phenomenological Heisenberg Hamiltonian $H = -2J S_A S_B$:

$$J = \frac{(E_{HS} - E_{BS})}{\langle S^2 \rangle_{HS} - \langle S^2 \rangle_{BS}} \quad \text{eq. (1)}$$

This approach covers the range from weak to strong coupling situations. BS wave functions were obtained employing the corresponding orbital transformation procedure implemented in ORCA.^[141] In the present context, a negative value for J corresponds to an 'antiferromagnetically coupled' or 'open-shell' singlet ground state.

For some species involved in the reaction pathways discussed below we find triplet ground states rather than (broken-symmetry) singlet states ($J = +25$ to $+534 \text{ cm}^{-1}$, cf. Table 3-4). In some instances we reoptimized the corresponding triplet structures, but we did not observe any significant energy lowering or structural change (e.g., 1 kcal mol^{-1} in the case of **1** with essentially unaltered structural features). Analysis of spin densities for all species investigated revealed that all magnetic interactions are caused by interactions of spin densities essentially localized on the copper ions with their formal d^9 electronic configurations. These Cu(II) based spin systems are antiferromagnetically coupled in most cases, giving rise to singlet ground states, but triplet ground states result in some instances as a consequence of ferromagnetic

spin coupling. The intricacies of magnetic coupling in related Cu_2O_2 systems are caused by the interplay between electronic and structural properties of the species studied are subject of ongoing research efforts^[142-151] and are - also in view of the general tendency of the B3LYP functional employed to generally overestimate the stability of high-spin over low-spin states for transition metal ions^[152] - outside the scope of our present study. The small energy differences between singlet and triplet species documented in Table 3-4 (below 2 kcal mol^{-1} in all cases) are insignificant in the context of our investigation of reaction pathways. Hence, for the present system we can safely exclude the possibility that copper based spin couplings give rise to a prominent two-state-reactivity scenario^[153-155] in the sense that spin crossover phenomena could provide alternative reaction pathways that significantly alter the relevance of the mechanistic scenario proposed below.^[63, 156]

Additional calculations were performed to support analysis of experimental IR- and resonance-Raman spectra. Here we used the UBP86 functional^[118, 157] based on the optimized (bs-) singlet structure for the full molecular model of the hydroxylated product, which we generated from the X-ray structure of **II**. It is well established that this level of DFT quite generally provides vibrational frequencies in good agreement with experimentally determined spectra.^[36, 158] Calculated frequencies were therefore used without further scaling.

3.4 X-ray Structure Analysis

3.4.1 Cu(I) complex (**Ia**)

The DAPA ligand and the corresponding copper complex were prepared according to the literature.^[115] In contrast to the facile synthesis of **I** and related bis(imine) complexes crystallographic characterization of these compounds is rare. Most recently a copper(I) complex with a ligand quite similar to DAPA (ethylene instead of propylene bridges) was structurally characterized, however, in this case a dinuclear complex with a Cu(I) to ligand ratio of 2 : 2 was obtained.^[159] After optimizing conditions in our crystallization experiments we succeeded in obtaining crystals of $[\text{Cu}(\text{I})_2(\text{DAPA})(\text{CH}_3\text{CN})_3](\text{ClO}_4)_2$ (**Ia**). The molecular structure of the cation of this complex is shown in Figure 3-2, bond distances and angles are given in Table 3-2.

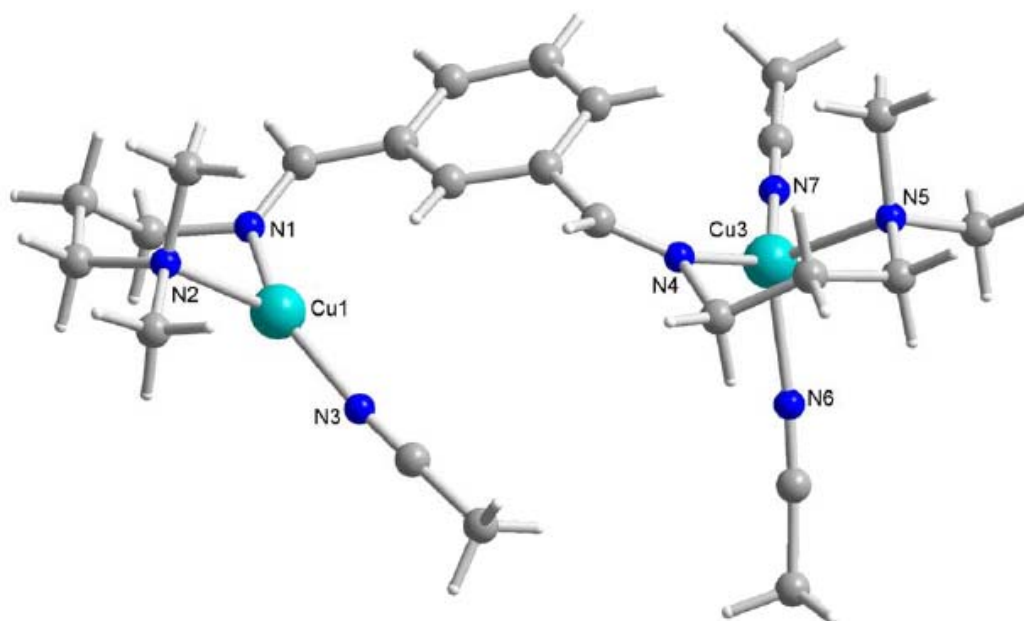


Figure 3-2: Molecular structure of the cation of **1**

Compound **1a** crystallizes in the monoclinic space group $P2_1$ with two complex cations and four complex anions per unit cell. The two copper(I)-centers are bridged by a *m*-xylyl-group with a Cu1...Cu3 separation of 7.1(1) Å. Each copper-ion is coordinated by one imine nitrogen (N1/N4) and one aliphatic amine nitrogen (N2/N5) per bidentate DAPA arm. As additional co-ligands one or two acetonitrile molecules are ligated to the copper ions. One N-bonded MeCN molecule completes the almost trigonal planar coordination geometry of Cu1. With two bound acetonitrile molecules the coordination geometry around Cu3 is best described as distorted tetrahedral. The formation of six membered chelate rings leads to values for the N1-Cu1-N2 and N4-Cu3-N5 angles of 96.7(3)° and 95.2(3)°, substantially deviating from ideal trigonal or tetrahedral geometry. The dihedral angle between the N1-Cu1-N2 and N4-Cu3-N5 planes is 53.09°. As expected, the Cu-N bond lengths of the tricoordinate Cu1 center are shorter than that of Cu3 (Table 3-2). The “harder” amine nitrogens N2 and N5 are bound more weakly to the copper(I) ion than the imine nitrogens N1 and N4.

Feringa and co-workers have reported the synthesis and characterization of a structurally related binuclear Cu(I)-complex, in which each copper center is coordinated to one bidentate ligand arm and one acetonitrile molecule.^[53] Comparison of this crystal structure with **1a** reveals quite similar Cu-N bond lengths, all in the range typical for tricoordinated Cu(I)-complexes,^[53, 160] while both complexes differ the in bond angles about the copper ions because of their different donor atom

environment (aliphatic amines vs. pyridine nitrogen donor atoms). A larger chelate ring size and a different Cu to ligand ratio are also responsible for significant differences in bond lengths and angles between **Ia** and a binuclear Cu(I) Schiff base complex characterized recently by Mukherjee and co-workers.^[159] Further, comparison of **I** with a related dinuclear macrocyclic Schiff base copper(I) complex previously described by Utz et al. as well as by Rieger and co-workers also shows differences in bond lengths and angles around the tetracoordinated Cu₃-center of **I**.^[47, 48] Most likely this is a consequence of the macrocyclic ligand that enforces a bowl shape of the complex and compared to **I** it has a much smaller Cu...Cu separation of 4.250(3) Å. Dinuclear copper(I) complexes of the non-macrocyclic ligand derivative have been described recently, however, for these no hydroxylation reactions were observed.^[161]

3.4.2 Cu(II) complex (II)

Oxygenation of the Cu(I) precursor **Ib** in dichloromethane leads to the Cu(II) complex Cu(II)₂-DAPA-OH **II**. Single crystals suitable for X-ray analysis were obtained by diffusion of diethyl ether into a solution of **II** in dichloromethane. The structure of the complex is shown in Figure 3-3, bond distances and angles are given in Table 3-3. Compound **II** crystallizes in the triclinic space group P-1 with Z = 2 and all atoms in general positions. Each of the two crystallographically independent copper atoms are coordinated by two nitrogen atoms and one oxygen atom of the ligand as well as one hydroxyl oxygen atom within a strongly distorted square planar geometry (Figure 3-3). There are two additional contacts to oxygen atoms of perchlorate anions of 2.4497(4) Å (Cu1-O11) and 2.6724(3) Å (Cu2-O13). If these contacts are taken into account the coordination around the copper atoms can be described as strongly distorted octahedral. In the case of **II** the copper atoms are connected via the perchlorate anions forming chains, which extend in the direction of the crystallographic a-axis.

Evidently the phenyl ring of the bis(imine) ligand has been hydroxylated upon the reaction of **Ib** with O₂, forming a phenoxo group that bridges the two Cu(II) centers; a second bridge is provided by hydroxide. The μ-hydroxo μ-phenoxo Cu₂ unit is coordinated by the two terminal amine and the two imine nitrogen atoms of the bis(imine) ligand, forming an almost perfectly planar dinuclear complex molecule with

a quadratic-planar coordination of each Cu(II) center. The Cu...Cu distance is 3.0(5) Å and the average Cu...N distance is 1.9(4) Å for the imine-nitrogens (N1 and N3) and 2.0(3) Å for the amine-nitrogens (N2 and N4) respectively.

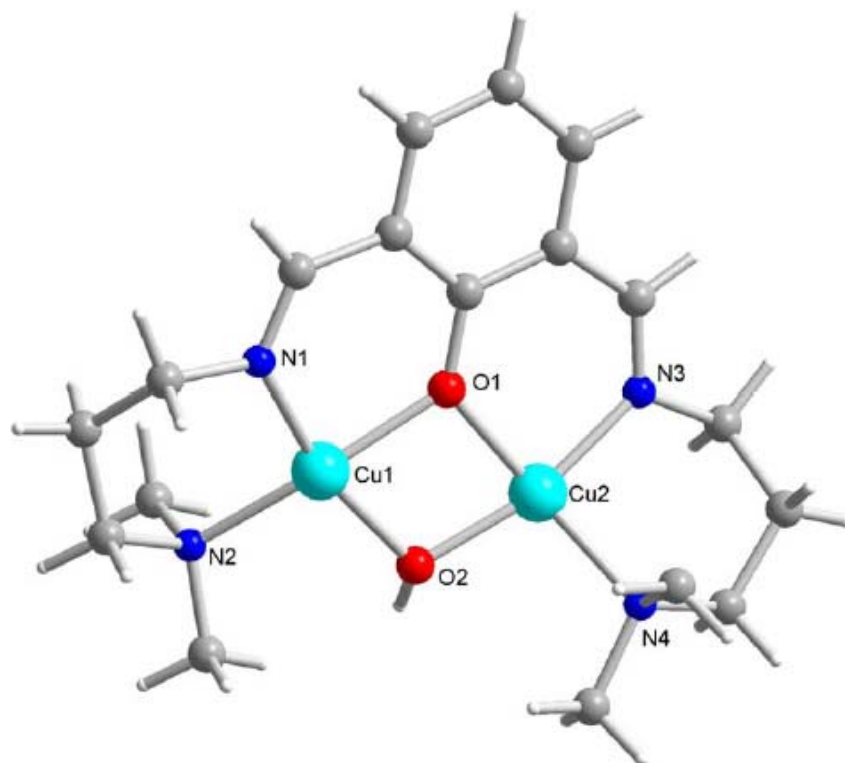


Figure 3-3: Molecular structure of the cation of II

Similar to the Cu(I) complex the N1-Cu1-N2 and N3-Cu2-N4 angles are 95.1(3)° and 97.8°, respectively which is caused in the six membered chelate ring formation. As expected, the molecular structure of II is very similar to the molecular structure of this complex published by Drew et al.^[56] The Cu...Cu distance in II is slightly longer (3.055 instead of 3.015 Å) which most likely is a consequence of the water molecule that is additionally coordinated to CuB in Drew's complex. Moreover, two perchlorate anions are coordinated at ~ 2.5 Å (*vide supra*).

Table 3-1: Crystal data and Structure Refinement for I and II.

Parameters	I	II
Empirical formula	C ₂₄ H ₃₉ N ₇ Cu ₂ P ₂ F ₁₂	C ₁₉ H ₃₂ N ₄ Cu ₂ Cl ₄ O ₁₀
Formula weight	842.64	745.37
Temperature (K)	173(2)	170(2) K
Crystal system	monoclinic	triclinic
Space group	P2(1) no.4	P-1
Wavelength (Å)	0.71073	0.71073
Unit cell dimensions	11.491(2) Å	a = 7.8818(9) Å α = 62.059(12)°
	25.391(5) Å β = 105.59(3)°	b = 13.9548(14) Å β = 84.902(14)°
	12.564(3) Å	c = 14.6487(18) Å γ = 81.658(13)°
Z	4	2
Density calcd. (Mg/m ³)	1.585	1.758
Absorpt. coeff. (cm ⁻¹)	1.386	1.948
F(000)	1712	760
Crystal size (mm)	0.25 x 0.1 x 0.12	0.2 x 0.2 x 0.1
θ range for data collected (°)	2.13 to 26.04	2.61 to 25.03
Index ranges	-14 ≤ h ≤ 13, -31 ≤ k ≤ 31, -14 ≤ l ≤ 15	-9 ≤ h ≤ 9, -16 ≤ k ≤ 16, -17 ≤ l ≤ 17
Reflection collected	24832	12085
Independent refl., Rint	13443, 0.1061	4681, 0.1250
Completeness to theta	97.7 % (theta = 26.04°)	93.9 % (theta = 25.03°)
Goodness-of-fit on F ²	0.780	0.998
R1 [I > 2σ(I)]	0.0532	0.0519
wR2 [I > 2σ(I)]	0.0845	0.1172
R1 [all data]	0.0805	0.1389
wR2 [all data]	0.1065	0.1319

Table 3-2: Selected Bond Distances and Angles for I (Å, °)

Cu(1)-N(3)	1.85(1)
Cu(1)-N(1)	1.960(9)
Cu(1)-N(2)	2.055(8)
Cu(3)-N(7)	1.96(1)
Cu(3)-N(6)	2.02(1)

Cu(3)-N(4)	2.019(9)
Cu(3)-N(5)	2.11(1)
N(3)-Cu(1)-N(1)	138.9(3)

Table 3-3: Selected Bond Distances and Angles for II (Å, °)

Cu(1) – O(2)	1.899(3)	Cu(2) – O(2)	1.899(4)
Cu(1) – O(1)	1.986(4)	Cu(2) – O(1)	1.991(3)
Cu(1) – Cu(2)	3.0546(11)	O(1) – C(1)	1.324(6)
Cu(1) – N(1)	1.938(4)	Cu(1) – N(2)	2.025(5)
Cu(2) – N(3)	1.948(5)	Cu(2) – N(4)	2.031(4)
N(1) – Cu(1) – N(2)	95.13	N(3) – Cu(2) – N(4)	97.8
Cu(1) – O(1) – Cu(2)	100.39	Cu(2) – O(2) – Cu(1)	107.07

3.5 Spectroscopic Investigations

3.5.1 UV-Vis spectroscopy

The UV/Vis spectrum of **II** in acetonitrile is shown in Figure 3-4. It exhibits two intense bands in the region between 200 – 300 nm and one band at 357 nm ($\epsilon = 10000 \text{ M}^{-1} \text{ cm}^{-1}$). The latter feature is absent in the spectrum of the Cu(I) precursor **I** which only shows a rising slope below 300 nm, exhibiting a couple of weak shoulders. The 357 nm band is therefore the most conspicuous UV/Vis-spectroscopic signature of the oxygenated complex. It has been assigned to a charge transfer transition from the Cu(II) centers to the hydroxylated bis(imine) ligand.^[162] At higher concentration a weak absorption band can also be detected at 663 nm which is assigned to a ligand-field transition of the square-planar Cu(II) centers.

The oxygenation of **I** to **II** proceeds only slowly in acetonitrile (see below); therefore we employed methanol as solvent as well. Figure 3-5 shows the spectra of **I** and **II** in methanol; the spectrum of **II** was obtained after bubbling O₂ through a solution of **I**. As in the spectrum of **II** in acetonitrile, an intense band is observed at 360 nm and a ligand-field band at 700 nm.

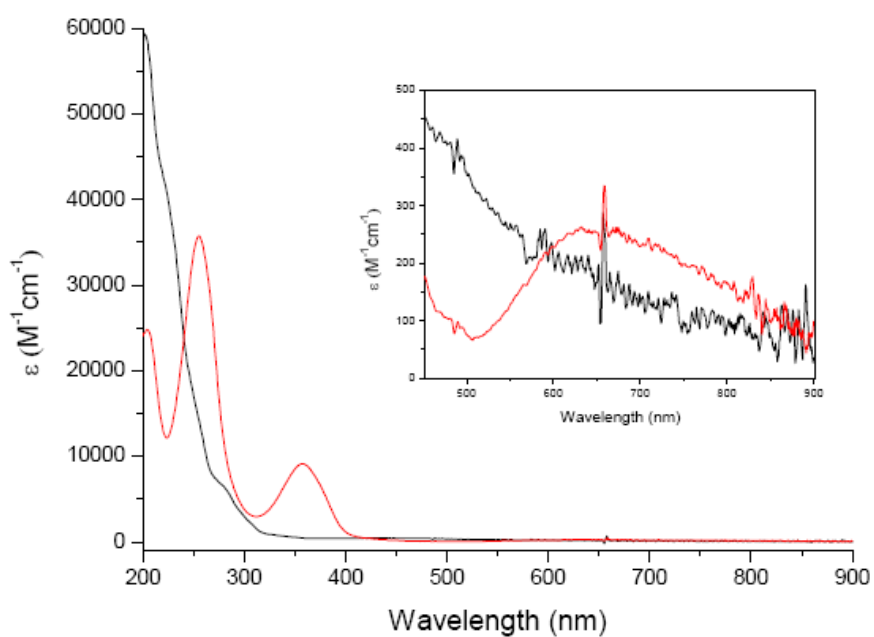


Figure 3-4: UV-Vis spectra of Ib (black line, $8 \times 10^{-5} mol/l$) in acetonitrile

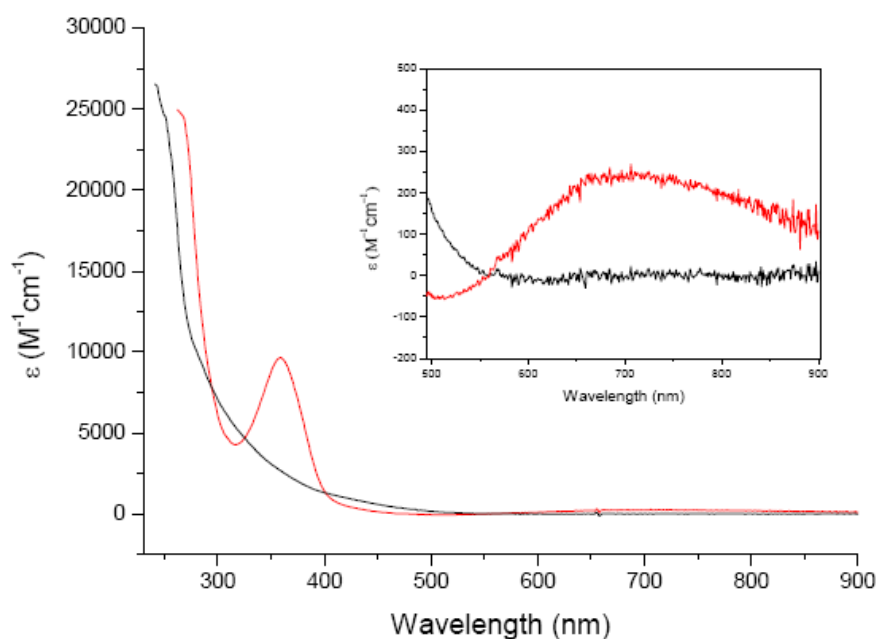


Figure 3-5: UV-vis showing the oxygenation of Ib to II (red) by bubbling O_2 through the solution of Ib (black line, $2,9 \times 10^{-4} mol/l$) in methanol

3.5.2 Vibrational spectroscopy

Infrared and Raman spectra of **I** and **II** were obtained from solid samples at room temperature and are presented in Figures 3-6 to 3-9. We also studied the ^{18}O -isotopomer of **II**, which was prepared by reaction of **I** with $^{18}\text{O}_2$. Spectral assignments were facilitated by comparison with computed harmonic frequencies at the bs-BP86/SVP level, which show an overall pleasing agreement with the experimental results (Figure 3-7). In contrast to our initial expectation $^{16}\text{O}/^{18}\text{O}$ isotopic substitution in **II** does not lead to the identification of a unique vibrational signature for a C-O stretching vibration. Detailed analysis of the computed spectra reveals instead that there are several normal modes with varying C-O stretch contributions. We here report only assignments of the most prominent vibrational features as a result of a careful correlation between measured and computed spectra. Figure 3-10 shows dominant atomic contributions to normal modes for the vibrations discussed below.

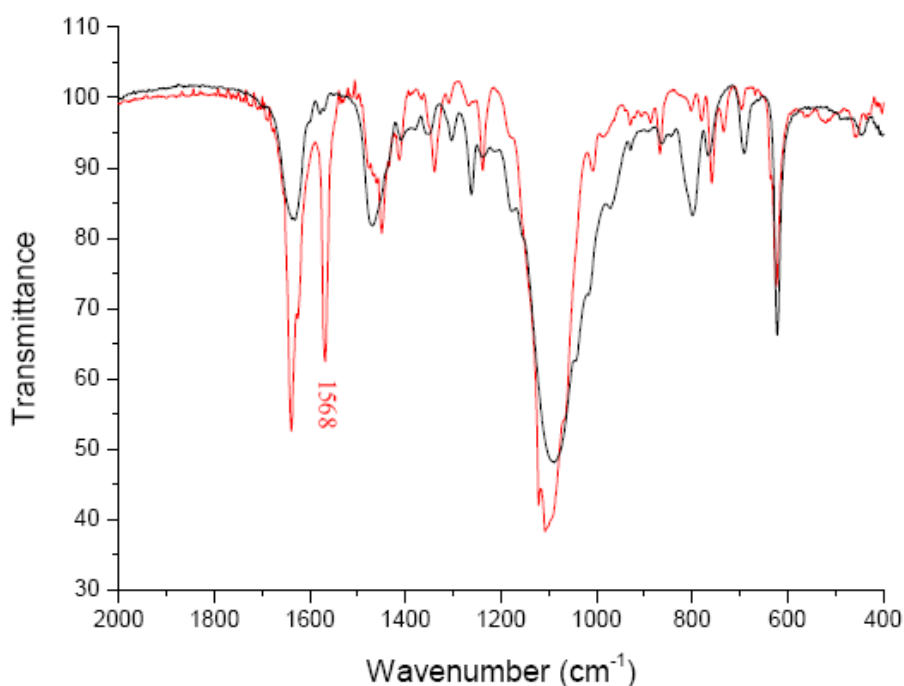


Figure 3-6: IR-spectra of Ib (black) and II (red)

The IR (Figures 3-6 and 3-7) and Raman (Figures 3-8 and 3-9) spectra of **I** and **II** show an intense signal at 1630 cm^{-1} which correlates with a normal mode in the computed spectra dominated by the symmetric stretching motion of the Schiff base C=N bonds (1622 cm^{-1} , cf. Figure 3-10); this band exhibits a second feature due the corresponding antisymmetric vibration (computed at 1615 cm^{-1} , not shown in Figure

3-10) with much lower intensity. Upon oxygenation of **I** an intense band appears in the spectrum of **II** at 1568 cm^{-1} (Figure 3-6). This band corresponds to a vibration at 1551 cm^{-1} in the computed spectrum (fg.3-10) and can be assigned to an asymmetric deformation mode in the aromatic ring in **II**. As consistently revealed by both, experimental and computed spectra, neither band shows any C-O participation. Buried among a series of bands between 1443 cm^{-1} and 1394 cm^{-1} which are caused by C-H stretching and bending vibrations of all parts of the ligand, the computed spectra exhibit an intense peak at 1424 cm^{-1} (shifted to 1420 cm^{-1} upon ^{18}O substitution) that contains some C-O stretching component. In the experimental spectra this signal occurs upon oxygenation of **I** at 1450 cm^{-1} (Figure 3-6) but does not show any significant isotopic shift in the spectrum of ^{18}O -**II**. One band at 1357 cm^{-1} in the spectrum of **I** moves to 1339 cm^{-1} in the spectrum of **II**. Comparison of the IR spectra of ^{16}O -**II** and ^{18}O -**II** (Figure 3-7) reveals a significant ^{18}O shift of this mode from 1339 cm^{-1} in ^{16}O -**II** to 1329 cm^{-1} in the spectrum of ^{18}O -**II**.

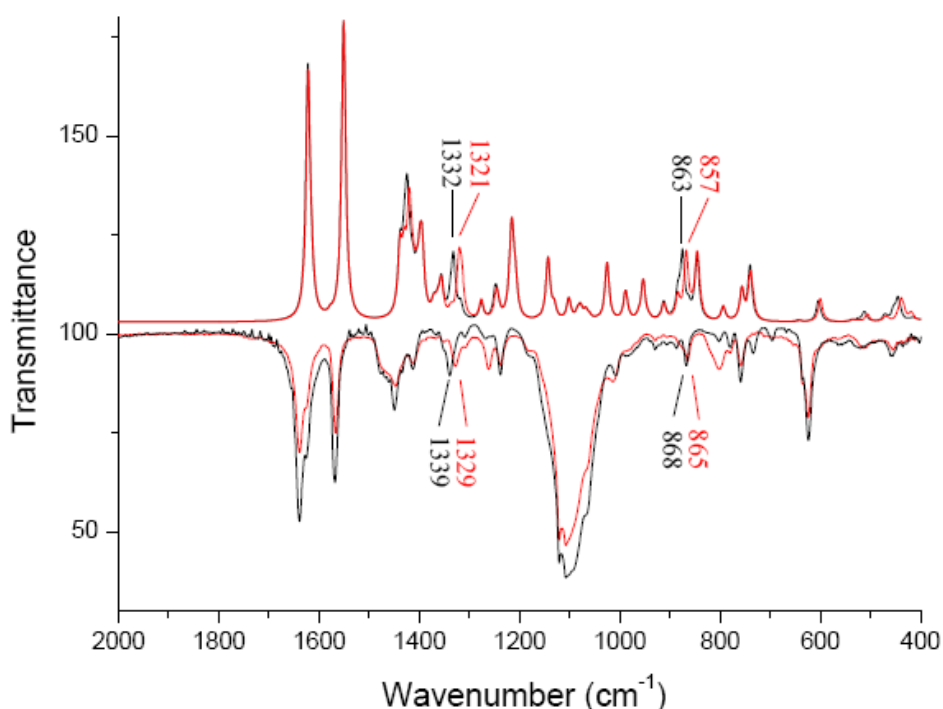


Figure 3-7: Experimental (bottom) and calculated (top) IR-spectra of **II (black) and $^{18}\text{O}_2$ -**II** (red) with isotope-sensitive bands**

Almost the same isotopic shift (11 cm^{-1}) is found in the computed spectra ($1332\text{ cm}^{-1} \rightarrow 1321\text{ cm}^{-1}$), in line with a significant C-O contribution to this normal mode (cf

Figure 3-10). At lower energy, there is a band at 866 cm^{-1} which upon isotopic substitution shifts to 861 cm^{-1} . This is reproduced by a computed vibration at 863 cm^{-1} , shifting to 857 cm^{-1} , which involves significant O-motion (cf Figure 3-10).

The FT-Raman spectra of **I** and **II** obtained with $\lambda_{\text{exc}}=1064\text{ nm}$ are shown in Figure 3-8. A comparison of the FT-Raman spectra of ^{16}O -**II** and ^{18}O -**II** (Figure 3-9) reveals only small isotopic shifts. After oxygenation of **I** two prominent new peaks appear at 1450 and 1257 cm^{-1} but only the latter has some minor C-O contribution: In the region around 1250 - 1280 cm^{-1} , where normally the (phenolate) C-O stretching vibration is found,^[109, 163] only the intense peak at 1257 shifts to 1254 cm^{-1} upon ^{18}O -substitution, and DFT reveals indeed some minor contribution from the C-O stretch to this vibration ($1249\text{ cm}^{-1} \rightarrow 1247\text{ cm}^{-1}$; not shown in Figure 3-9). Three less intense peaks with small isotope shifts are observed at 1313 cm^{-1} (shifting to 1308 cm^{-1}), 1330 cm^{-1} (shifting to 1327 cm^{-1}) and 1371 cm^{-1} (shifting to 1366 cm^{-1}). The lowest-energy one may correspond to the vibration calculated at 1317 cm^{-1} , shifting to 1315 cm^{-1} (cf Figure 3-10).

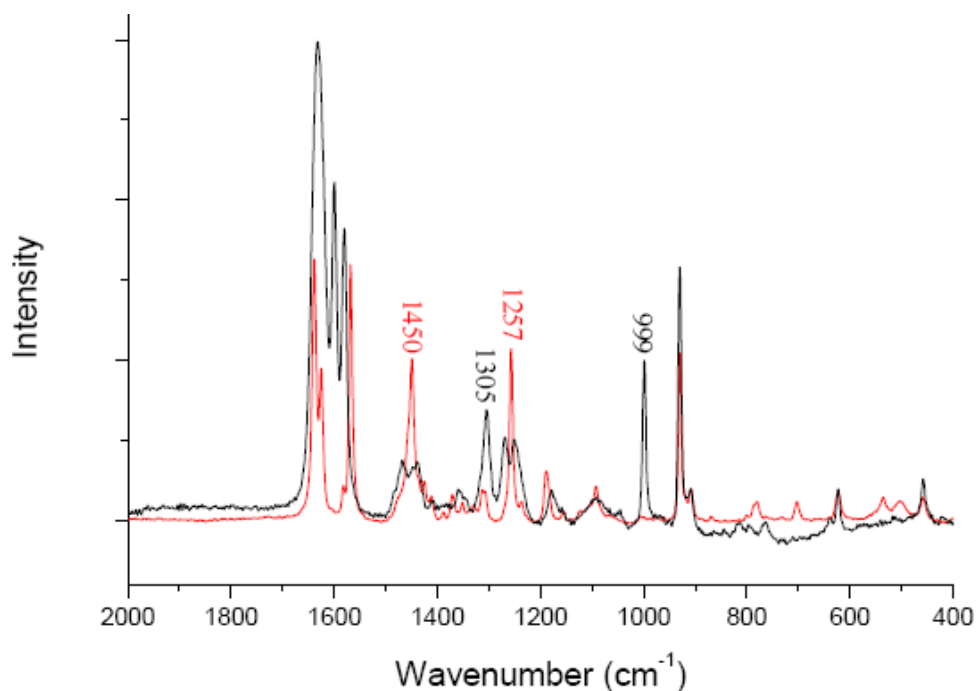


Figure 3-8: FT-Raman-spectra of Ib (black) and II (red)

To conclude, there is only one vibration with a strong isotope shift (-10 cm^{-1}) which is located at 1339 cm^{-1} (exp.; 1332 cm^{-1} calc.) and has mostly IR intensity. It has the most prominent C-O contribution of the spectral range investigated. Some other

vibrations show minor isotope shifts of the order of -3 to -5 cm^{-1} , depending upon the admixture of the C-O stretching motion.

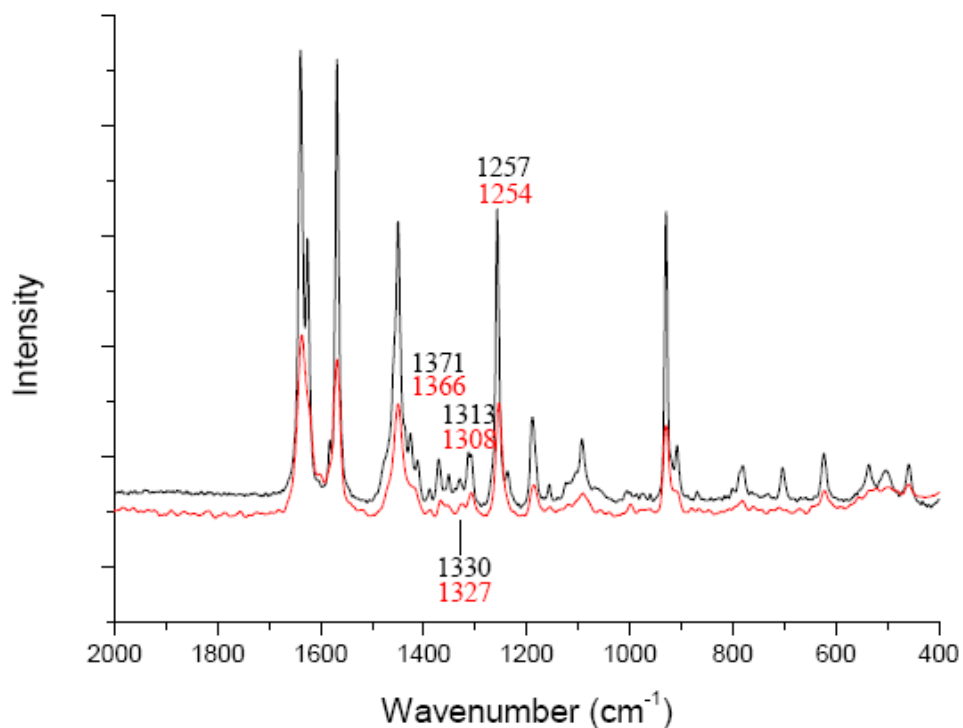


Figure 3-9: FT-Raman-spectra of II (black) and ^{18}O -II (red)

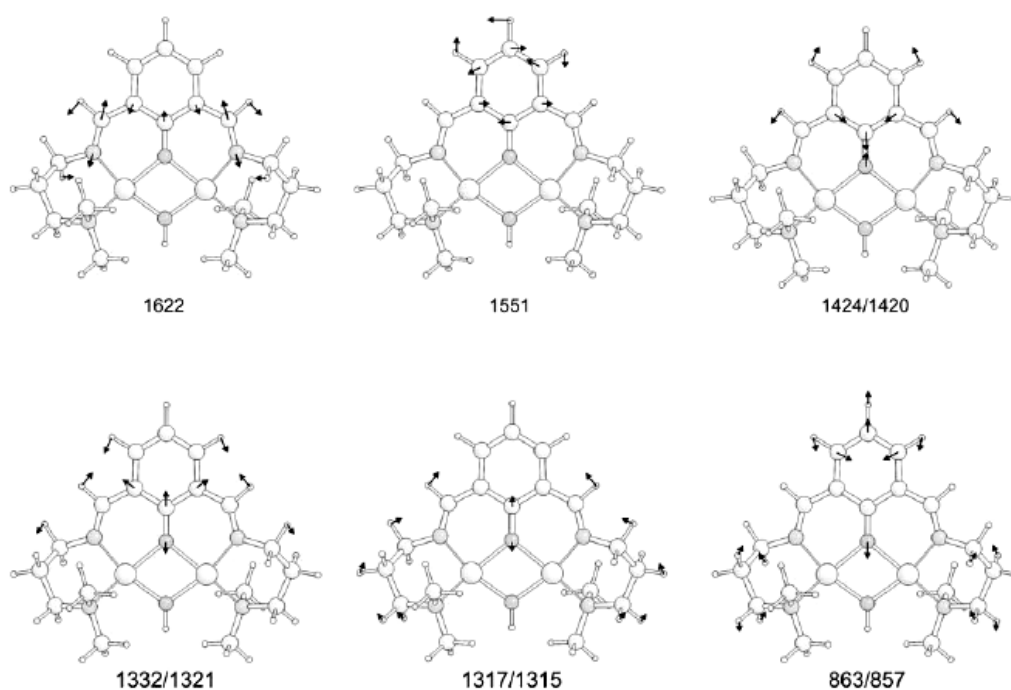
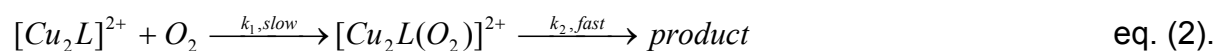


Figure 3-10: Eigenvectors of the most important vibrations of structure 3 (corresponding to complex II)

3.6 Kinetic Investigations

Yellow solutions of **Ia** in methanol turn immediately green when exposed to dioxygen, forming **II**. Time-resolved spectra could be obtained using low temperature stopped-flow techniques; a typical example of the oxidation reaction in methanol is shown in Figure 3-11. The spectra resemble those obtained previously by some of us in kinetic studies of the related imine systems $[\text{Cu}_2(\text{HBPB-H})(\text{CH}_3\text{CN})_2](\text{BF}_4)_2$ and $[\text{Cu}_2\text{mac}(\text{CH}_3\text{CN})_2](\text{ClO}_4)_2$ (HBPB = 1,3-bis[N-(2-pyridylethyl)formimidoyl]benzene; mac = 3,6,9,17,20,23-Hexaaza-tricyclo [23.3.1.1]triaconta-1(29),2,9,11(30),12(13),14,16,23, 25,27-decaene).^[48] Again, similar to these systems, we could not detect the build-up of a dioxygen adduct. This is in contrast to the complex $[\text{Cu}_2(\text{XYL})]$ reported by Karlin and co-workers where spectroscopic detection of such an intermediate was possible at low temperatures.^[29, 30, 109] The lack of a detectable O_2 -intermediate most likely is the consequence of a rate-determining formation of the reactive intermediate and much faster consecutive reactions according to the following general equation:



Immediately after the dioxygen adduct is formed it further reacts to the product(s) and therefore cannot be observed spectroscopically. As a consequence, no kinetic data for the reaction of the peroxo complex to the hydroxylated product complex could be obtained.

The absorbance vs time traces could be fitted using one exponential or the sum of two or three exponential functions at different temperatures (cf Figure 3-11). Acceptable fitting over a larger temperature range was, however, not possible. Moreover, we observed a linear dependence on the dioxygen concentration for two rate constants with an intercept. This result was not surprising insofar as similar difficulties had been encountered for the complexes $[\text{Cu}_2(\text{HBPB-H})(\text{CH}_3\text{CN})_2](\text{BF}_4)_2$ (here a more detailed discussion on the different possible reaction pathways has been described) and $[\text{Cu}_2\text{mac}(\text{CH}_3\text{CN})_2](\text{ClO}_4)_2$ (*vide supra*). From the present findings we can at least state that one part of the rate law should contain the term $k_{\text{obs}} [\text{O}_2]$, confirming the occurrence of a dioxygen adduct as an intermediate. The reaction proved to be faster than observed for $[\text{Cu}_2(\text{HBPB-H})(\text{CH}_3\text{CN})_2](\text{BF}_4)_2$ and for

$[\text{Cu}_2\text{mac}(\text{CH}_3\text{CN})_2](\text{ClO}_4)_2$ and therefore required low temperature stopped-flow techniques. This is understandable as the ligands HBPB-H and mac stabilize the copper(I) complexes more than DAPA.

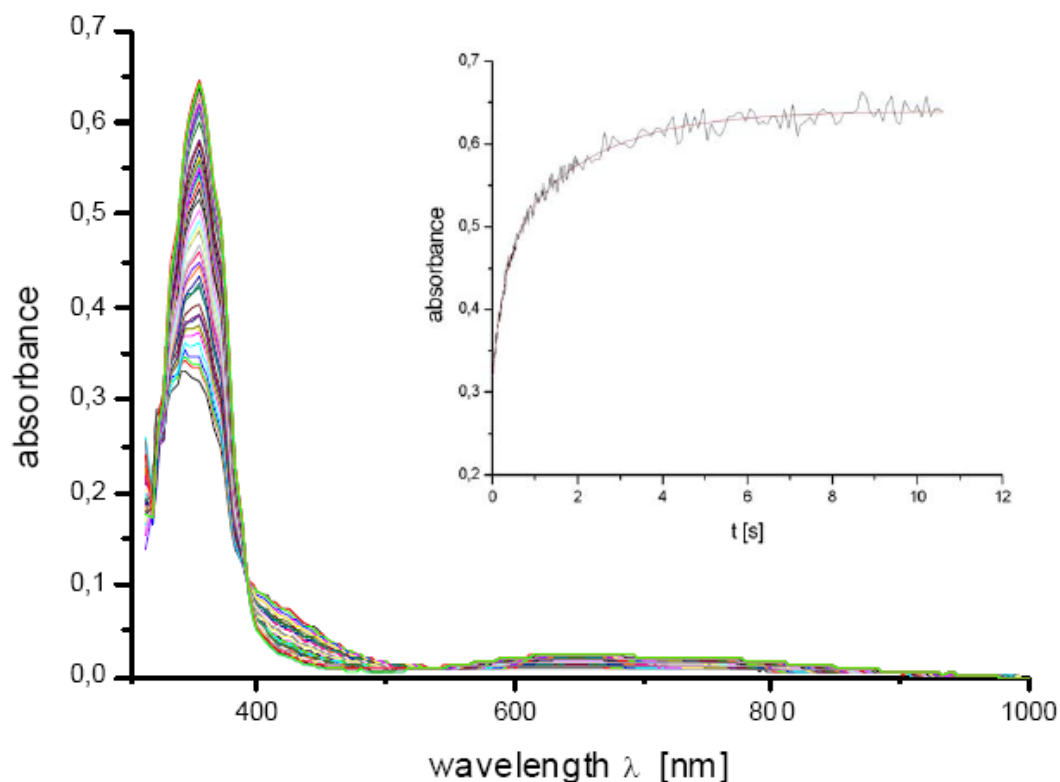


Figure 3-11: Spectral changes during reaction of I with dioxygen in methanol ($T = -60.1$ °C, $[\text{complex}] = 0.1$ mmol/l, $[\text{O}_2] = 4.25$ mmol/l, $t = 10.605$ s)

Insert: Absorbance vs. time trace at 353 nm and fit to the sum of two exponentials ($k_{\text{obs}1} = 3.1 \pm 0.2 \text{ s}^{-1}$; $k_{\text{obs}2} = 0.41 \pm 0.03 \text{ s}^{-1}$)

The hydroxylation of **Ib** leading to **II** was also investigated in acetonitrile. In this case, however, a much slower reaction was observed. This can be attributed to the fact that acetonitrile binds fairly strongly to the Cu(I) centers of **Ib** and has to be replaced by O_2 in the course of the hydroxylation reaction. Loss of acetonitrile ligands bound to **I** is, of course, impeded if the reaction is performed in this solvent. If, in contrast, the reaction is performed in methanol, the acetonitrile ligands of **Ia** obviously are exchanged in a first reaction step; i.e., prior to binding of O_2 . This follows from the observation that in this solvent no isotope effect on the binding of O_2 is observed (see below).

In the course of the present study, DFT calculations indicated several thermally accessible pathways from a $\mu\text{-}\eta^2\text{:}\eta^2$ peroxo adduct to the hydroxylated final product (*cf* next Section) involving proton transfer steps that should show prominent primary kinetic isotopic effects upon ligand deuteration. In order to experimentally check these predictions, further kinetic investigations based on the deuterated DAPA-complex **I^D** were performed. The substitution of **Ib** by **I^D** was expected to *decrease* the reaction rate in the presence of rate-determining H-atom or proton transfer steps or leave it unchanged in the absence of such reactions.^[164] Importantly, the rate of the oxygenation reaction of **Ia** in methanol was unchanged, indicating the absence of a significant KIE (Figure 3-12). In acetonitrile, on the other hand, the reaction of **I^D** containing the deuterated ligand was found to be approximately 2.6 times *faster* (KIE = 0.38) than of **Ib** containing the non-deuterated ligand (Figure 3-13).

The lack of a primary KIE in MeOH and the observation of an *inverse* deuterium effect in CH₃CN are *not* compatible with the presence of a rate-determining proton transfer step in the reaction phase after formation of the π -complex. The inverse deuterium effect in CH₃CN is rather attributed to the reaction phase *before* formation of the σ -complex; i.e., the binding of O₂: Due to the geometry of the complex the O-O-axis in the peroxo-adduct points to the C-H bond of the aromatic ring; O₂ binding thus is hindered by the C-H stretching motion of the H-atom at the C₂ atom of the phenylene spacer, and due to the smaller D-C vibration amplitude O₂ binding proceeds faster in the deuterated than in the non-deuterated complex. Since O₂ binding is also the rate-limiting process in methanol, the inverse deuterium effect should in principle appear in this solvent as well. However, this is not observed, which can be attributed to the fact that this solvent is weaker coordinating than acetonitrile, thus diminishing the steric congestion in the transition state leading to the dioxygen adduct and, correspondingly, the influence of the C-H stretching motion on the formation of this adduct.

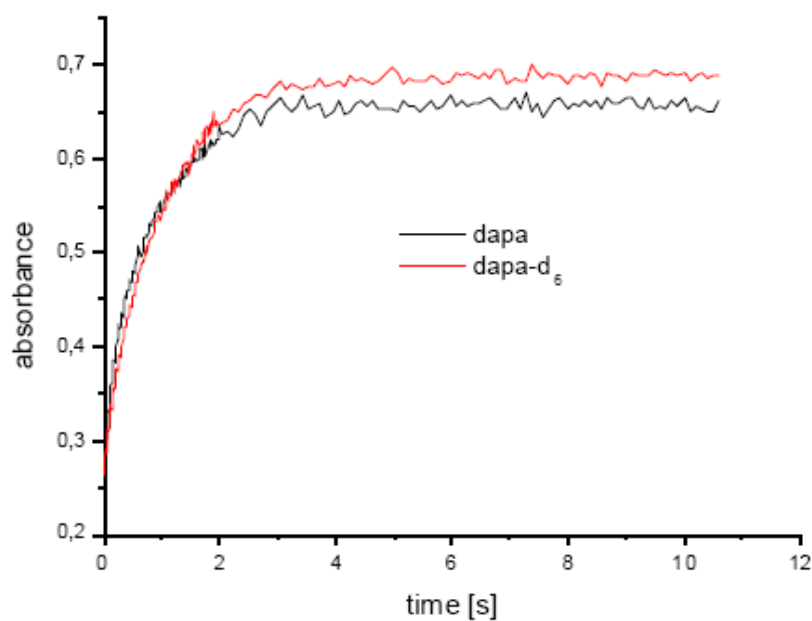


Figure 3-12: Absorbance during oxygenation of Ia at 353 nm in Methanol.
[T= -60,1°C; [dapa]=0,1 mM; [dapa-d₆]= 0,1 mM; [O₂]= 4,25mM; t= 10,6 s]

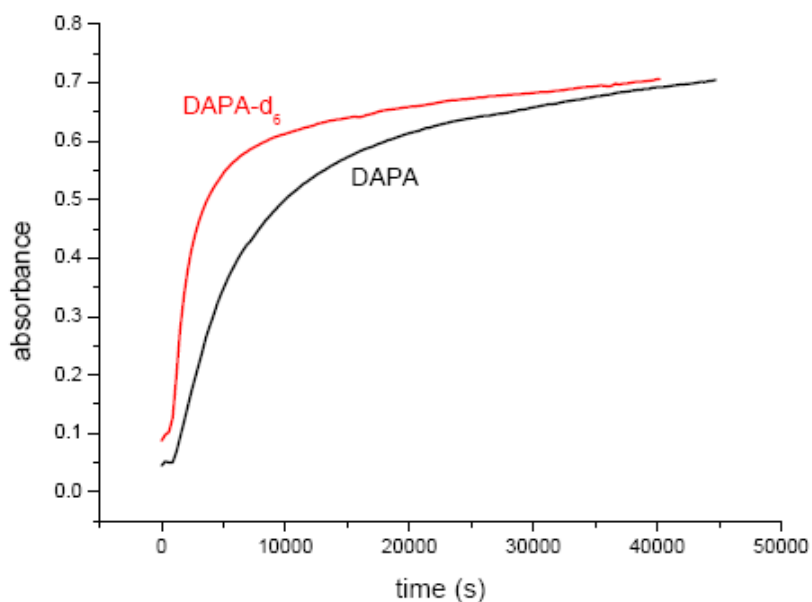


Figure 3-13: Absorbance at 358 nm for the DAPA- (Ib, black) and DAPA-d₆-complex (1^D, red) during oxygenation in acetonitrile.

3.7 Quantum Chemical Investigations on Reaction Pathways

As discussed in the Computational Details section above, we assume throughout this study that all elementary steps involved in the reaction pathways investigated take place on a ground state singlet potential energy surface. In other words, we inherently suppose that the spin flip evidently occurring upon binding of O₂ with its triplet ground state to the bare copper(I) complex occurs as part of the initial steps leading to formation of peroxo complex **1**. These steps, which include solvent exchange at the Cu(I) sites and potentially prominent spin flip phenomena, are not studied here.^[165-170] Instead we decidedly concentrate on the fate of the initially formed peroxo Cu₂O₂ species **1** and the elementary steps that are involved in reaction pathways leading to the product of the aromatic hydroxylation (**3**) which corresponds to complex **II**. All relevant intermediates and transition structures are compiled in Figure 3-14; corresponding energies are collected in Table 3-4.

Several minima resulted from geometry optimizations performed for the starting point of our quantum chemical investigation, the side-on $\mu\text{-}\eta^2\text{:}\eta^2\text{-peroxo}$ intermediate **1**; for the sake of brevity we only consider the most stable isomers directly involved in the reaction pathways discussed below. **1** exhibits a significant butterfly distortion of the Cu₂O₂ moiety indicative of substantial strain introduced by the ligand framework, which obviously does not allow for the formation of the planar arrangement of this subunit identified experimentally in unstrained systems.^[4, 171] Interestingly, we were unable to localize a bis($\mu\text{-oxo}$) isomer for the present ligand environment, although such a species should generally be more stable than the peroxo intermediate for bidentate N-donor ligand environments of Cu₂O₂ cores such as present here.^[3, 32, 172-178] Even carefully preoptimized bis($\mu\text{-oxo}$) structures obtained by constrained geometry optimizations, in which the ideal core substructure was kept fixed while the rest of the structure was optimized, fell back into a peroxo structure in subsequent unconstrained optimization runs. We take this finding as another consequence of the significant strain introduced by the ligand framework, which is not flexible enough to allow for the formation of a tighter bis($\mu\text{-oxo}$) core with its closer Cu-Cu contact (2.74–2.79 Å) compared to the larger Cu-Cu distance found in the peroxo cores (3.37–3.56 Å).^[4, 171]

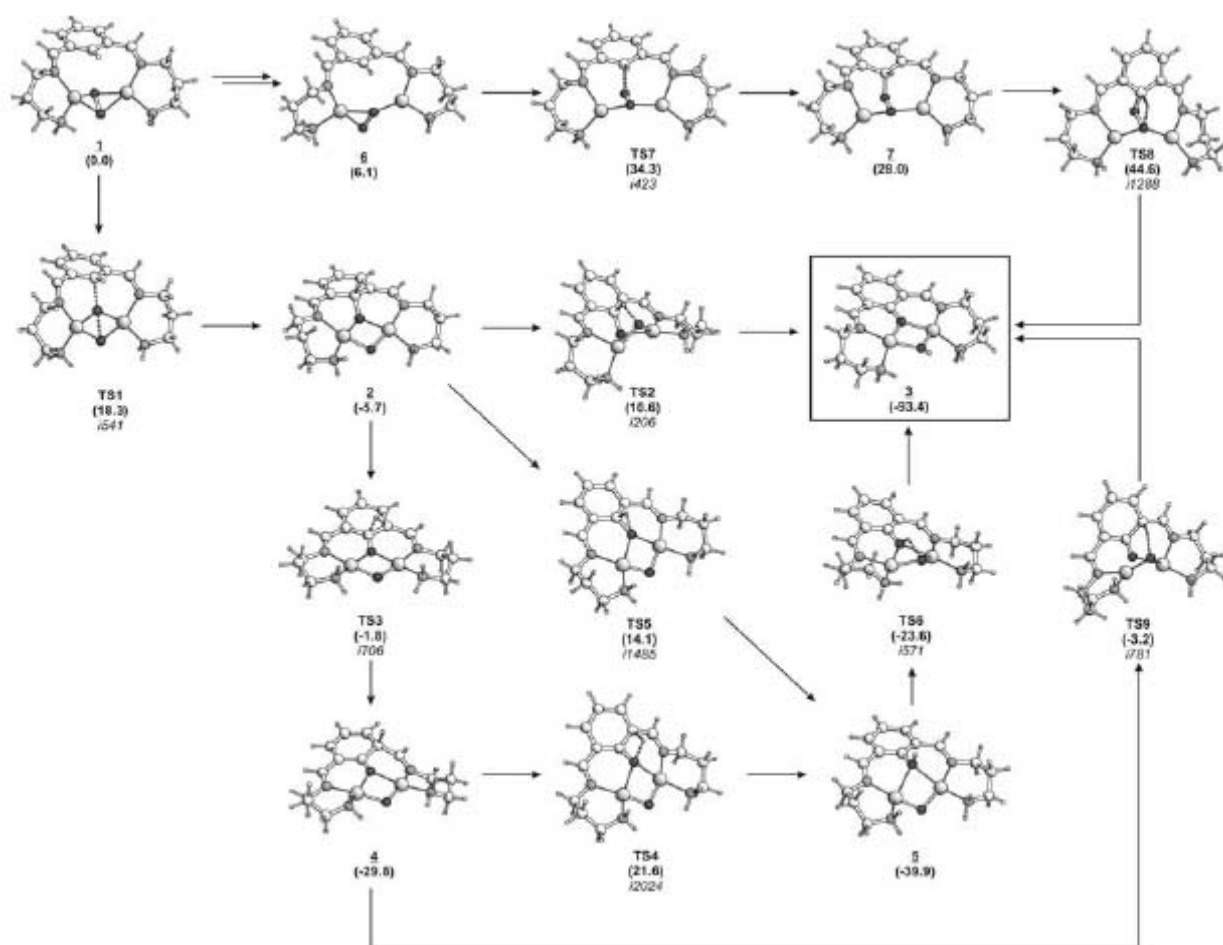


Figure 3-14: Reaction pathways identified for the hydroxylation reaction starting from the μ - η^2 : η^2 peroxy complex I (Gibbs free energies at 298 K in kcal mol⁻¹ relative to I; UB3LYP/TZVP+COSMO//UB3LYP/SVP+COSMO results).

Starting from **1** we localized a transition structure (**TS1**) for the O-O bond cleavage, that resembles to a large extent the corresponding transition structure for the peroxy/bis(μ -oxo) core isomerisation identified in our previous study on the aliphatic hydroxylation reactivity of a Cu₂O₂ complex bearing unstrained bidentate N-donor ligands.^[179] In the present system, however, **TS1** represents a multicenter transition state for the simultaneous O-O bond cleavage and C-O bond formation. IRC calculations confirm the direct connection of this transition state with the peroxy minimum **1** and the arenium-like σ -complex **2**, without occurrence of an intermediate bis(μ -oxo) species. This electrophilic attack of the aromatic ring is connected with a

barrier of $18.3 \text{ kcal mol}^{-1}$, and formation of the σ -intermediate **2** is exoergic by $5.7 \text{ kcal mol}^{-1}$.

We identified three pathways for the decay of the σ -complex **2**. A somewhat unexpected but conceptually strikingly simple path is the direct, highly exoergic formation of the final product of the overall reaction; i.e., formation of the μ -hydroxo- μ -phenolato complex **3** ($\Delta G_R = -93.4 \text{ kcal mol}^{-1}$ with respect to **1**) is possible in a single step after passage of **TS2**. In this transition structure the proton at the tetrahedral phenyl-carbon of the σ -complex **2** is abstracted by the μ -oxo atom bridging the two copper ions. The unusually low imaginary frequency of $i206 \text{ cm}^{-1}$ for this proton transfer step is a consequence of the participation of several atoms in the transition normal mode resulting from the excessive deformation about the Cu_2O_2 moiety necessary to bend the μ -oxo atom over into a bonding range with the proton transferred. Somewhat counterintuitively, however, a rather modest barrier of $16.5 \text{ kcal mol}^{-1}$ results for this step, in spite of the highly strained nature of this transition state. Quite obviously this elementary step profits from significant stabilizing Coulomb interactions between the proton transferred and the high negative charge of the μ -oxo atom (formally an O^{2-}). Also, using qualitative Hammond arguments, the large exothermicity of this step ($\Delta G_R = -87.7 \text{ kcal mol}^{-1}$ with respect to **2**) might be seen as another factor contributing to the lowering of the barrier. In fact, already at this point product formation appears feasible under the thermal conditions of the experiment: once the barrier of $18.3 \text{ kcal mol}^{-1}$ connected with **TS1** is surmounted, subsequent proton transfer via **TS2** should be efficient as its barrier is even lower by about 2 kcal mol^{-1} .

The situation is, however, more complicated than that. The arenium intermediate **2** can actually rearrange almost barrierless ($\Delta G^\ddagger = 3.9 \text{ kcal mol}^{-1}$) via **TS3**, the transition structure of a [1,2]H-shift across the phenyl ring, to form the thermodynamically rather stable dienone **4** ($\Delta G_R = -24.1 \text{ kcal mol}^{-1}$). Hence, any amount of the σ -intermediate **2** formed will immediately decay to yield the dienone rather than passing the significantly larger barrier **TS2** that would lead to direct product formation. Decay of the dienone intermediate via a [1,3]H-shift onto the phenolate oxygen atom to form the more stable phenol intermediate **5** ($\Delta G_R = -10.1 \text{ kcal mol}^{-1}$) is unlikely to occur because of the excessively high barrier connected

with this step via **TS4** ($\Delta G^\ddagger = 51.4 \text{ kcal mol}^{-1}$). Yet another route to phenol formation was found via **TS5** that connects the σ -complex **2** with **5**, but this path has a much higher barrier ($\Delta G^\ddagger = 19.8 \text{ kcal mol}^{-1}$) than **TS2** and constitutes the kinetically least favorable step among the three routes identified for the decay of **2**. Thus, even though formation of the intermediate **5** would provide a strong thermodynamic driving force and subsequent formation of the product complex **3** via **TS6** could occur with a moderately low barrier of $16.3 \text{ kcal mol}^{-1}$, this intermediate is unlikely to play any role in the course of the overall reaction because unfavorably high barriers preclude its formation from **2**.

With the somewhat unexpected nature of **TS2** in mind we actually located a corresponding transition structure **TS9** leading directly from **4** to the final product **3**, that obviously profits from the same driving force provided by the large proton affinity of the bridging μ -oxo atom. This step represents the most favorable pathway we could find for product formation from dienone **4**. With a barrier of $26.6 \text{ kcal mol}^{-1}$, however, this step appears high enough to prevent an immediate decay of the dienone intermediate. Because all other barriers surrounding **4** are even higher (i.e., reaction back to **2** via **TS3** with $\Delta G^\ddagger = 28.0 \text{ kcal mol}^{-1}$, or phenol formation via **TS4** with $\Delta G^\ddagger = 51.4 \text{ kcal mol}^{-1}$), *the dienone should be thermodynamically as well as kinetically stable enough to attribute to it a significant life time under the experimental conditions*. Because the barriers in question are related to proton transfer transition states these elementary steps should be subject to substantial H/D kinetic isotope effects (KIE) upon deuteration of the 2-position of the phenyl ring. Indeed, H/D exchange of the respective hydrogen in the optimized stationary points **4** and **TS9** yields an increase of the corresponding barrier by $1.8 \text{ kcal mol}^{-1}$ for the most favorable route for the dienone decay. This corresponds to a classical KIE of 21.4 at 298.15 K. Qualitative consideration of quantum mechanical tunneling^[180] employing a simple one-dimensional model^[181] significantly increases the predicted KIE to 27.1 (298.15 K). We thus predict a situation in which it might actually be possible to identify this species by experimental means even at room temperature employing a deuterated ligand framework. Given the fact that it represents the only relevant non-aromatic intermediate in the mechanistic scenario established so far, we suggest NMR spectroscopy as a promising tool for its experimental identification.

As an alternative to the reaction paths considered up to this point, we identified a route to product formation commencing with an initial rearrangement of the $\mu\text{-}\eta^2\text{:}\eta^2$ peroxo species **1** to a $\mu\text{-}\eta^2\text{:}\eta^1$ coordinated isomer **6**, which is less stable than **1** by 6.1 kcal mol⁻¹. From **6** electrophilic attack of the aromatic ring via **TS7** leads to the formation of σ -complex **7**, a thermodynamically highly unfavorable counterpart of **2** (i.e. less stable by 33.7 kcal mol⁻¹). From **7**, proton transfer with simultaneous O-O bond cleavage via **TS8** leads to formation of the hydroxylated product **3**. With formation of two thermodynamically unfavorable intermediates and two energetically demanding reaction barriers, this reaction sequence can effectively be seen as a unimolecular decomposition of **1** (assuming reaction kinetics with pre-equilibrium) with an overall barrier of 44.6 kcal mol⁻¹ related to **TS8**. Thus, with the highest effective barrier identified in our entire study, this reaction channel is certainly unlikely to contribute to product formation.

Summarizing this part of our investigation we note that we identified four alternative reaction pathways leading from the $\mu\text{-}\eta^2\text{:}\eta^2$ peroxo species **1** to the hydroxylated product **3**. Three thermally accessible pathways to product formation were identified, all of which involve the decay of the σ -intermediate **2**. Formation of **2** requires passage of an activation barrier of 18.3 kcal mol⁻¹ via **TS1** corresponding to the electrophilic attack of the aromatic ring by the peroxo Cu₂O₂ core. **2** can rearrange almost without activation barrier to the dienone intermediate **4**, which we propose as a key intermediate in the course of the aromatic hydroxylation reaction. For the energetically least demanding route leading from **4** to product formation via **TS9** we predict an effective barrier of 26.6 kcal mol⁻¹. Consequently, for the overall mechanistic scenario established here, this last proton transfer constitutes the rate limiting step for product formation. The preceding electrophilic attack via **TS1** is energetically significantly less demanding by 8.3 kcal mol⁻¹. For the rate limiting step we predict a large H/D-KIE, which might allow future characterizations of the dienone intermediate by NMR techniques.

Why then did the dienone intermediate escape any experimental detection in our hands so far? An intuitively striking explanation for the experiments performed in methanol is certainly the participation of this protic solvent in the proton transfer steps in the latter phase of the reaction sequence. In this case intermolecular proton

transfer steps will most likely provide much lower barriers than those identified in our computations, which were performed employing a continuum solvent model but without explicit consideration of solvent molecules. But also in experiments using aprotic solvents, we searched in vain for any trace of this intermediate. Spurred by recent reports on the potential importance of counter ions for related systems^[161, 182] we investigated the influence of a single $[\text{ClO}_4]^-$ counter ion on the rate limiting step of the mechanistic scenario suggested above. And indeed, compared to the computed barrier height of $26.6 \text{ kcal mol}^{-1}$ for the step $4 \rightarrow \text{TS9}$ a dramatically lower barrier of only $7.5 \text{ kcal mol}^{-1}$ results for the corresponding process $4 \cdot \text{ClO}_4 \rightarrow \text{TS9} \cdot \text{ClO}_4$ (Figure 3-15)! This result implies a high reaction rate for this elementary step at room temperature, which straightforwardly explains the lack of any experimental evidence for the occurrence of a stable dienone intermediate prior to product formation or any prominent KIE in acetonitrile or CH_2Cl_2 .

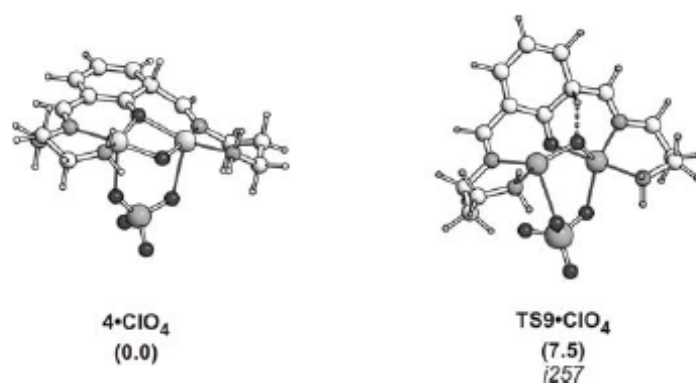


Figure 3-15: Dienone $4 \cdot \text{ClO}_4$ and transition structure $\text{TS9} \cdot \text{ClO}_4$ leading to product formation optimized in the presence of a coordinating ClO_4^- counter ion (Gibbs free energies at 298 K in kcal mol^{-1} relative to $4 \cdot \text{ClO}_4$; UB3LYP/TZVP+COSMO//UB3LYP/SVP+COSMO results)

In order to substantiate this quantum-chemical result the hydroxylation reaction was repeated in an aprotic solvent, acetonitrile, with the Cu(I) DAPA complex having a non-coordinating anion, BPh_4^- (**1c**). Under these conditions a significantly slower reaction as compared to the Cu(I) complex with perchlorate as counterion (**1b**) was observed (cf. Figure 3-14). This indeed supports the presence of a rate limiting proton transfer step leading from the dienone to the final product, which gets markedly accelerated in the presence of a coordinating counterion.

Table 3-4: Computed energy contributions (in atomic units) used to obtain relative free energies G_{rel} (in kcal mol⁻¹) and magnetic properties of all species discussed in the text.

Species	$G_{\text{B3LYP/SVP/au}}$	$\Delta G_{\text{corr/au}}^{\text{a}}$	$E_{\text{B3LYP/TZVP/au}}^{\text{b}}$	$G_{\text{B3LYP/TZVP/au}}^{\text{c}}$	$G_{\text{rel/kcal mol}^{-1}}$	$J/\text{cm}^{-1}_{\text{d}}$	$\langle\alpha \beta\rangle^{\text{e}}$
1	-4195.60056	0.31044	-4197.35914	-4197.04870	0.0	25.0	0.24
TS1	-4195.56551	0.31172	-4197.33120	-4197.01949	18.3	-1325.4	0.54
2	-4195.60553	0.31473	-4197.37254	-4197.05781	-5.7	-23.5	0.13
TS2	-4195.58272	0.30871	-4197.34045	-4197.03175	10.6	251.1	0.15
3	-4195.75172	0.31483	-4197.51234	-4197.19750	-93.4	-521.8	0.23
TS3	-4195.59967	0.30969	-4197.36128	-4197.05159	-1.8	-84.5	0.21
4	-4195.64395	0.31271	-4197.40890	-4197.09619	-29.8	-307.2	0.26
TS4	-4195.56457	0.30689	-4197.32116	-4197.01427	21.6	-38.0	0.21
5	-4195.66128	0.31292	-4197.42523	-4197.11231	-39.9	530.1	0.04
TS5	-4195.57355	0.30669	-4197.33293	-4197.02623	14.1	-516.6	0.31
6	-4195.59091	0.30904	-4197.34809	-4197.03906	6.1	534.1	0.24
TS6	-4195.63820	0.31198	-4197.39824	-4197.08625	-23.6	-166.0	0.22
TS7	-4195.55689	0.30944	-4197.30342	-4196.99398	34.3	-241.6	0.62
7	-4195.56043	0.30960	-4197.31375	-4197.00415	28.0	-332.1	0.35
TS8	-4195.53386	0.30495	-4197.28254	-4196.97760	44.6	-3366.1 ^f	1.00 ^f
TS9	-4195.60805	0.30862	-4197.36248	-4197.05385	-3.2	285.1	0.04
4•ClO₄	-4195.66999	0.31918	-4958.43118	-4958.11200	0.0		
TS9•ClO₄	-4955.17452	0.31666	-4958.41677	-4958.10011	7.5		

^a Thermal corrections to $G(298.15)$ computed at the B3LYP/SVP+COSMO level;

^b Total energies of single point calculations at the B3LYP/TZVP+COSMO level;

^c $E_{\text{B3LYP/TZVP}} + \Delta G_{\text{corr}}$; ^d Spin coupling constant computed according to eq. 2 (see text);

^e Overlap integral of the magnetic orbitals;

^f magnetic coupling constant involving a closed-shell singlet solution, no bs wave function found.

3.8 Summary and Discussion

In the preceding sections structural, spectroscopic, kinetic and quantum chemical investigations of the ligand hydroxylation reaction mediated by a Cu bis(imine) complex have been presented. Starting from a structural analysis of the Cu(I) complex **I** and the Cu(II) product **II** exhibiting a hydroxylated ligand the optical absorption and vibrational spectra have been analyzed. Special attention was directed to reproduce the structural and spectroscopic properties of complex **II** by quantum-chemical means. The kinetic analysis of the ligand hydroxylation provided evidence for O₂-binding being the rate-limiting step in the overall reaction. The conversion of **I** to **II** was found to proceed much faster in methanol than in acetonitrile, which was attributed to the fact that the acetonitrile ligands of the Cu(I) precursor **I** are displaced in the course of O₂ binding. Moreover, an inverse kinetic isotope effect was evidenced for the reaction in acetonitrile which was rationalized by a sterically congested transition state leading to the peroxo adduct. In methanol, however, no KIE was observed. Finally, a DFT analysis of the oxygenation reaction demonstrated that the dominant barrier after O₂ binding is represented by the electrophilic attack of the $\mu\text{-}\eta^2\text{:}\eta^2$ peroxo intermediate **1** on the arene ring. Nevertheless, on the basis of the activation energy (18.3 kcal/mol) this reaction is thermally allowed, in agreement with the experimental observation. Given the fact that the B3LYP functional employed has been shown to overestimate barrier heights by 4-7 kcal mol⁻¹,^[183] the actual barrier height might rather be in the range of 10-15 kcal mol⁻¹.

The DFT investigation of the reactivity of the Cu(II) peroxo intermediate **1** formed by reaction of the Cu(I) precursor and O₂ indicated the presence of four pathways to the hydroxylated final product **3**. One of the pathways studied involves the rearrangement of the $\mu\text{-}\eta^2\text{:}\eta^2$ peroxo structure to a $\mu\text{-}\eta^2\text{:}\eta^1$ peroxo intermediate that subsequently attacks the aromatic ring. In the present system, however, this pathway is associated with an overall barrier of 44.6 kcal/mol which renders it less likely for product formation. In this context it is interesting to note that Siegbahn has suggested a related sequence (i.e., peroxide attack followed by O-O bond cleavage) as key steps for the *ortho*-hydroxylation of phenolate in the catalytic cycle of tyrosinase, but with an overall barrier of only 14.4 kcal mol⁻¹.^[106] Alternative pathways were not

reported in this study. In contrast, all energetically favorable pathways identified in our study involve a direct decay of the $\mu\text{-}\eta^2\text{:}\eta^2$ peroxy intermediate **1** without rearrangement to an alternative peroxide coordination mode.

The energetically most favorable route commences with a direct electrophilic attack of the aromatic ring by the peroxy moiety to form an arenium ion, which subsequently undergoes an almost barrierless proton shift to form a rather stable dienone intermediate (**4**). A second proton transfer step from the dienone directly leads to product formation. We have identified several alternative pathways with moderate barrier heights that would actually be thermally accessible under the experimental conditions. None of these pathways, however, can compete with the energetically most favorable pathway, even assuming potential errors in computed relative energies as large as 7 kcal/mol, and so we feel safe to suggest a single pathway as a general mechanistic scenario for the system under study.

This scenario involves as a key intermediate in the conversion of the peroxy complex to the hydroxylated product the dienone intermediate **4**, which should eventually be detectable experimentally. We attribute the fact that we (and others) were unable so far to identify such an intermediate to several factors: first of all, explicit participation of protic (or Lewis-basic) solvent molecules (which have not been considered in our calculations) in the proton transfer steps after formation of the σ -complex **2** might lead to drastically lowered barriers. Secondly, the key proton transfer steps might occur in an intermolecular fashion, involving initial deprotonation of the σ -complex by another copper dioxygen intermediate. A third factor contributing to the rapid decay of the dienone the counterion has explicitly been identified in the Computational Section: Compared to the calculated barrier height of 26.6 kcal/mol for the decay of **4** via **TS9**, a dramatically lowered barrier of 7.5 kcal/mol was found for the corresponding process $\mathbf{4}\cdot\mathbf{ClO}_4 \rightarrow \mathbf{TS9}\cdot\mathbf{ClO}_4 \rightarrow \text{product } (\mathbf{3})$. This hypothesis is supported by a measurement of the hydroxylation reaction in acetonitrile employing a Cu(I) BPh₄ complex; in this case a significantly lower reaction rate as compared to the Cu(I) perchlorate salt is observed. In order to directly detect the dienone intermediate **4** further experimental studies have to be performed. The present system, however, appears less suitable for these investigations as binding of O₂ is

also associated with a thermal barrier, probably precluding accumulation of a dienone species at low temperatures.

Another notable, and somewhat surprising result of our quantum chemical analysis is the finding that no stable bis(μ -oxo) isomer is formed in the ligand environment studied here. Based on the experience gathered in related investigations put forward by many groups, we would actually expect preferential formation of a bis(μ -oxo) species within the chelating bidentate N-donor ligand environment of the system studied here. Yet, the initial steps take place without intermediate formation of a bis- μ -oxo species. While the initial transition state **TS1** exhibits structural features nearly identical to O-O bond breaking transition states leading to the formation of a bis- μ -oxo species in related ligand environments,^[179] it represents in the present case a multicenter transition state for the O-O bond cleavage and simultaneous σ -attack of the aromatic ring by the peroxy moiety. We view this finding as a consequence of the rather tight coordination sphere of the bis-imine ligand that brings the breaking O-O bond in the Cu_2O_2 subunit in **TS1** into close proximity of the aromatic ring, ideally oriented for direct orbital interactions with the aromatic π -system to generate the σ -complex **2** in a single step.

The mechanistic scenario established here has implications for the ligand hydroxylation reaction occurring in Karlin's prototype system, the binuclear copper complex $[\text{Cu}_2(\text{XYL})]$,^[29, 30] upon reaction with O_2 . In full agreement with our present results, Pidcock et al. implied a μ - η^2 : η^2 peroxy complex as active species and excluded the occurrence of a corresponding bis(μ -oxo) species in a spectroscopic analysis of this reaction.^[109] These authors rationalized the electrophilic attack of the Cu_2O_2 moiety onto the aromatic ring in terms of qualitative frontier orbital arguments. Within this picture, it was convincingly argued that the HOMO of the arene system overlaps with an unoccupied orbital of the electrophile, which can either be the π^*_{σ} or the σ^* orbital of the side-on peroxy dicopper core (Figure 3-16a). Based on the particularities of the coordination geometry present in the tridentate ligand environment in that study, an attack via the σ^* peroxide orbital was considered unlikely, and a preferred, symmetry allowed pathway via the π^*_{σ} orbital was suggested. The geometry of the initial transition state **TS1** optimized for the copper bis(imine) complex here, however, differs essentially from the assumed transition

state geometry discussed by Pidcock et al., and it is in fact the σ^* orbital of the peroxy group, and not the π^*_{σ} orbital, that is involved in the electrophilic attack on the arene ring. In particular, the rather rigid ligand framework studied in the present work does not allow for a tilt of the aromatic ring along the O-O axis of the Cu_2O_2 group in the course of this elementary step – which would indeed exclude any constructive orbital interaction between the σ^* peroxy orbital with the aromatic π -system. Instead the arene ring and the Cu_2O_2 group rotate in the transition state about axes *perpendicular* to the O-O vector such that the σ^* orbital now interacts with the aromatic π -system from *below* in a symmetry allowed fashion that mediates the initial step along the hydroxylation pathway (Figure 3-16b).

Another interesting implication for the mechanism of Karlin's XYL system relates to the observation of an NIH-shift in studies employing a modified xylyl ligand that was methylated in 2-position of the aromatic core.^[20, 184] This observation could in fact straightforwardly be rationalized assuming the formation of a dienone as a key intermediate, in analogy to the mechanistic scenario developed here. A subsequent C-N cleavage, in analogy to the cleavage of the methylene-N(amine) bond in the XYL-system, would, however, appear unlikely in a bis(imine) complex due to the double-bond character of the C-N linkage.

The present results are also relevant to the enzyme tyrosinase, specifically the *ortho*-hydroxylation of tyrosine mediated by the *oxy* form of this enzyme. Of crucial importance for this reaction is the orientation of phenolic substrates with respect to the binuclear copper active site. Experimental information on this point has mostly been derived from spectroscopic studies on the bonding of inhibitors to tyrosinase.^[185, 186] Alternatively, it has been proposed that an external tyrosine substrate is oriented at the active site of Ty in the same way as Phe49 in the *Limulus oxy* Hc structure.^[23, 187] The recently solved structure of *Streptomyces castaneoglobisporus* tyrosinase has revealed a very similar arrangement with Tyr98 (provided by the associated caddie-protein) extending into the active site pocket like a potential substrate.^[14, 101] An external phenolic substrate may be preoriented at the active site in a similar geometry (Figure 3-2).

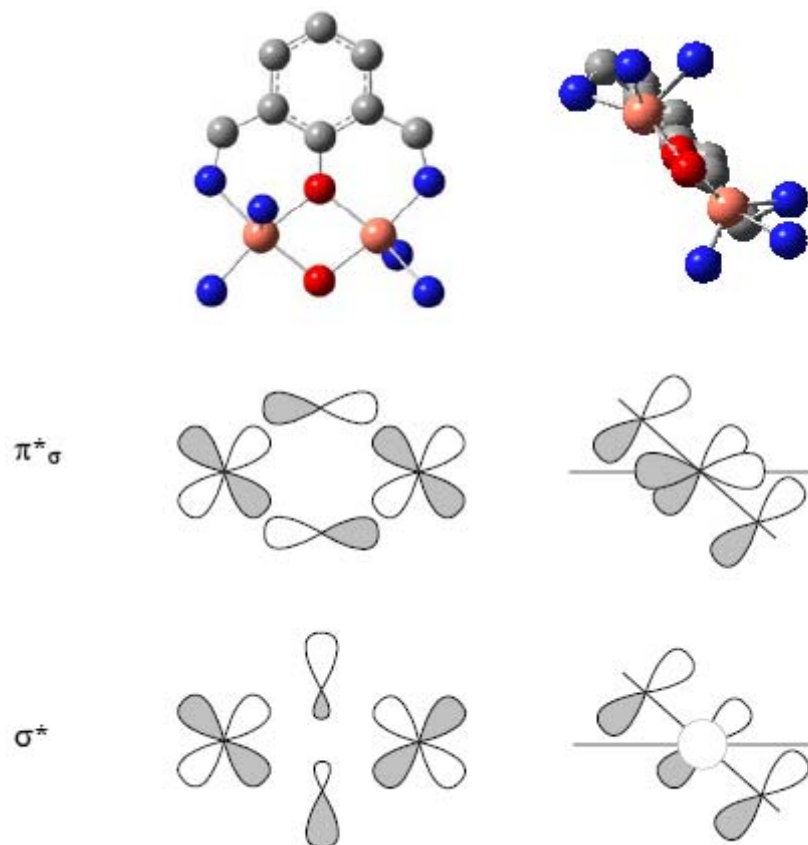


Figure 3-16a: Geometries in the transition states leading to the σ -complex: Karlin-complex

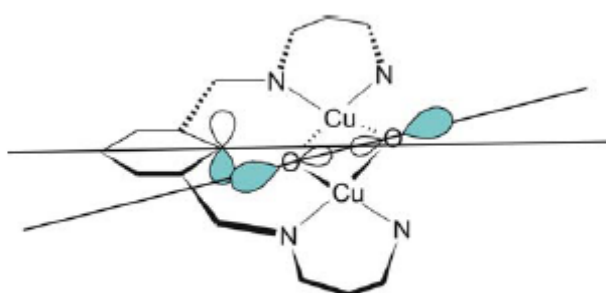


Figure 3-16b: Geometries in the transition states leading to the σ -complex: bis(imine)complex (see text)

The analysis of the hydroxylation pathway in the Cu₂ bis(imine) complex thus has shown that besides the previously discussed π^*_σ pathway a second pathway for the oxygenation chemistry mediated by binuclear copper site does exist, i.e., electrophilic attack of the substrate by the σ^* orbital of side-on bound peroxide. For systems exhibiting more structural flexibility than the Cu bis(imine) systems both pathways might be operative. Importantly, the presence of a second orbital pathway provides additional flexibility for the position of the aromatic substrate with respect to the Cu₂O₂ unit in the transition state leading to the σ -complex. This is of relevance both for the enzyme tyrosinase and for copper model systems which are active in the hydroxylation of external substrates.^[42, 46, 188] In all of these cases the σ^* orbital directed along the prolonged O-O vector just has to “hit” the π -system of the substrate (except for the nodal plane of the C-orbitals) from an arbitrary angle in order to mediate hydroxylation. This structural flexibility in the transition state accounts for the wide occurrence of oxygenation reactions in binuclear copper dioxygen systems exhibiting largely different ligand structures and explains the fact that these reactions are not limited to a few systems with special geometries.

3.9 Unpublished Material

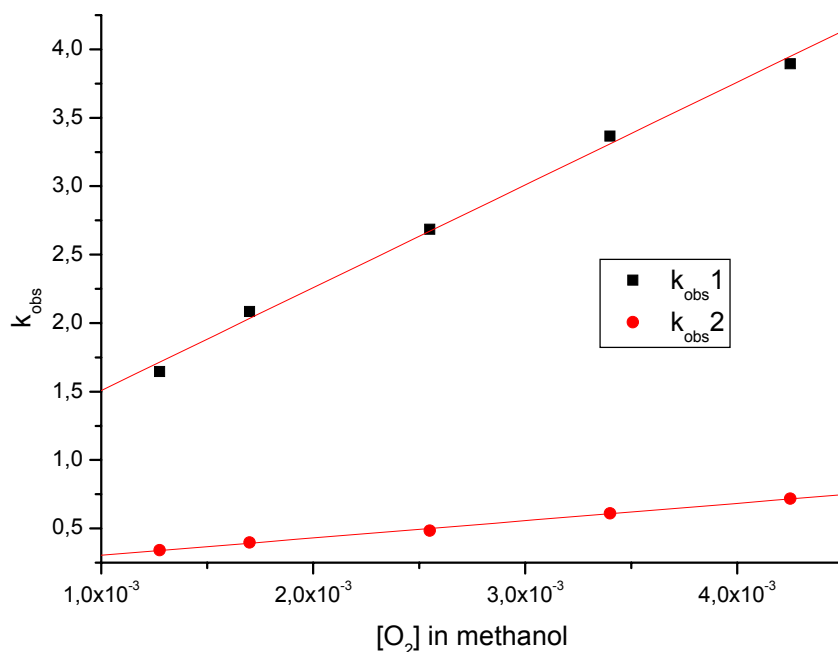
3.9.1 Kinetic Investigations

As described above, during the analysis of the oxidation of **1a** with dioxygen, we could not detect the formation of a dioxygen intermediate like a peroxo complex. Compared with the reaction in acetonitrile the oxidation in methanol is much faster. Here it was possible to fit the absorbance vs time traces using the sum of two exponential functions. Two independent rate constants could be determined which indicates two independent reaction steps. In a limited temperature range a linear dependence on the dioxygen concentration for the two rate constants with an intercept was obtained as shown in Figure 3-17.

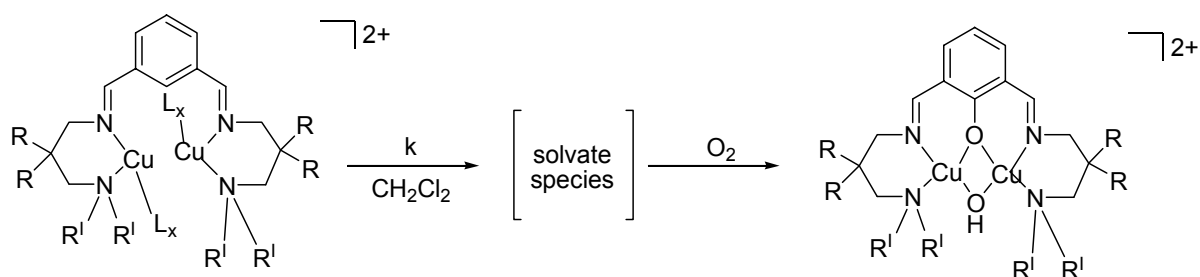
The two reactions that are depending on dioxygen concentration indicate the existence of different solvated complex species. This is already known from earlier studies by the Schindler group and the Feringa group that in solutions of related complexes several species can exist.

Table 3-5: Measured reaction rates of the reaction of Ia with O₂ in methanol at -60,1°C

O ₂ [mM]	k _{1obs/s⁻¹}	k _{2obs/s⁻¹}
1.25	1.65 ± 0.05	0.34 ± 0.01
1.77	2.08 ± 0.06	0.40 ± 0.02
2.55	2.69 ± 0.06	0.49 ± 0.01
3.4	3.37 ± 0.06	0.61 ± 0.02
4.25	3.89 ± 0.08	0.72 ± 0.02

**Figure 3-17: Dependence of the reaction constants k_{obs1} and k_{obs2} on dioxygen concentration in methanol [Ia] = 1 x 10⁻⁴ mol/l, T = -60,1°C**

These complexes are mainly different in regard to the number of coordinated acetonitrile molecules.^[49, 189] For our system such a variety of species is also suggested and might cause some kind of problems, because acetonitrile molecules compete significantly with dioxygen as a ligand at the copper site.^[48] (Figure 3-18)

**Figure 3-18: Several complex species existing in solution**

Additionally, depending on the concentration of copper(I) cations and acetonitrile molecules, the formation of mononuclear copper(I) species and uncoordinated ligand or even the formation of copper(I) polymers might be possible.^[162] The intercepts could indicate responsible reaction behavior, however, more likely is a consequence of preliminary reorganisation steps prior to the reaction with dioxygen. In our efforts to simplify the kinetic behavior by reducing the distribution of species in solution, copper(I) salt or acetonitrile was added. Unfortunately these attempts did not simplify the reaction behavior. It was not possible to fit the time traces over a large temperature range. Therefore more detailed analysis could not be performed and activation parameters ΔH^\ddagger and ΔS^\ddagger could not be determined.

Related investigations were also performed in dichloromethane as solvent. Compared to the measurements in methanol, the oxidation reaction of the complex was significantly slower. Most importantly, in this solvent no dependence on dioxygen concentration for both reaction rate constants could be observed (Figure 3-19). Unfortunately, "clean" fitting was not possible due to the large errors for the data fitting. However, the observations support that an additional intermediate is formed, probably the dienone that has been predicted from theoretical calculations as described above.

Table 3-6: Measured reaction rates of the reaction of Ia with O₂ in CH₂Cl₂ at 20,0°C

O ₂ [mM]	k ₁ _{obs} × 10 ⁻² /s ⁻¹	k ₂ _{obs} × 10 ⁻² /s ⁻¹
2.15	15 ± 2	4.3 ± 0.1
1.935	15 ± 1	4.1 ± 0.1
1.72	13. ± 2	3.2 ± 0.2
1.505	15 ± 2	3.6 ± 0.1
1.29	13. ± 4	2.7 ± 0.1
1.075	15 ± 1.	3.2 ± 0.2

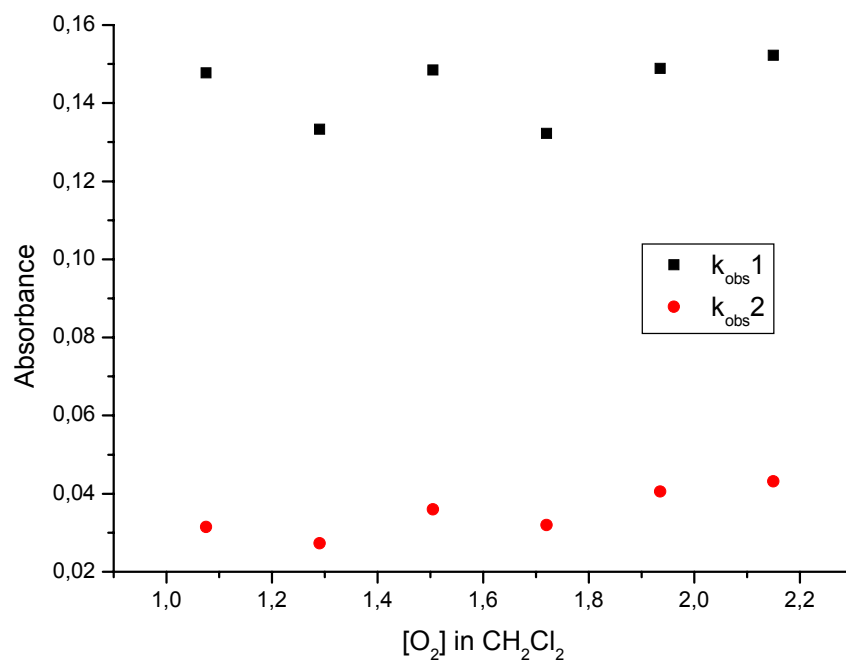


Figure 3-19: Dependence of the reaction constants $k_{\text{obs}1}$ and $k_{\text{obs}2}$ on dioxygen concentration in dichloromethan $[I_a] = 1 \times 10^{-4}$ mol/l, $T = 20^\circ\text{C}$

Copper complexes with phenanthroline and bipyridine as ligands

4.1 A Copper(I) complex with an adamantane derivative as ligand

4.1.1 Introduction

It is well known that bidentate chelate ligands with nitrogen donor atoms are suitable for complexation of copper(I) ions. Therefore numerous copper(I) complexes with ligands such as bipyridine or phenanthroline have been synthesized. Furthermore several of these complexes are also suitable to coordinate unsaturated hydrocarbons e.g. olefins or alkynes. As described in chapter 1.4 there is a great interest to investigate such copper complexes containing unsaturated compounds in regard to their possible catalytic properties and application in organic synthesis. The research group of Prof. Schreiner (JLU Gießen) is interested in the functionalization of adamantane derivatives and examples are shown in Figure 4-1.^[190, 191]

Adamantane (tricyclo[3.3.1.1^{3,7}]decane) is a cycloalkane and the simplest diamondoid. Its formal structure consists of four cyclohexane molecules attached in the chair conformation. In nature traces of adamantane can be found in some rock crystals or in petroleum, where it was discovered first 1933. Its name derived from the Greek *adamantinos*, due to its diamond-like structure. Adamantane is the most stable isomer of C₁₀H₁₆. As an unfunctionalized hydrocarbon, adamantane itself is not very useful in contrast to its derivatives that are applied for example in pharmaceutical products. .

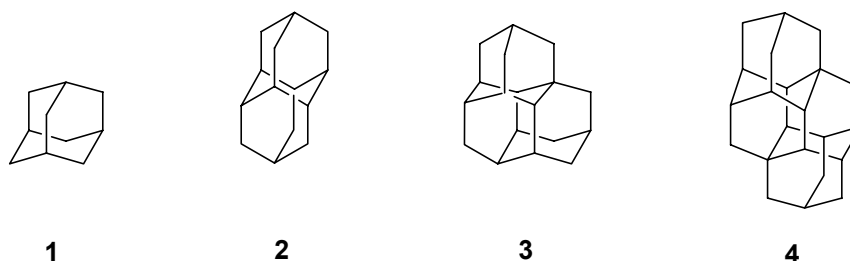


Figure 4-1: Adamantane and derivatives: adamantane (1), diamantane (2), triamantane (3) and [121] tetramantane (4)^[190, 191]

In collaboration with the Schreiner group it was decided to try to use the adamantane derivative tetracyclo[7.3.1.1^{4,12}.0^{2,7}]tetradeca-6,11-diene (**tctd**) shown in Figure 4-2 as ligand for the complexation of copper(I). This derivative could show some potential for the formation of coordination polymers.

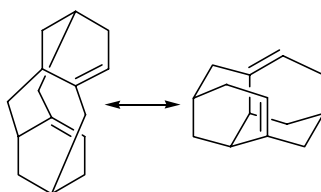
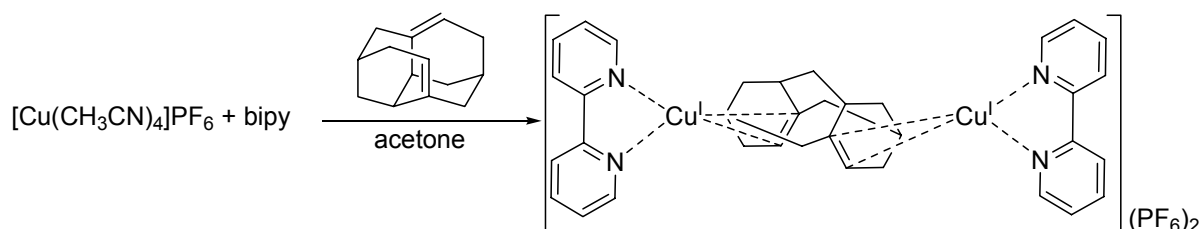


Figure 4-2: Tetracyclo[7.3.1.1^{4,12}.0^{2,7}] tetradeca-6,11-diene (tctd**)**

4.1.2 Results

Due to the facile preparation of related copper(I) complexes, the synthesis and characterization of a copper(I) complex with **tctd** as ligand seemed to be a facile experiment that should be performed. And indeed, applying the same experimental conditions as for the synthesis of the related complex $[\text{Cu}(\text{bipy})\text{COD}]\text{PF}_6$ ^[68], $[\text{Cu}_2(\text{bipy})_2(\text{tctd})](\text{PF}_6)_2 \times \text{C}_3\text{H}_6\text{O}$ could be obtained.



The molecular structure of the cation of $[\text{Cu}_2(\text{bipy})_2(\text{tctd})](\text{PF}_6)_2$ is shown in Figure 4-3 (crystallographic data are presented in Tables 4-1 and 4-2). The unit cell contains one complex molecule, one solvent molecule (acetone) and two anions.

Each copper center is coordinated with two nitrogen atoms of bipy and one double bond of the adamantyl derivative **tctd**. The coordination sphere of the copper centers is almost square planar, which is common for ternary copper olefin complexes.^[65-67, 192] Due to this the Cu-N bond lengths have typical values around 2,0(2) and are in good agreement with those found in similar ternary complexes.^[65-67, 192] Furthermore, comparable values for the Cu-C_{olefin} distances were observed.

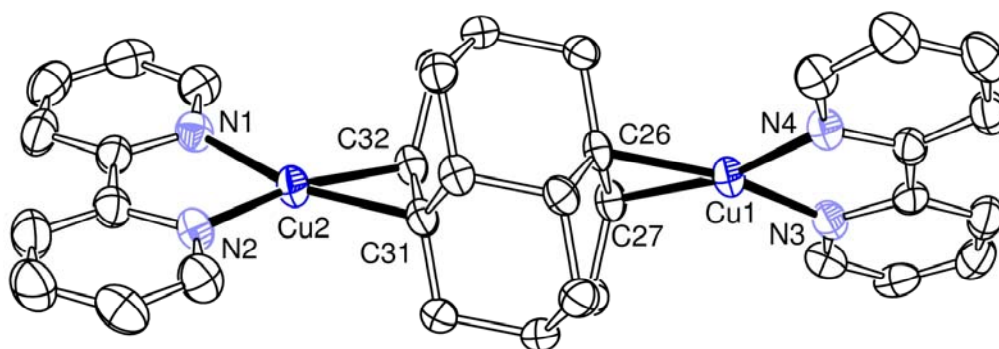


**Figure 4-3: ORTEP plot of $[\text{Cu}_2(\text{bipy})_2(\text{tctd})]^{2+}$
(50% probability ellipsoids) hydrogen atoms omitted for clarity**

The double bonds lengths C(25)-C(26) and C(31)-C(32) showed with values of 1,40(5) and 1,38(6) a clear widening compared to the average value of 1,33 Å for a simple uncoordinated double bond. Due to the fact that the uncoordinated tctd has not been characterized crystallographically yet, a detailed comparison of the bond lengths and angles is not possible.

Table 4-1: Crystal data and structure refinement for $[\text{Cu}_2(\text{bipy})_2(\text{tctd})]^{2+}$

Empirical formula	$\text{C}_{37} \text{H}_{40} \text{Cu}_2 \text{F}_{12} \text{N}_4 \text{O} \text{P}_2$		
Formula weight	973.75	F(000)	988
Temperature (K)	193(2) K	Crystal size (mm)	0.28 x 0.08 x 0.28
Crystal system	triclinic, p-1	θ range for data collected ($^\circ$)	2.66 to 28.14
Space group	P-1 no.2	Index ranges	$-10 \leq h \leq 11$, $-14 \leq k \leq 14$, $-24 \leq l \leq 26$
Wavelength (Å)	0.71073	Reflection collected	17289
Unit cell dimensions[Å / $^\circ$]	a = 8.50(2)	Independent refl., Rint	8570, 0.0709
	b = 11.31(3)	Completeness to theta	90.5% ($\theta = 28, 14^\circ$)
	c = 20.49(5)	Goodness-of-fit on F^2	0.888
$\alpha = 91.5(3)$			
$\beta = 92.9(3)$			
$\gamma = 100.8(3)$			
Z	2	R1 [$ I > 2\sigma(I)$]	0.0452
Density calcd. (Mg/m^3)	1.671	wR2 [$ I > 2\sigma(I)$]	0.1021
Volume [Å ³]	1935.8(8)	R1 [all data]	0.0914
Absorpt. coeff. (cm^{-1})	1.277	wR2 [all data]	0.1220

Table 4-2: Selected bond lengths and angles [Å, °] for [Cu₂(bipy)₂(tctd)]²⁺

Cu(2)-N(1)	1.99(1)	Cu(1)-C(27)	2.02 (4)
Cu(2)-N(2)	1.98(1)	C(31)-C(32)	1.38(6)
Cu(1)-N(3)	1.99(3)	C(26)-C(27)	1.40(5)
Cu(1)-N(4)	1.99 (3)	N(1)-Cu(2)-N(2)	83.2 (1)
Cu(2)-C(31)	2.04(4)	C(32)-Cu(2)-C(31)	40.1(2)
Cu(2)-C(32)	2.00(3)	N(3)-Cu(1)-N(4)	83.3(2)
Cu(1)-C(26)	2.04(3)	C(26)-Cu(1)-C(27)	40.2(2)

4.2 Copper(I) complexes with bicyclopropylidene and dicyclopropylacetylene as ligands

4.2.1 Introduction

In organometallic chemistry unsaturated compounds such as bicyclopropylidene **bcp** (a) and dicyclopropylacetylene **dcpa** (b) (depicted in Figure 4-4) play an important role for the synthesis of special molecules with remarkable properties.^[193-195] In that regard Armin de Meijere and co-workers successfully used dcpa for the facile preparation of octacyclopropylcubane and some of its isomers.^[196] Due to these novel reactions, transition metal complexes with bcp and dcpa as ligands are assumed to have interesting properties and should be investigated in more detail.

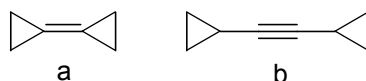
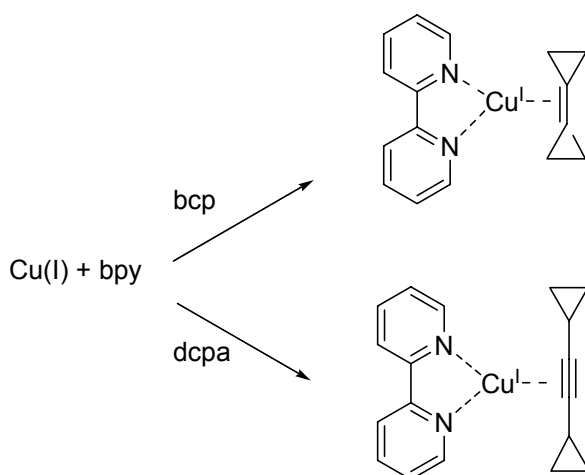


Figure 4-4: Bicyclopropylidene bcp (a) and dicyclopropylacetylene dcpa (b)

In collaboration with the research group of Prof. A. de Meijere (University of Göttingen) it was possible to prepare successfully the complexes $[\text{Cu}(\text{bipy})(\text{bcp})]\text{PF}_6$ and $[\text{Cu}(\text{bipy})(\text{dcpa})]\text{PF}_6$. This is already a quite interesting and important result because so far, only one transition metal complex containing bcp as ligand has been synthesized and characterized by de Meijere and co-workers.^[195]



To gain a better understanding of the coordination ability of these ligands and in regard to investigate further possible applications of their complexes as catalysts we were interested in preparing and investigating complexes with bcp and dcpa as

ligands. Prior to the investigations described herein, a bcp nickel complex was successfully synthesized and characterized by L. Römmling in the Schindler group.^[197]

4.2.2 Results

4.2.2.1 [Cu(bipy)(bcp)]PF₆

By mixing copper(I) salt, bipyridine and an excess of the olefin bcp the complex [Cu(bipy)(bcp)]PF₆ could be synthesized in acceptable yields. Crystals suitable for X-ray analysis were obtained and the molecular structure of the cation is depicted in Figure 4-5. Selected bond lengths and angles are presented in Tables 4-3 and 4-4.

The geometry of [Cu(bipy)(bcp)]PF₆ is best described as square planar. The copper(I) center is coordinated by two pyridyl nitrogen atoms and by the double bond of the olefin. Due to the space group C2/c there is a plane of symmetry in the molecule. The values of 1.98(2) Å for Cu-N- and of 1.96(2) Å for Cu-C-distances are comparable to related ternary copper(I) olefin complexes.^[64, 66, 67, 192, 198]

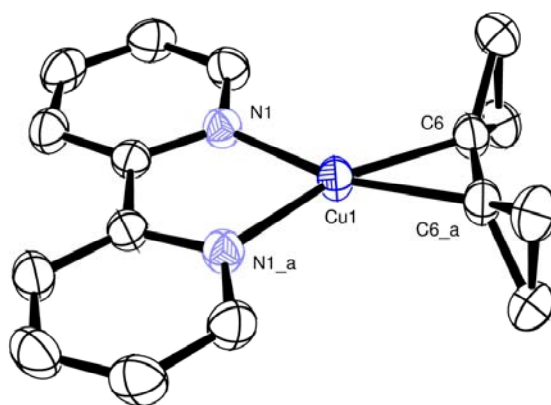


**Figure 4-5: ORTEP plot of [Cu(bipy)bcp]⁺
(50% probability ellipsoids) hydrogen atoms omitted for clarity**

Due to the changed hybridization of the coordinated carbon atoms from sp² to sp³, the primal planar bicyclopropylidene shows an out of plane bending of both cyclopropyl groups. In that regard an expansion of the coordinated double bond compared to the uncoordinated ligand from 1,31 to 1,36(3) Å is observed. In comparison with the previously described cobalt complex the out of plane bending of the ligand is less with 23,19° (compared to 40°). Furthermore the minor expansion of

the coordinated double bond (1,36(3) Å compared to 1,40 Å in the cobalt complex) confirms that the Cu(I) ion is a poor π -back bonding transition metal cation. As expected, the bonds in this complex can be described as predominately σ bonds from alkenes to the copper ion.^[64-67] This weak π back bonding interaction is also observed with dicyclopropylacetylene as ligand in the complex [Cu(bipy)dcpa]PF₆ described below.

4.2.2.2 [Cu(bipy)dcpa]PF₆

In the same way as [Cu(bipy)bcp]PF₆ was synthesized it was possible to obtain the analogous alkyne complex with dicyclopropylacetylene (dcpa) as ligand. Treatment of [Cu(CH₃CN)₄]PF₆ and bipyridine with dcpa in acetone gave [Cu(bipy)dcpa]PF₆ as a yellow-orange solid, which was characterized by NMR-spectroscopy. After diffusion of diethylether into the solution yellow crystals suitable for X-ray structure analysis could be obtained. The molecular structure of the cation of [Cu(bipy)dcpa]PF₆ is shown in Figure 4-6 while selected bond lengths and angles are given in Tables 4-5 and 4-6. The coordination environment of the copper(I) ion is almost trigonal planar with two pyridine nitrogen atoms and a side-on bound dicyclopropylacetylene molecule.

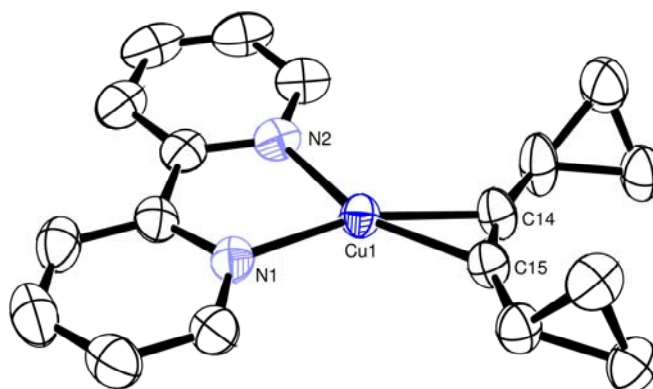


**Figure 4-6: ORTEP plot of [Cu(bipy)dcpa]⁺
(50% probability ellipsoids) hydrogen atoms omitted for clarity**

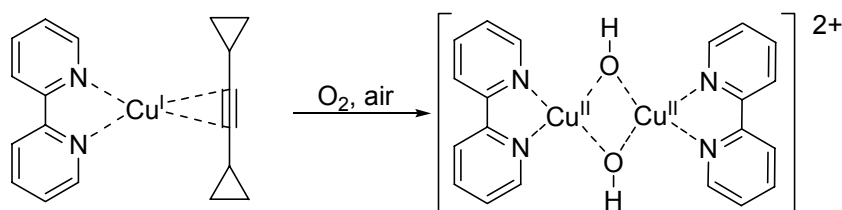
As expected the observed bond angle N(1)-Cu(1)-N(2) and the distances N(1)-Cu(1) / N(2)-Cu(1) and Cu(1)-C(14) / Cu(1)-C(15) are comparable to those determined in the structure of [Cu(bipy)bcp]PF₆. The carbon-carbon bond length of the coordinated dcpa molecule (1.23(4) Å) is only slightly larger than in the free molecule (1.197(3) Å).^[199] This is in line with the only slightly elongated triple bond of dcpa compared to

a related acetylene complex (C-C bond length 1.188(11) Å) and to an uncoordinated acetylene molecule (1.204 Å).^[67] As a consequence of the changed hybridization (sp to sp²) of the coordinated carbon atoms the bonds adjacent to the triple bond are also bended. Due to this, the two cyclopropyl rings are bended out of plane as depicted in Figure 4-6.

4.2.2.3 Reactivity towards dioxygen

As described in the introduction the activation of molecular oxygen by copper complexes plays a central role in synthetically useful stoichiometric and catalytic conversions of organic molecules and also in biological systems. Furthermore, dioxygen adduct complexes are very important species in this regard.^[3, 4, 21, 200-202] However, it is quite difficult to isolate and characterize these reactive intermediates. Therefore, it seemed a good idea to use alkenes or alkynes as ligands, thus stabilizing the copper(I) unit but additionally to provide a ligand that could be easily substituted by dioxygen during the oxidation process. Thus, in a bench top experiment [Cu(bipy)bcp)PF₆ and [Cu(bipy)dcpa)PF₆ were dissolved in acetone and the solution was cooled to -80°C. After dioxygen had been bubbled through the cold solution, the color turned slowly pale blue, but no dioxygen adduct complex with intensive color could be detected in this preliminary test.

Unfortunately, the experiment demonstrated that a simple copper complex with only bipyridine as ligand could not stabilize a "dioxygen" adduct complex under these conditions. However, still an interesting oxidation reaction occurred. According to the following equation the oxidation of [Cu(bipy)dcpa)PF₆ led to a bis(μ-hydroxo)dicopper(II) complex as product and its structure is shown in Figure 4-7 (crystal data, bond distances and angles are presented in Tables 4-7 and 4-8).



Oxidation of the coordinated dcpa was not observed. As depicted in Figure 4-7, the dcpa molecule is not coordinated to the copper centre anymore. Therefore, a

binuclear copper(II) complex was formed in which both copper ions are bridged by a hydroxido group of the inserted oxygen. It is assumed that this hydroxido group is formed from a bis- μ -oxo precursor and traces of water due to the fact, that these crystals were obtained by oxidation of $[\text{Cu}(\text{bipy})\text{dcpa}]\text{PF}_6$ with air instead of using dry dioxygen.

Each unit cell contains one binuclear copper(II) complex and two distorted PF_6^- anions. At a first glance the structure of the cation seems to be symmetrical but the determined space group $C2/c$ reveals a monoclinic crystal system. Due to this the Cu_2O_2 core is only almost planar. The $\text{Cu}(\text{II})\text{-N}$ and $\text{Cu}(\text{II})\text{-O}$ distances as well as the O-Cu-O and Cu-O-Cu angles are in line with the metric parameters of closely related complexes.^[203, 204]

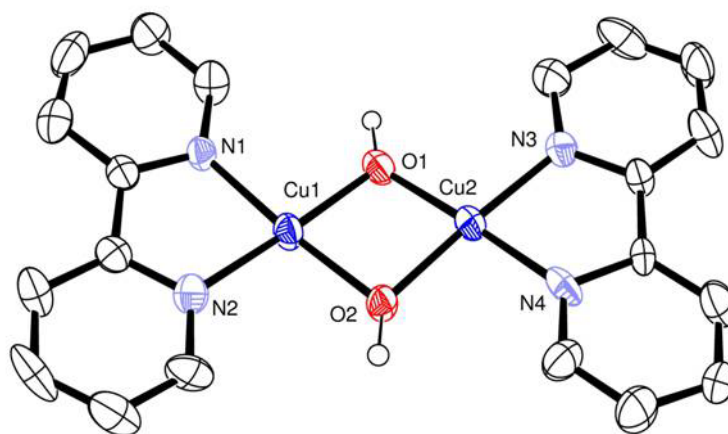


**Figure 4-7: ORTEP plot $[\text{Cu}_2(\text{bipy})_2(\text{OH})_2]^{2+}$
(50% probability ellipsoids) hydrogen atoms omitted for clarity**

Table 4-3: Crystal data and structure refinement for [Cu(bipy)bcP]PF₆

Empirical formula	C ₈ H ₈ Cu _{0.5} F ₃ N ₁ P _{0.5}		
Formula weight	222.41	F(000)	896
Temperature (K)	200 (2)	Crystal size (mm)	0.35 x 0.35 x 0.25
Crystal system	monoclinic	θ range for data collected (°)	2.67 to 28.27
Space group	C2/c, no.15	Index ranges	-11 ≤ h ≤ 11, -19 ≤ k ≤ 19, -17 ≤ l ≤ 16
Wavelength (Å)	0.71073	Reflection collected	10033
Unit cell dimensions[Å / °]	a = 8.98(2) b = 14.63(1) c = 13.13(9) α = 90 β = 96.6(1) γ = 90	Independent refl., Rint	2101, 0.0284
		Completeness to theta	49.5% (theta= 28.27°)
		Goodness-of-fit on F ²	1.091
Z	8	R1 [>2σ(I)]	0.0266
Density calcd. (Mg/m ³)	1.724	wR2 [>2σ(I)]	0.0725
Volume [Å ³]	1713.9(2)	R1 [all data]	0.0312
Absorpt. coeff. (cm ⁻¹)	1.431	wR2 [all data]	0.0745

Table 4-4: Selected bond lengths and angles [Å, °] for [Cu(bipy)bcP]PF₆

Cu(1)-N(1)	1.98(2)	C(11)-Cu(1)-C(12)	40.7(1)
Cu(1)-N(2)	1.98(2)	C(11)-Cu(1)-N(2)	158.8(7)
Cu(1)-C(11)	1.96 (2)	C(12)-Cu(1)-N(2)	118.1(6)
Cu(1)-C(12)	1.96(2)	C(11)-Cu(1)-N(1)	118.1(6)
C(11)-C(12)	1.36 (3)	C(12)-Cu(1)-N(1)	158.7(7)
N1-Cu(1)-N2	83.2(8)		

Table 4-5: Crystal data and structure refinement for [Cu(bipy)dcpa]PF₆

Empirical formula	C ₁₈ H ₁₈ CuF ₆ N ₂ P		
Formula weight	470.85	F(000)	952
Temperature (K)	193(2)	Crystal size (mm)	0.2 x 0.32 x 0.04
Crystal system	monoclinic	θ range for data collected (°)	2.17 to 26.01
Space group	P2(1)/n (no. 14)	Index ranges	-13 ≤ h ≤ 13, -10 ≤ k ≤ 10, -23 ≤ l ≤ 22

CHAPTER 4

Wavelength (Å)	0.71073	Reflection collected	13372
Unit cell dimensions [Å / °]	a = 11.12(2) b = 8.97(2) c = 18.92(1) α = 90 β = 96.6(2) γ = 90	Independent refl., Rint	3584, 0.0596
		Completeness to theta	97.4% (theta= 26,01°)
		Goodness-of-fit on F ²	1.005
Z	4	R1 [>2σ(I)]	0.0470
Density calcd. (Mg/m ³)	1.671	wR2 [>2σ(I)]	0.1238
Volume [Å ³]	1872.2(4)	R1 [all data]	0.0699
Absorpt. coeff. (cm ⁻¹)	1.315	wR2 [all data]	0.1388

Table 4-6: Selected bond lengths and angles [Å, °] for [Cu(bipy)dcpa]PF₆

Cu(1)-C(14)	1.95(4)	C(14)-Cu(1)-N(2)	118.9(2)
Cu(1)-C(15)	1.96(4)	C(15)-Cu(1)-N(2)	155.3(2)
Cu(1)-N(2)	1.98(3)	C(14)-Cu(1)-N(1)	158.0(2)
Cu(1)-N(1)	1.99(3)	C(15)-Cu(1)-N(1)	121.6(2)
C(14)-C(15)	1.23(4)	N(2)-Cu(1)-N(1)	83.0(2)
C(14)-Cu(1)-C(15)	36.8(2)		

Table 4-7: Crystal data and structure refinement for [Cu₂(bipy)₂(OH)₂](PF₆)₂

Empirical formula	C ₂₀ H ₁₈ Cu ₂ F ₁₂ N ₄ O ₂ P ₂		
Formula weight	761.39	F(000)	3008
Temperature (K)	193(2) K	Crystal size (mm)	0.16 x 0.08 x 0.24
Crystal system	monoclinic	θ range for data collected (°)	2.64 to 28.05
Space group	C2/c (No. 15)	Index ranges	-29<=h<=29, -18<=k<=18, -21<=l<=21
Wavelength (Å)	0.71073	Reflection collected	22725
Unit cell dimensions [Å / °]	a = 24.4(1) b = 14.1(3) c = 16.1(3) α = 90 β = 112.5(3) γ = 90	Independent refl., Rint	5775, 0.1850
		Completeness to theta	92.8% (theta= 28,05°)
		Goodness-of-fit on F ²	0.880
Z	8	R1 [>2σ(I)]	0.0853

CHAPTER 4

Density calcd. (Mg/m ³)	1.977	wR2 [$I > 2\sigma(I)$]	0.1915
Volume [Å ³]	5116.5	R1 [all data]	0.1900
Absorpt. coeff. (mm ⁻¹)	1.905	wR2 [all data]	0.2506

Table 4-8: Selected bond lengths and angles [Å, °] for [Cu₂(bipy)₂(OH)₂](PF₆)₂

N(1)-Cu(1)	1.96(9)	O(2)-Cu(1)	1.95(7)
N(2)-Cu(1)	1.96(8)	Cu(1)-Cu(2)	2.91(2)
N(3)-Cu(2)	1.96(8)	N(2)-Cu(1)-N(1)	82.2(4)
N(4)-Cu(2)	1.96(1)	O(1)-Cu(1)-O(2)	80.9(3)
O(1)-Cu(2)	1.94(6)	O(1)-Cu(2)-O(2)	81.5(3)
O(1)-Cu(1)	1.94(7)	N(4)-Cu(2)-N(3)	82.5(4)
O(2)-Cu(2)	1.93(9)		

4.3 Copper(I) complexes with phenanthroline and derivatives as ligands

4.3.1 Introduction

Considering “greener chemistry”, today catalysis plays a more and more important role in organic chemistry.^[205-207] In an effort to synthesize single stereoisomers for production and marketing of new drugs, asymmetric catalysis will play an integral part in future applications. Therefore the asymmetric preparation of enantiomerically pure compounds has become an extremely important aspect in organic synthesis and a challenge for academic and industrial chemists.

Chelating diphospane ligands are commonly used as chiral catalysts due to their successful application in Rh(I) complexes for asymmetric hydrogenation and for many other asymmetric reactions.^[208-215] Recently it has been recognized that chelating ligands containing nitrogen donor atoms such as phenanthroline can also be used as catalysts for asymmetric synthesis. 1,10 phenanthroline is well known as analytical reagent and can be used as a template for the preparation of chiral ligands. The chiral information can be introduced by chiral groups at the 2-,3-,8- and/or 9- position (I,II) or by ring fusion (III) depicted in Figure 4-8.^[216]

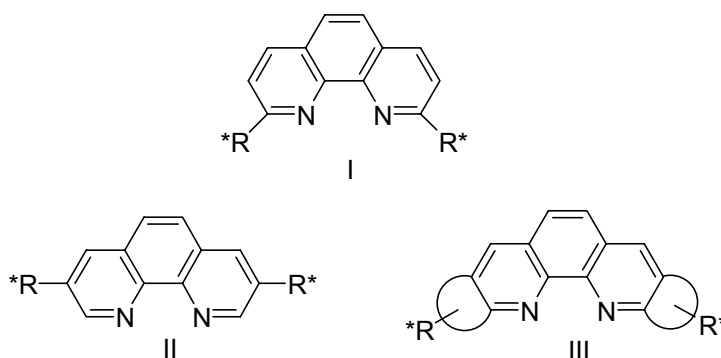


Figure 4-8: Ligand templates^[216]

The research group of Prof. Elke Schoffers (Chemistry Department, Western Michigan University, Kalamazoo, USA) is trying to prepare such modified phenanthroline ligands and to investigate their properties towards enantioselective recognition reactions. Therefore these ligands are modified either by introducing chiral groups or by introducing epoxide groups into the ring system which causes the loss of aromaticity and planarity, shown in Figure 4-9.^[214, 216, 217]

In regard to the application as asymmetric catalysis we thought it could be interesting to investigate the properties of copper containing complexes of such functionalized phenanthroline derivatives. From this a collaboration with the group of Prof. Schoffers developed and several Cu(I) and Cu(II) complexes of numerous phenanthroline ligands were synthesized and structurally characterized during my diploma thesis.^[218] A selection of the used ligands are depicted in Figure 4-9.

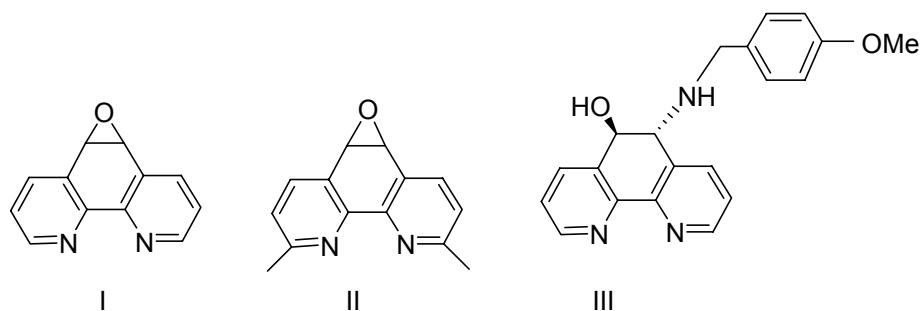


Figure 4-9: Phenanthroline derivatives used as ligands:

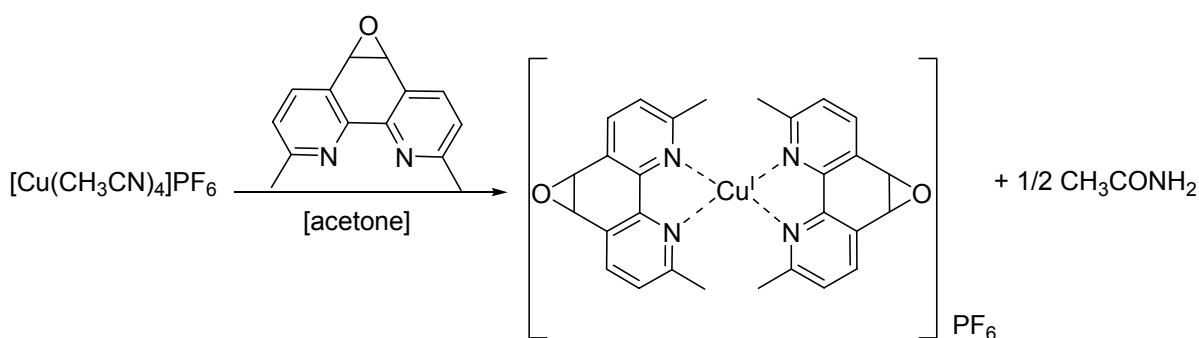
**1,10-phenanthroline-5,6-epoxide (I), 2,9-dimethyl-1,10-phenanthroline-5,6-epoxide (II)
5,6-dihydro-[1,10]phenanthroline-5,6-aminoalcohol (III)**

So far tests on these complexes as catalysts in asymmetric synthesis have not been performed yet because it was not the goal of this thesis. Such experiments will be performed in the future in the Schoffers group.

4.3.2 Results

4.3.2.1 $[\text{Cu}(\text{dmpe})_2]\text{PF}_6 \times 1/2 \text{CH}_3\text{CONH}_2$

An interesting reaction was observed when 2,9-dimethyl-1,10-phenanthroline-5,6-epoxide (II) (dmpe) as a ligand was mixed with $[\text{Cu}(\text{CH}_3\text{CN})_4]\text{PF}_6$ in a stoichiometric ratio in acetone.



Crystals of the complex $[\text{Cu}(\text{dmpe})_2]\text{PF}_6 \times 1/2 \text{CH}_3\text{CONH}_2$ were obtained and the molecular structure of the cation of $[\text{Cu}(\text{dmpe})_2]\text{PF}_6$ is shown in Figure 4-10. Crystal data, bond lengths and angles are presented in Tables 4-9 and 4-10.

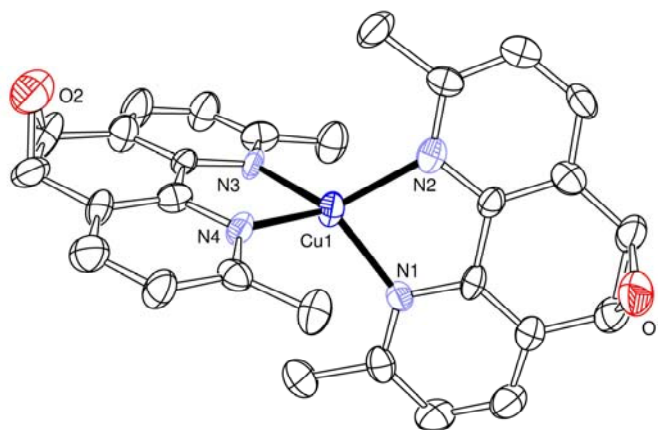


**Figure 4-10: ORTEP plot of $[\text{Cu}(\text{dmpe})_2]^+$ (50% probability ellipsoids)
hydrogen atoms omitted for clarity**

The unit cell contains the fourfold coordinated complex cation $[\text{Cu}(\text{dmpe})_2]^+$, a PF_6^- anion and furthermore an acetamide molecule (in every second unit cell) depicted in Figure 4-11.

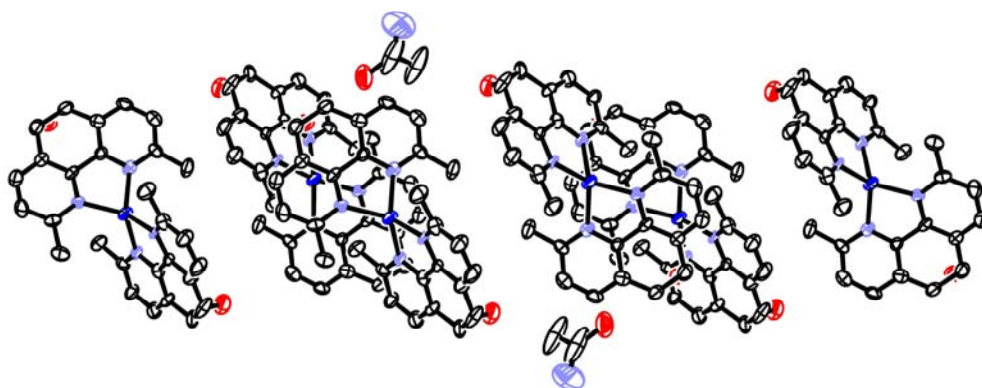
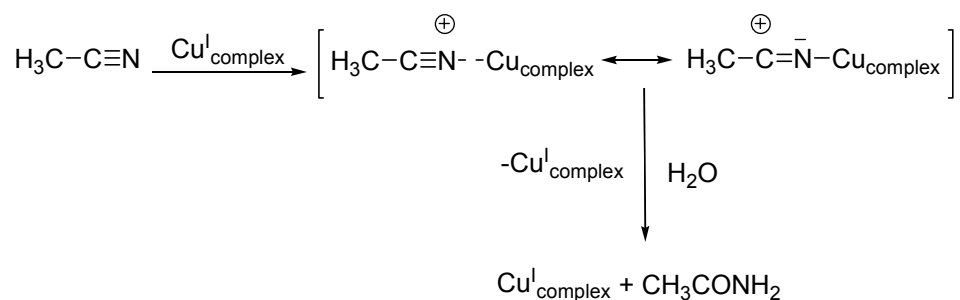


**Figure 4-11: ORTEP ellipsoid plot of a part of the unit cell of
 $[\text{Cu}(\text{dmpe})_2]^+ \times 1/2 \text{CH}_3\text{CONH}_2$ (50% probability ellipsoids)
hydrogen atoms omitted for clarity**

This is quite amazing due to the fact that no acetamide was added to the reaction solution. Nevertheless, under certain conditions the formation of this acetamide molecule can be assumed and explained. The formation of an amide as intermediate

during hydrolysis of nitrils is well known. Such hydrolysis of nitrils catalysed by acids or bases are a common method to synthesize carbon acids. Therefore, since a catalytic effect caused by protons or hydroxyl ions can be excluded, it might be possible, that the copper cation is responsible for the formation of acetamide from acetonitrile. Acetonitrile is present from the starting material $[\text{Cu}(\text{CH}_3\text{CN})_4]\text{PF}_6$ and traces of water might be present in the dried absolute acetone. This furthermore explains why acetamide instead of the corresponding carbon acid was formed.



Unfortunately the quality of the obtained crystals was not great. The structural refinement was not so good showed disorder problems encountered with the epoxide groups and the acetamide molecules. Due to this the formation of acetamide is assumed but not clearly proofed. Therefore efforts in obtaining better quality single crystals have to follow as well as further investigations to gain a better understanding of the described catalytic reaction.

The structure of the cation in Figure 4-10 shows a distorted tetrahedral geometry. The copper(I) ion is coordinated by the four nitrogen atoms of the phenanthroline ligands, whereas the formation of five membered chelate rings leads to values for the $\text{N}(1)-\text{Cu}(1)-\text{N}(2)$ and $\text{N}(3)-\text{Cu}(1)-\text{N}(4)$ angles of $82,6(3)^\circ$ and $83,0(3)^\circ$, significantly deviating from ideal tetrahedral angle. Due to sterical demand both phenanthroline molecules are coordinated almost at right angles. Furthermore, the epoxide groups in the middle ring of the phenanthroline molecule are responsible for the loss of aromaticity. Due to this and to the sterical effects of the methyl groups, there is no planarity of the ligand system anymore and the disordered oxygen atoms are standing out of plane. With $2,01(6)$ and $2,02(6)$ Å the values of the Cu-N bonds are comparable to those of related Cu(I) phenanthroline complexes.^[219, 220]

Table 4-9: Crystallographic data for [Cu(dmpe)₂]PF₆ x 1/2 CH₃CONH₂

Empirical formula	C ₂₉ H _{26,5} CuF ₆ N _{4,5} O _{2,5} P		
Formula weight	686.56	F(000)	2800
Temperature (K)	200(2)	Crystal size (mm)	0.1 x 0.15 x 0.2
Crystal system	monoclinic.	θ range for data collected (°)	1.88 to 28.29
Space group	C2/c (no 15)	Index ranges	-30 ≤ h ≤ 24, -15 ≤ k ≤ 14, -29 ≤ l ≤ 32
Wavelength (Å)	0.71073	Reflection collected	14882
Unit cell dimensions[Å / °]	a = 23.17(6) b = 11.67(3) c = 24.10(6) α = 90 β = 115.9(4) γ = 90	Independent refl., R _{int}	6984, 0.1901
		Completeness to theta	95.9 % (theta= 28.29°)
		Goodness-of-fit on F ²	0.862
Z	8	R1 [>2σ(I)]	0.0752
Density calcd. (Mg/m ³)	1.556	wR2 [>2σ(I)]	0.1403
Volume [Å ³]	5860(2)	R1 [all data]	0.3127
Absorpt. coeffic. (cm ⁻¹)	0.876	wR2 [all data]	0.2138

Table 4-10: Selected bond lengths (Å) and bond angles (°) for [Cu(dmpe)₂]PF₆ x 1/2 CH₃CONH₂

Cu(1)-N(1)	2.01(6)	N(3)-Cu(1)-N(4)	83.0(3)
Cu(1)-N(2)	2.01(6)	N(1)-Cu(1)-N(4)	116.6(2)
Cu(1)-N(3)	2.01(6)	N(1)-Cu(1)-N(3)	130.6(2)
Cu(1)-N(4)	2.02(6)	N(2)-Cu(1)-N(3)	121.0(3)
N(1)-Cu(1)-N(2)	82.6(3)	N(4)-Cu(1)-N(2)	129.4(3)

4.4 Efforts to synthesize a copper-oxo-species

4.4.1 Introduction

As described above the challenge to synthesize and fully characterize a copper oxo species is still open. Because it is a highly reactive intermediate responsible for many oxidizing processes, isolation and characterization of such a species failed so far. Recently Schroeder, Holthausen and Schwarz could successfully generate a copper-oxo-complex with phenanthroline as ligand via ESI.^[63] Based on these results it seemed promising to use derivatives of phen and bipy as ligands in an attempt to stabilize such a species. Therefore, several copper(I) complexes with bipyridine, phenanthroline and its derivatives as ligands were reacted with air, pure dioxygen or ozone.

As mentioned above, dimethylphenanthroline **dmp** has been used as reagent for the detection of copper(I) ions since 1960. Because of the intense color of its copper(I) complexes it is still a common and commercial available detection reagent and was therefore used by us in our first attempts to obtain an oxo-complex. In general bidentate ligands with nitrogen donor atoms such as dmp, phen or the related bipy coordinate to Cu(I) in a ratio of 2:1 or 3:1 (ligand to Cu(I) center). In this regard we obtained as expected the $[\text{Cu}(\text{dmp})_2]^+$ complex cation with two dmp molecules coordinated to one copper ion, depicted in Figure 4-12. Due to this the copper(I) center and its oxidation state +I is stabilized and the reactivity towards dioxygen is rather low.

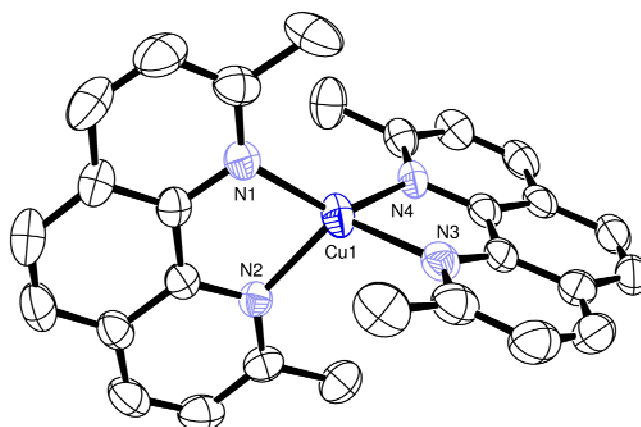


Figure 4-12: ORTEP plot of $[\text{Cu}(\text{dmp})_2]^+$ (50% probability ellipsoids)
hydrogen atoms omitted for clarity

To facilitate a reaction with dioxygen it is absolutely necessary to generate a complex with a Cu(I) to ligand ratio of 1:1. Here dioxygen is then supposed to coordinate to the copper center and form a "dioxygen adduct" complex. Therefore one dmp ligand of $[\text{Cu}(\text{dmp})_2]^+$ has to be substituted by an only weakly coordinated ligand such as an olefin. In that regard the olefin cyclooctadiene seemed to be suitable to saturate the coordination sphere of the copper(I) center being weakly bonded and appropriate for substitution.

Due to the fact that bipy has related ligation properties as phen or dmp and due to the facile preparation of the olefin complex $[\text{Cu}(\text{bipy})\text{COD}]^+$, this complex was synthesized to investigate its reaction behavior towards dioxygen. The complex $[\text{Cu}(\text{bipy})\text{COD}]^+$ is already known from the literature and has been described in chapter 1.4.

4.4.2 Results

4.4.2.1 Reactivity of $[\text{Cu}(\text{bipy})\text{COD}]^+$ towards dioxygen

To gain first insights into the reactivity of this complex a bench top experiment was performed. After having cooled a solution of $[\text{Cu}(\text{bipy})\text{COD}]^+$ in acetone to -80°C , pure dioxygen was bubbled through this solution. This facile procedure allows rapid detection of thermal unstable dioxygen-adducts which usually can be recognized by an intensive color. However, it was observed that $[\text{Cu}(\text{bipy})\text{COD}]^+$ only reacted very slowly with dioxygen while the yellow color of the solution turned to blue. UV-vis spectroscopic investigations using stopped-flow technique were performed. The spectral changes that occurred during the reaction of $[\text{Cu}(\text{bipy})\text{COD}]^+$ with dioxygen in acetone are shown in Figure 4-13. The decrease of the maximum at 339 nm indicates the decomposition of the complex; only weak d-d product bands were observed. The insert shows the data fit to the sum of two exponential functions at 339 nm. Two reaction rate constants could be determined, which reveals the existence of a parallel or consecutive reaction. From previous studies of related systems from S. Goldstein and G. Czapski it is well known that such reactions with dioxygen are very complex.^[221, 222]

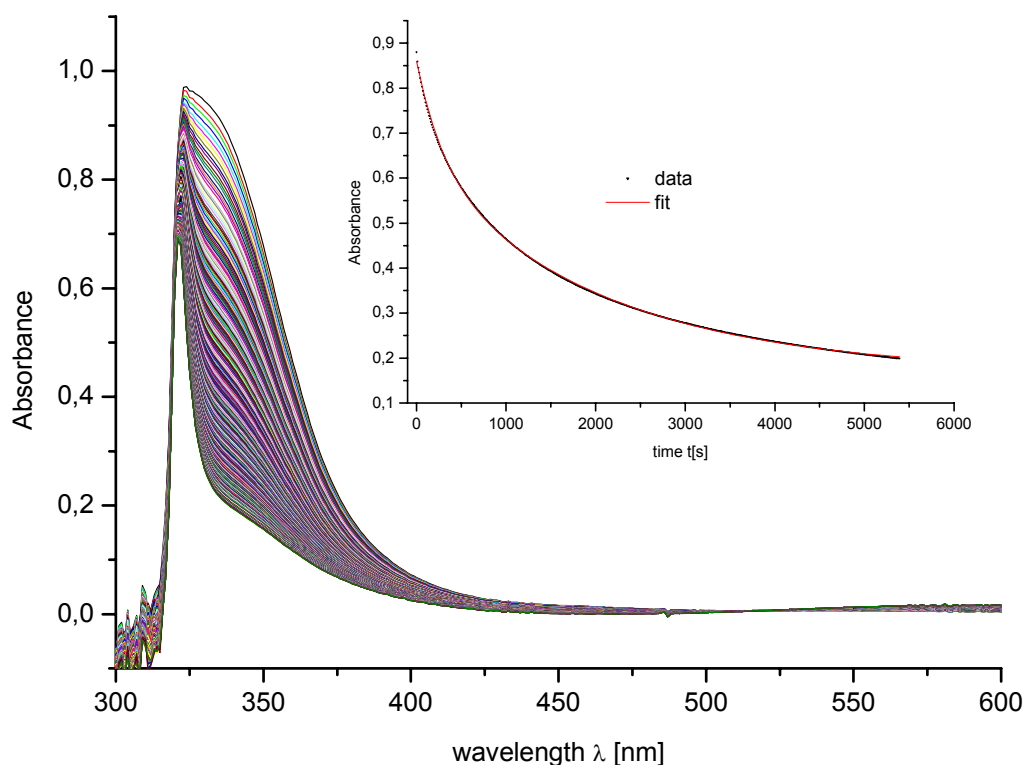


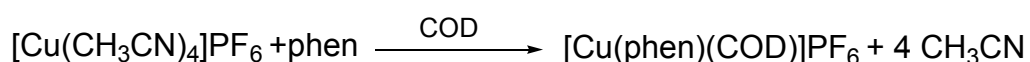
Figure 4-13: Spectral changes during reaction of $[\text{Cu}(\text{bipy})\text{COD}]^+$ with dioxygen in acetone ($T = 20\text{ }^\circ\text{C}$, $[\text{complex}] = 1.0\text{ mM}$, $[\text{O}_2] = 4.0\text{ mM}$, $t = 5400\text{ s}$)

Insert: Absorbance vs. time trace at 339 nm and fit to the sum of two exponentials ($k_{\text{obs}1} = 3.72 \times 10^{-3} \pm 4 \times 10^{-5}\text{ s}^{-1}$; $k_{\text{obs}2} = 4.94 \times 10^{-4} \pm 3 \times 10^{-6}\text{ s}^{-1}$)

Unfortunately, no formation of a dioxygen adduct complex could be detected during the oxidation reaction. An analogue reaction behavior was expected for the related complex $[\text{Cu}(\text{phen})\text{COD}]^+$, which was synthesized easily according to the preparation method as for the bipy complex.

4.4.2.2 $[\text{Cu}(\text{phen})\text{COD}]\text{PF}_6$

Mixing phenanthroline, 1,5-cyclooctadiene (COD) and Cu(I) salt afforded a grey material that could be recrystallized from acetone. By ether diffusion crystals suitable for X-ray structural analysis were obtained.



The ORTEP representation of $[\text{Cu}(\text{phen})\text{COD}]^+$ is shown in Figure 4-14, crystal data, bond lengths and angles are presented in Tables 4-11 and 4-12. In contrast to

[Cu(bipy)COD]PF₆ the complex [Cu(phen)COD]PF₆ has not been described in the literature so far.

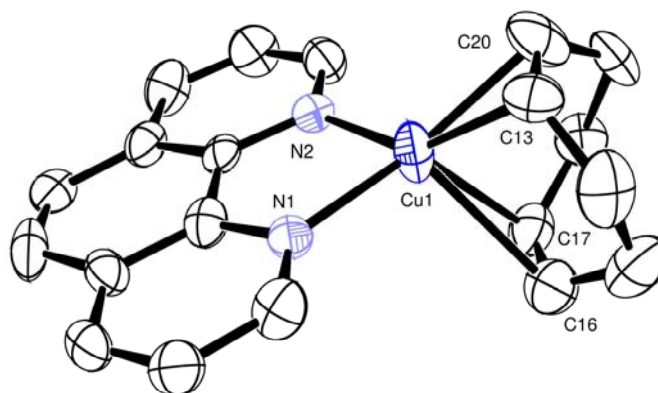
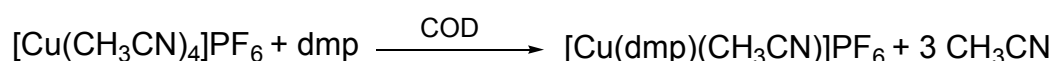


Figure 4-14: ORTEP plot of [Cu(phen)COD]⁺ (50% probability ellipsoids) hydrogen atoms omitted for clarity

The structure of the cation [Cu(phen)COD]⁺ shows a distorted tetrahedral geometry coordinated with two nitrogen atoms of the phenanthroline ligand and two double bonds of the COD ligand. The Cu-N bonds (av 2,0 Å) are shorter than Cu-N bond of related copper(I) complexes of phen, bipy and their derivatives.^[68, 198, 223-225] In contrast the coordination of the ligand COD is only weak due to the longer Cu-C_{olefin} bonds in comparison with related ternary complexes.^[64-66] Furthermore the C=C bond distance of 1,31 Å is similar to the values of uncoordinated cyclooctadiene.^[226]

4.4.2.3 Efforts to synthesize a [Cu(dmp)COD]⁺ complex

Since it was not possible to detect a dioxygen adduct complex using [Cu(bipy)COD]⁺ or [Cu(phen)COD]⁺ it seemed to be necessary to use ligands with more sterical demand such as dmp. However, it was not possible to synthesize [Cu(dmp)COD]⁺ according to the preparation of [Cu(phen)COD]⁺: instead of coordinated COD, an acetonitrile molecule coordinates to the copper center:



The crystals obtained during this synthesis were suitable for crystallographic characterization and the determined molecular structure is shown in Figure 4-15. The coordinated acetonitrile molecule acts as an additional ligand and saturates the

coordination sphere of the copper(I) ion. In this case acetonitrile molecules compete with COD for the coordination site of the copper centre due to the sterical effects of the dmp ligand. Its methyl groups prevent coordination of COD that is a much weaker ligand for copper(I) ions compared to acetonitrile. The crystal structure of this complex shows a three coordinated copper(I) ion and has already been reported previously by M. Munakata et al. in 1989.^[227] The reported crystal data, bond lengths and angles are consistent with our data.

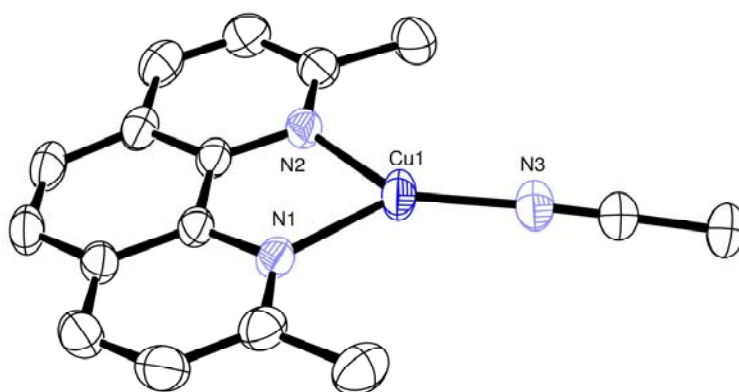
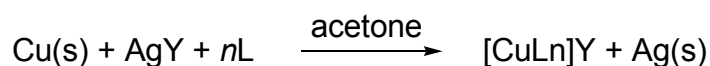


**Figure 4-15: ORTEP plot of $[\text{Cu}(\text{dmp})\text{CH}_3\text{CN}]^+$
(50% probability ellipsoids) hydrogen atoms omitted for clarity**

Due to the strong ligated acetonitrile molecule and the stability of $[\text{Cu}(\text{dmp})\text{CH}_3\text{CN}]^+$ towards oxidation with air, the reactivity of this complex towards dioxygen is extremely slow and no formation of a dioxygen adduct complex could be observed.

Further efforts to synthesize a $[\text{Cu}(\text{dmp})\text{COD}]^+$ - or another $[\text{Cu}(\text{dmp})\text{olefin}]^+$ -complex (to gain more reactivity) also failed despite modified reaction conditions (concentration, solvent) and always resulted in the formation of three coordinated Cu(I) centres with acetonitrile as additional ligand instead of the olefin.

To avoid this unfavorable coordination it made sense to use a preparation route for these complexes without using tetrakis-acetonitrile-copper(I) salts as educt. Such a new oxidation-based synthetic route was recently developed by B. A. Ghandi et al.^[228] Copper powder is reacted with a silver salt according to the following equation:



But even with this method it was not possible to obtain the target molecules. Again molecular structures demonstrated that only crystals of 1:2 ratio of Cu(I) to dmp-ligand could be obtained. The structure of $[\text{Cu}(\text{dmp})_2]^+$ is shown in Figure 4-12. Crystal data, bond lengths and angles are given in Tables 4-13 and 4-14.

Table 4-11: Crystallographic data for $[\text{Cu}(\text{phen})\text{COD}]^+$

Empirical formula	$\text{C}_{40}\text{H}_{40}\text{Cu}_2\text{F}_{12}\text{N}_4\text{P}_2$		
Formula weight	993.78	F(000)	2016
Temperature (K)	200 (2)	Crystal size (mm)	0.1 x 0.1 x 0.4
Crystal system	monoclinic	θ range for data collected ($^\circ$)	1.71 to 28.34
Space group	PC(1)/n (no 14)	Index ranges	$-32 \leq h \leq 32$, $-9 \leq k \leq 9$, $-31 \leq l \leq 31$
Wavelength (\AA)	0.71073	Reflection collected	45562
Unit cell dimensions [\AA / $^\circ$]	a = 24.13(3) b = 6.89(8) c = 24.19(3) $\alpha = 90$ $\beta = 100.6(2)$ $\gamma = 90$	Independent refl., Rint	9662, 0.0674
		Completeness to theta	98.0% (theta = 28.34 $^\circ$)
		Goodness-of-fit on F^2	1.089
Z	4	R1 [$ I > 2\sigma(I) $]	0.1735
Density calcd. (Mg/m^3)	1.670	wR2 [$ I > 2\sigma(I) $]	0.4101
Volume [\AA^3]	3953.5(8)	R1 [all data]	0.2180
Absorpt. coeff. (cm^{-1})	1.251	wR2 [all data]	0.4307

Tab. 4-12: Selected bond lengths (\AA) and bond angles ($^\circ$) for $[\text{Cu}(\text{phen})\text{COD}]^+$

Cu(1)-N(1)	2.01(1)	C(13)-Cu(1)-N(1)	114.9(5)
Cu(1)-N(2)	2.01(1)	C(20)-Cu(1)-N(1)	149.3(6)
Cu(1)-C(13)	2.09(2)	C(20)-Cu(1)-N(2)	113.7(6)
Cu(1)-C(20)	2.12(2)	C(13)-Cu(1)-C(20)	38.0(6)
Cu(1)-C(17)	2.34(2)	C(17)-Cu(1)-N(2)	98.9(5)
Cu(1)-C(16)	2.48(2)	C(17)-Cu(1)-N(1)	120.6(5)
C(16)-C(17)	1.31(2)	C(16)-Cu(1)-N(1)	102.7(5)
C(20)-C(13)	1.37(2)	C(16)-Cu(1)-N(2)	125.2(5)
N(1)-Cu(1)-N(2)	84.2(4)	C(16)-Cu(1)-C(17)	31.4(5)
C(13)-Cu(1)-N(2)	146.7(5)		

Tab. 4-13: Crystallographic data for [Cu(dmp)₂]CF₃SO₃

Empirical formula	C ₂₉ H ₂₄ Cu F ₃ N ₄ O ₃ S		
Formula weight	629.12	F(000)	1288
Temperature (K)	193(2) K	θ range for data collected (°)	2.38 to 26.06
Crystal system	monoclinic	Reflection collected	19731
Space group	P2(1)/n	Independent refl., Rint	5364, 0.0882
Wavelength (Å)	0,71073	Completeness to theta 26.06	98.1 %
Unit cell dimensions [Å / °]	a = 13.55 (3) b = 11.09(2) c = 18.47(4) α = 90 β = 96.2(3) γ = 90	Index ranges	-16<=h<=16, -13<=k<=13, -22<=l<=22
Density calcd. (Mg/m ³)	1.513	Goodness-of-fit on F ²	0.884
Z	4	R1 [I>2σ(I)]	0.0489
Volume [Å ³]	2761.4(10)	wR2 [I>2σ(I)]	0.1057
Absorpt. coeff. (mm ⁻¹)	0.926	R1 [all data]	0.1000
Crystal size [mm]	0.16 x 0.08 x 0.08	wR2 [all data]	0.1237

Tab. 4-14: Selected bond lengths (Å) and bond angles (°) for [Cu(dmp)₂]CF₃SO₃

Cu(1)-N(1)	2.01 (3)	N(1)-Cu(1)-N(4)	131.4(1)
Cu(1)-N(2)	2.06 (3)	N(1)-Cu(1)-N(4)	131.4(1)
Cu(1)-N(3)	2.05(3)	N(3)-Cu(1)-N(2)	113.2(1)
Cu(1)-N(4)	2.02(3)	N(4)-Cu(1)-N(3)	82.3 (1)
N(1)-Cu(1)-N(2)	82.3 (1)	N(4)-Cu(1)-N(2)	122.2(1)
N(1)-Cu(1)-N(3)	129.5(1)	N(4)-Cu(1)-N(2)	122.2(1)

4.4.2.4 Oxidation with dioxygen

Despite the unfavorable aspect of two coordinated dmp molecules and an expected minor reactivity towards dioxygen, first attempts were made to oxidize this complex. First of all the [Cu(dmp)₂]⁺ was treated with air and after a few days crystals were obtained suitable for X-ray crystallographic studies.



Although it turned out that the crystals were either twinned or badly grown and thus did not allow a perfect determination of the crystal structure, it was at least possible to obtain a clear picture of the cation of the formed complex. The molecular structure of the product is shown in Figure 4-16 and crystallographic data, selected bond lengths and angles are given in Tables 4-15 and 4-16.

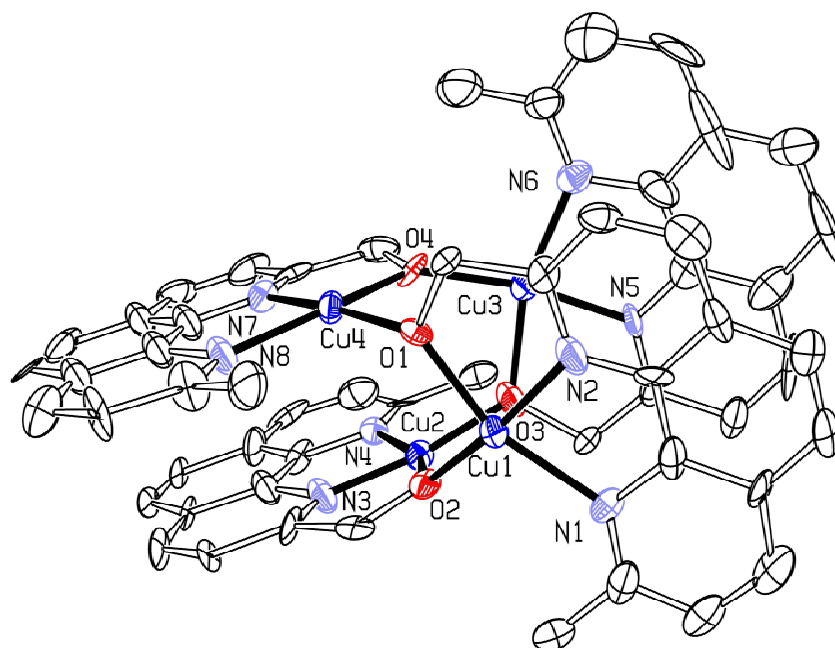


Figure 4-16: ORTEP plot of $[\text{Cu}_4(2\text{-methoxy-9-methyl-phenanthroline})_4]^{4+}$ (50% probability ellipsoids) hydrogen atoms omitted for clarity

The structure of the cation depicted in Figure 4-16 consists of four dimethylphenanthroline molecules, each two of them parallel and almost at right angles to the remaining two. The four copper centres, each in a distorted square planar environment, are each ligated by two phenanthroline nitrogen atoms and by two oxygen atoms which act as bridge between opposed copper centres.

The crystal structure shows that hydroxylation of a ligand methyl group occurred during the oxidation reaction with the result, that the copper(II) ion is now coordinated to the inserted oxygen of the alkoxide group. Recently, a related reaction has been observed by Maiti et al. who reported, that during the reaction of a copper(II) superoxo complex similar C-H substrate oxygenation was observed. In this work a copper oxo complex was proposed as reactive intermediate, responsible for the hydroxylation.^[229] Most likely the oxidation $[\text{Cu}(\text{dmp})_2]^+$ with dioxygen follows the same reaction pathway and the postulated mechanism is depicted in Figure 4-17.

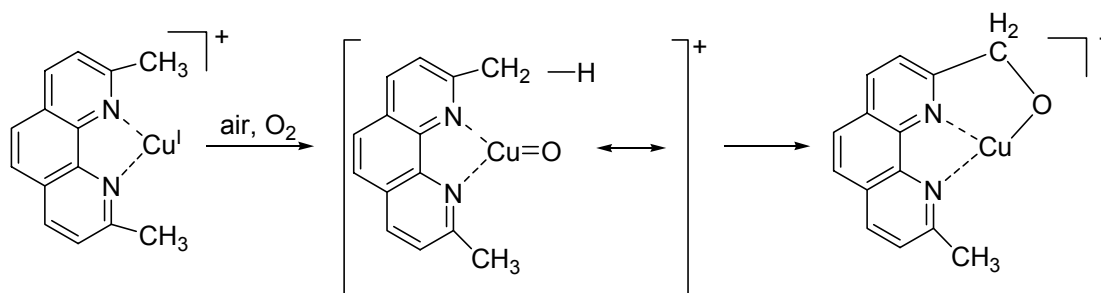


Figure 4-17: $[\text{Cu}(\text{dmp})_2]^+ + \text{O}_2$;

Proposed reaction pathway: Generation of a copper-oxo species?

Therefore, during the hydroxylation reaction of the $[\text{Cu}(\text{dmp})_2]^+$ complex should be the reactive intermediate an oxo species such as $\text{Cu}(\text{II})\text{O}^-$ ($\leftrightarrow \text{Cu}(\text{III})=\text{O}$) or $\text{Cu}(\text{III})\text{O}^-$ (i.e. $\{\text{CuO}\}^{2+}$).^[229-231] However, so far it was not possible to detect or isolate this intermediate. The methyl groups cannot stabilize such a reactive dioxygen intermediate and have been oxidized themselves. Therefore, more oxidant resistant and bulky groups such as CF_3 or tert-butyl at the positions 2 and 9 of the phenanthroline ligand system seem to be more appropriate for stabilizing such an intermediate. Furthermore phenanthroline derivatives with more bulky substituents offer the possibility to synthesize complexes with a copper(I) to ligand ratio of 1:1. These complexes are supposed to be more reactive towards dioxygen and may form an oxo species that can be detected and even isolated.

4.4.2.5 Ozonolysis

As the studied complexes showed only minor reactivity towards dioxygen an alternative strategy was applied. In iron chemistry Grapperhaus et al. reported previously that an iron(IV) oxo complex could be generated by ozonolysis of an iron(III)-cyclam-acetato complex.^[232] The formation of this oxo-species occurred during the reaction of ozone with an iron cyclam complex in an acetone/water mixture at -80°C . The generation of the iron oxo species could be detected by UV-vis- and Mössbauer analysis and the following mechanism, depicted in Figure 4-18 for the formation of this species was proposed.

With this background it seemed promising to use a similar approach for the synthesis of a copper oxo complex. Therefore, a solution of $[\text{Cu}(\text{dmp})_2]^+$ in acetone was cooled to -80°C and ozone (using different amounts/concentrations) was bubbled through it.

Interestingly a large number of different color changes occurred during the reaction process (Figure 4-19).

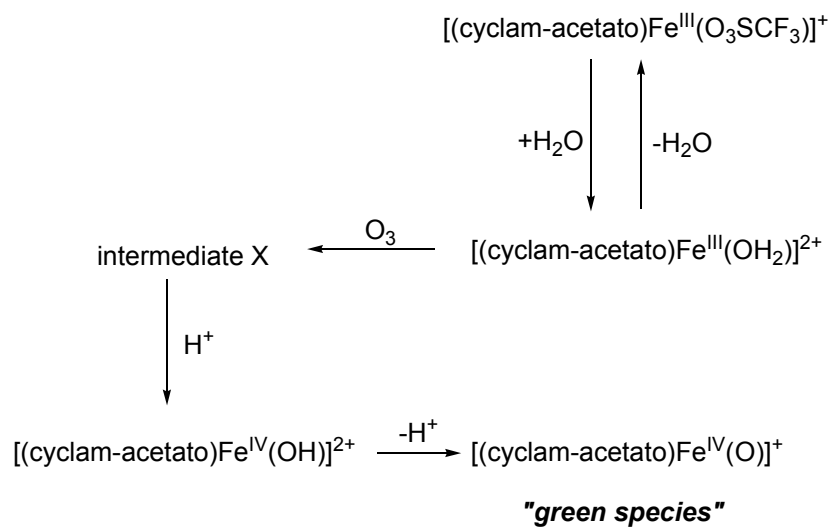


Figure 4-18: Generation of an iron(IV)oxo species by oxidizing with O₃

The color of the solution immediately turned from red to brown to green and blue. After warming the color of the solution turned again red. The spectral changes that occurred during the reaction under these conditions are shown in Figure 4-20.

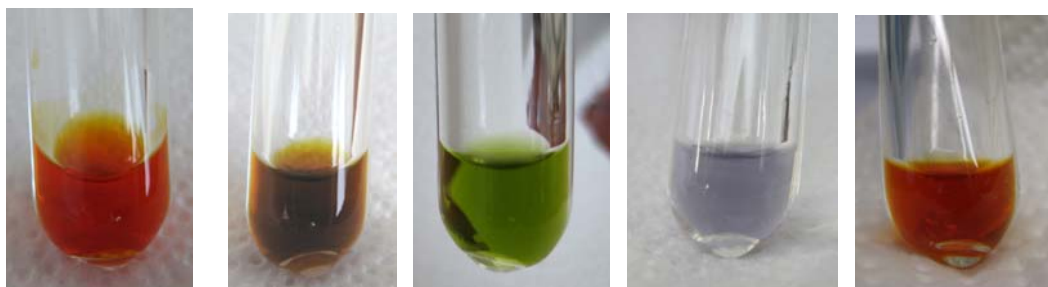


Figure 4-19: [Cu(dmp)₂]⁺ + O₃

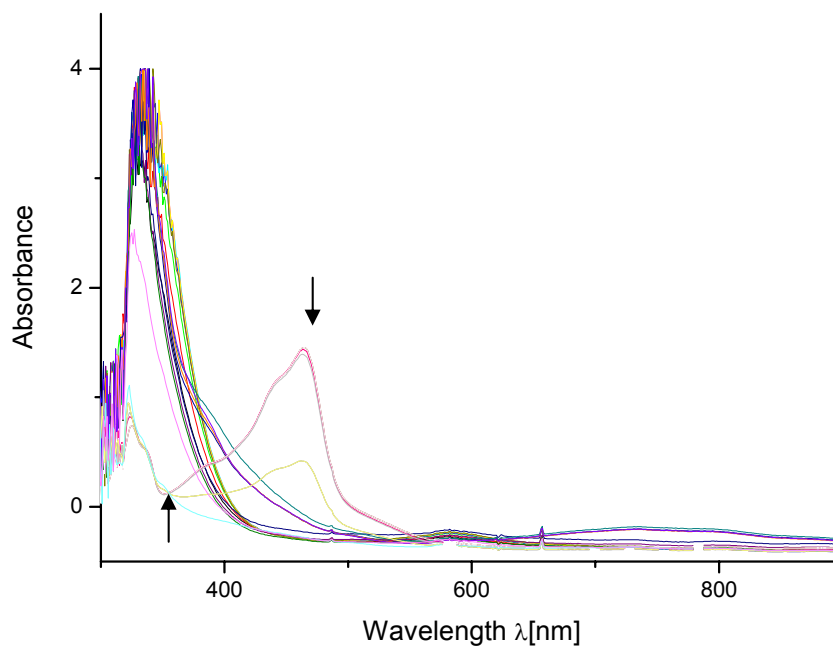


Figure 4-20: Spectral changes during reaction of $[\text{Cu}(\text{dmp})_2]^+$ with ozone in acetone ($T = -80^\circ\text{C}$, $[\text{complex}] = 1.0 \text{ mmol/l}$)

A buildup of an absorbance maximum at 327 nm and a decrease of absorbance at 460 nm could be observed. Interestingly the spectra detected after warming the solution to RT corresponds to the educt-spectra. These findings reveal a reversible formation of a possible “ O_2^- or O_3^- ” adduct complex as intermediate. So far it was not possible to detect spectroscopically any intermediate such as a dioxygen, an ozonide or an oxo species. The reaction is extremely interesting, however again it is more likely that it is possible to analyze the different intermediate products if a sterically more demanding phenantroline ligand will be used.

Tab. 4-15: Crystallographic data for [Cu₄(2-methoxy-9-methyl-phenanthroline)₄](CF₃SO₃)₄

Empirical formula	C _{17.14} H _{12.86} Cu _{1.14} F _{3.43} N _{2.29} O _{4.57} S _{1.14}		
Formula weight [g/mol]	498.41	θ range for data collected (°)	2.09 to 22.47
Temperature (K)	173(2) K	Reflection collected	18411
Z	7	Independent refl., Rint	9199, 0.0619
Wavelength (Å)	0.71073	Completeness to theta	98.0% (theta= 28.34°)
Unit cell dimensions [Å / °]	a = 13.92(3) b = 16.57(3) c = 19.12(4) α = 108.5(3) β = 98. 2(3) γ = 109.3(3)	Goodness-of-fit on F ²	2.773
		R1 [>2σ(I)]	0.2017
		Index ranges	-14<=h<=14 -17<=k<=17 -20<=l<=20
Density calcd. (Mg/m ³)	1.526	wR2 [>2σ(I)]	0.5646
Volume [Å ³]	3795.4(13)	R1 [all data]	0.2239
Absorpt. coeffic. (cm ⁻¹)	1.310	wR2 [all data]	0.5773
F(000)	1754		

Tab. 4-16: Selected bond lengths (Å) and bond angles (°) for [Cu₄(2-methoxy-9-methyl-phenanthroline)₄](CF₃SO₃)₄

Cu(1)-N(2)	1.86(3)	O(2)-Cu(1)-O(5)	95.1(7)
Cu(1)-O(2)	1.897(2)	N(2)-Cu(1)-O(2)	161.9(8)
Cu(1)-O(1)	2.01(2)	O(1)-Cu(1)-N(1)	160.4(7)
Cu(1)-N(1)	2.13(2)	N(2)-Cu(1)-O(5)	102.8(8)
Cu(1)-O(5)	2.33(2)	O(1)-Cu(1)-O(5)	100.3(7)
O(2)-Cu(1)-O(1)	92.8(6)	N(1)-Cu(1)-O(5)	87.2(7)
N(2)-Cu(1)-N(1)	78.8(9)	N(2)-Cu(1)-O(1)	81.9(8)
O(2)-Cu(1)-N(1)	104.6(7)		

4.5 Experimental Section

4.5.1 Materials and Reagents

Commercial reagents were used as obtained without further purification. Solvents were dried according to standard procedures. Absolute (dry) acetone for kinetic measurements was either obtained commercially (Acros) or by distillation of analytical grade acetone. All handling (as well as storage) of oxygen sensitive compounds and materials used in the kinetic studies was carried out in a glove box (M. Braun, Germany, O₂ < 0,1 ppm, H₂O < 0,1 ppm) under an argon atmosphere.

4.5.2 Physical Measurements

UV-vis spectra were measured using an Agilent 8453 diode-array spectrophotometer.

¹H NMR spectra were recorded on a Bruker-Aspect 2000/3000 400-MHz spectrometer by Dr. Hausmann (Institute for Organic Chemistry, JLU-Giessen).

4.5.3 Kinetic Measurements

Kinetic measurements of slower reactions were carried out using a stopped-flow unit (HI)-Tech Scientific SFA20 Rapid Kinetics Accessory) connected to the Agilent spectrophotometer.

Kinetic measurements of faster reactions were performed using a home built low temperature stopped-flow unit. A more detailed description of the stopped-flow technique and the used instruments has been described previously.^[97, 117] Additional information on the kinetics of inorganic reactions have been described in chapter 2. Data fitting was performed using Specfit and Origin (OriginLab Corporation, Northhampton, MA, USA).

The solutions of the copper(I) complexes were prepared in the glove box and then transferred into quartz cuvettes or glass syringes with attached valves. The concentration of the copper(I) complex solutions usually was adjusted to 1,0 x 10⁻⁴ mol/l.

A dioxygen saturated solution was prepared by bubbling dioxygen for 20 minutes through acetone. The solubility of dioxygen in acetone is 8.0 mmol/l at 20°C.^[116]

4.5.4 X-ray Crystallography

X-ray data were collected either on a Siemens SMART CCD diffractometer of the Forschungszentrum Karlsruhe or on a STOE Imaging Plate Diffraction System of the Justus-Liebig-University. Intensity data were collected on a Siemens SMART CCD 1000 diffractometer or on a STOE Imaging Plate Diffraction System equipped with a low temperature system (Karlsruher Glastechnisches Werk). The X-ray crystallographic data were collected by the ω -scan technique. The collected reflections were corrected for absorption, Lorentz and polarization effects.^[233] All structures were solved by direct methods and refined by least-squares techniques using the SHELX-97 program package.^[234] The hydrogen atoms were positioned geometrically and all non-hydrogen atoms were refined anisotropically, if not mentioned otherwise.

4.5.5 Synthesis of the complexes

The ligands bicyclopropylidene **bcp**, dicyclopropylacetylene **dcpa**, and Tetracyclo[7.3.1.1^{4,12}. 0^{2,7}]tetradeca-6,11-diene **tctd** were prepared by the research groups of Prof. A. de Meijere (bcp, dcpa) and Prof. P. Schreiner (tctd). The phenanthroline derivative 2,9-dimethyl-phenepoxide was prepared by co-workers of Prof. E. Schoffers. The Cu(I) salts [Cu(CH₃CN)₄]PF₆/ BF₄/ SbF₆/ CF₃SO₃ were prepared according to a procedure described in the literature.^[115]

4.5.5.1 [Cu₂(bipy)₂(tctd)](PF₆)₂

To a stirred solution of 37.2 mg (0.1 mmol) [Cu(CH₃CN)₄]PF₆ in 3 ml acetone 15.6 mg (0.1 mmol) of 2,2'-bipyridine was added. The resulting red solution was stirred furthermore for 2 hours and then an excess amount of tctd (160 mg, 0.8 mmol) was added. The solution was filtered through a pad of zeolite. Diffusion of diethyl ether into the solution at room temperature resulted in the formation of light yellow crystals suitable for X-ray structure determination.

4.5.5.2 [Cu(bipy)bcp]PF₆

37.2 mg (0.1 mmol) of [Cu(CH₃CN)₄]PF₆ and 15.6 mg (0.1 mmol) of 2,2'-bipyridine were dissolved in 3 ml acetone. After addition of 16 mg (0.2 mmol) of bicyclopropylidene the reaction mixture was stirred for 10 minutes and the color of the solution turned pale yellow. Vapor diffusion of diethyl ether into the complex solution yielded single crystals of [Cu(bipy)bcp]PF₆ suitable for X-ray characterization.

¹H-NMR (400 MHz, acetone d₆, δ/ppm):

1.59 (b s 8H), 7.87 (t 2H); 8.36 (t 2H); 8.7 (d 2H); 8.96 (d 2H)

¹³C-NMR (100 MHz, acetone d₆, δ/ppm):

9.1, 124.3, 129.3, 143.1, 151.1, 153.9

4.5.5.3 [Cu(bipy)dcpa]PF₆

38.8 mg (0.36 mmol) of dicyclopropylacetylene were added to a mixture of 37.2 mg (0.1 mmol) of [Cu(CH₃CN)₄]PF₆ and 15.6 mg (0.1 mmol) of bipyridine in 3 ml acetone under stirring. After 10 minutes the color of the solution turned pale yellow. Crystals suitable for X-ray characterization were obtained after several days by diffusion of ether into the solution at -5°C.

¹H-NMR (400 MHz, acetone d₆, δ/ppm):

0.56 (m 2H); 0.79 (m 2H); 1.36 (m 1H); 7.92 (t 2H); 8.41 (t 2H); 8.71 (d 2H); 9.01 (d 2H)

¹³C-NMR (100 MHz, acetone d₆, δ/ppm):

152.6, 150.8, 141.5, 127.7, 122.9, 80.8

4.5.5.4 [Cu₂(bipy)₂(OH)₂]²⁺

38.8 mg (0.36 mmol) of dicyclopropylacetylene were added to a mixture of 37.2 mg (0.1 mmol) of [Cu(CH₃CN)₄]PF₆ and 15.6 mg (0.1 mmol) of bipyridine in 3 ml acetone under stirring. After 10 minutes the color of the solution turned pale yellow. After

exposure to air, the color of the solution turned slightly blue and after a few days blue crystals suitable for X-ray characterization were obtained.

4.5.5.5 [Cu(phen)COD]PF₆

To a stirred solution of 372.7 mg (1 mmol) [Cu(CH₃CN)₄]PF₆ and 180.2 mg (1 mmol) 1,10-phenanthroline in 5 ml acetone an excess of 1,5-cyclooctadiene (3.24 g, 30mmol) in 5 ml acetone was added drop wise. The pale yellow solution turned grey and after stirring for one hour a grey colored precipitate was obtained which was collected by filtration and dried in vacuum. Dissolution of the complex in acetone and diffusion of diethyl ether at room temperature resulted in colorless crystals suitable for X-ray structural analysis.

¹H-NMR (400 MHz, acetone d₆, δ/ppm):

2.80 (s 8H), 5.95 (s 4H), 8.18 (q 2H), 8.32 (s 2H), 8.95 (dd 2H), 9.36 (dd, 2H)

¹³C-NMR (100 MHz, acetone d₆, δ/ppm)

30, 18.6, 127.6, 128.9, 131.3, 140.8, 145.2, 152.4

4.5.5.6 [Cu(dmp)₂]CF₃SO₃

To a stirred solution of 100 mg (0.481 mmol) 2,9-dimethylphenanthroline in acetone an excess of copper powder (1 g) and 123 mg (0.481 mmol) AgCF₃SO₃ were added portion wise. The bright red solution was stirred for 1 hour and then filtered off. Slow diffusion of diethyl ether resulted in red crystals suitable for X-ray structural analysis.

4.5.5.7 [Cu₄(2-methoxy-9-methyl-phenanthroline)₄]⁴⁺

In the glove box, a solution of [Cu(dmp)₂]CF₃SO₃ in acetone (1.0 mmol/l) was filled in a small test tube which was closed with a septum. Exposure to air resulted in a blue colored solution after several days. After 2 weeks blue crystals suitable for X-ray characterization were obtained.

4.5.6 Ozonolysis

In a typical experiment a solution of $[\text{Cu}(\text{dmp})_2]\text{CF}_3\text{SO}_3$ in acetone (1.0 mmol/l) was filled in a small test tube which was closed with a septum (in the glove box). If necessary, the solution was filtered to remove trace amounts of silver impurities.

The test tube was placed in a Dewar filled with ethanol at $-80\text{ }^\circ\text{C}$. The temperature of the solution was monitored during the reaction and remained constant within $5\text{ }^\circ\text{C}$. A stream of ozone provided by an ozone generator (Ozonosan PM 80, Germany) was passed through the solution for 10 - 30 min. Within 3 min the red color of the solution initially fades to brown, green and blue. For UV-vis measurements during ozonolysis, the reaction was performed in a quartz UV-vis cell closed with a septum at $-80\text{ }^\circ\text{C}$ up to room temperature with a constant ozone stream during the measurements.

Nickel-olefin complexes

5.1 Introduction

Nickel catalyzed reactions are of high interest in organic chemistry and play an integral role in laboratory as well as in industry. It is well known that various Ni(0) complexes are responsible for catalytic induced reactions such as oligomerization of alkenes, dienes and alkynes as well as C-C-coupling reactions. As mentioned before the catalytic dimerization of 1,3-butadiene to 1,5 cyclooctadiene (COD) using Ni(0) phosphane complexes as catalysts is performed on industrial scale and the mechanism of the reaction was investigated by Wilke and co-workers. [75, 81-85] Despite the fact that Ni(0) complexes are very air sensitive, several of these complexes were synthesized and characterized successfully in the Schindler group. For some of these complexes the reaction behavior was also investigated in detail. [235, 236] Interestingly, only a few Ni(0) bipyridine complexes with unsaturated hydrocarbons as ligands have been described so far. Amongst others H. Weiss could successfully synthesize and characterize the first nickel cyclopropene complex, which was demonstrated to be a crucial intermediate during the oxidative cyclization of cyclopropenes at the nickel(0) site.

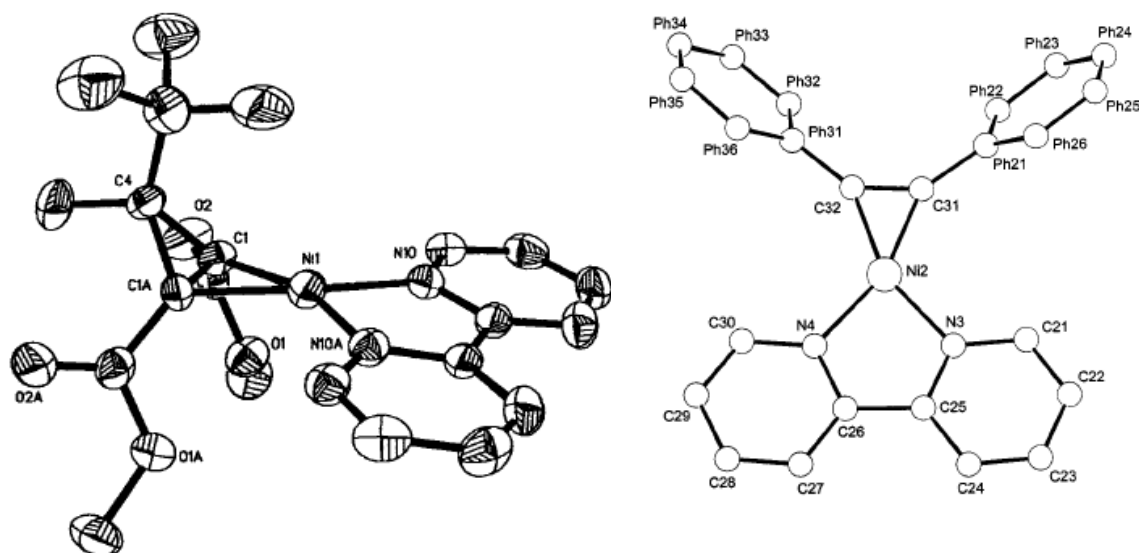


Figure 5-1: Right: ORTEP plot of nickel(0) cyclopropene complex^[235]
(50% probability ellipsoids) hydrogen atoms omitted for clarity

Left: Molecular structure of 2,2-bipyridyl (η^2 -diphenylacetylene)nickel^[79]

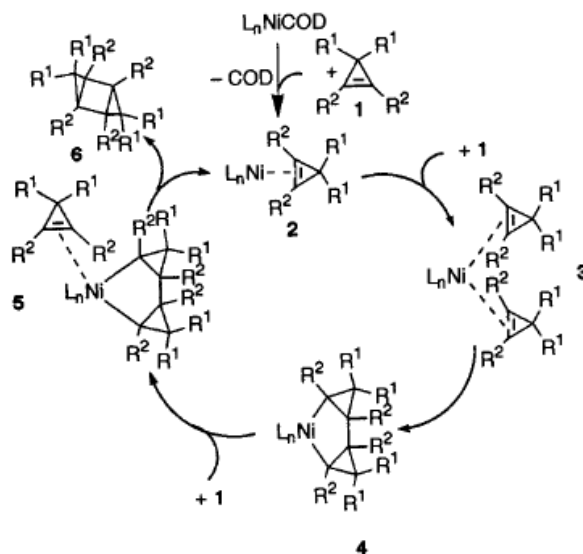


Figure 5-2: Proposed mechanism for the catalytic oxidative cyclization of cyclopropenes with Ni(0) complexes

The structure is depicted in Figure 5-1, the mechanism in Figure 5-2. Another previously reported bipyridine complex is the 2,2-bipyridyl (η^2 -diphenylacetylene)nickel complex, characterized by Eisch and co-workers (Figure 5-1).^[79]

5.2 Ni(0) complex with dcpa and bcp as ligands

To gain a better understanding of the properties of Ni(0) complexes with unsaturated compounds as ligands in regard to their possible application as catalysts in organic synthesis, we thought it could be interesting to prepare and to investigate Ni(0) complexes with bipyridine and unsaturated ligands. Within the collaboration with the research group of de Meijere from the University of Göttingen the olefin bicyclopropylidene **bcp** (a) and the alkyne dicyclopropylacetylene **dcpa** (b) were used as special ligands for complexation of Ni(0). (Figure 5-3) This is in complete analogy to the copper(I) complexes with these ligands described in chapter 4.2.

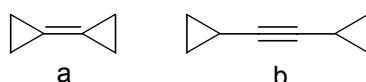
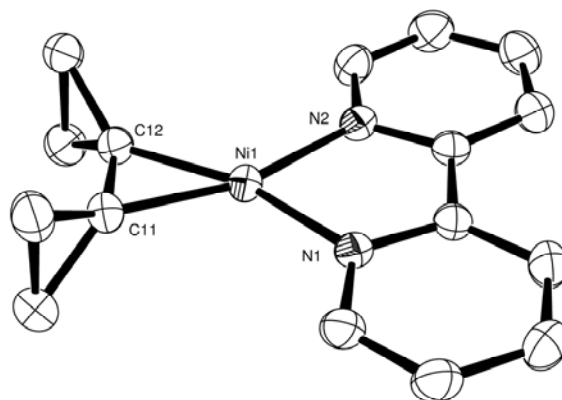


Figure 5-3: Bicyclopropylidene (a) and dicyclopropylacetylene (b)

Prior to the investigations of the nickel dcpa complex described herein, a bcp nickel complex was successfully obtained by L. Römmling in the Schindler group.^[197]

Crystals of [Ni(bipy)bcp] were characterized by X-ray studies and the reaction of the precursor [Ni(bipy)COD] with bcp was investigated kinetically using stopped flow technique. The proposed mechanism was in line with the one previously postulated by H. Weiss, which is depicted in Figure 5-2. The determined structure of the obtained [Ni(bipy)bcp] is shown in Figure 5-4 and the reaction mechanism is depicted in Figure 5-5.



**Figure 5-4: ORTEP plot of [Ni(bipy)bcp] ^[197]
(50% probability ellipsoids) hydrogen atoms omitted for clarity**

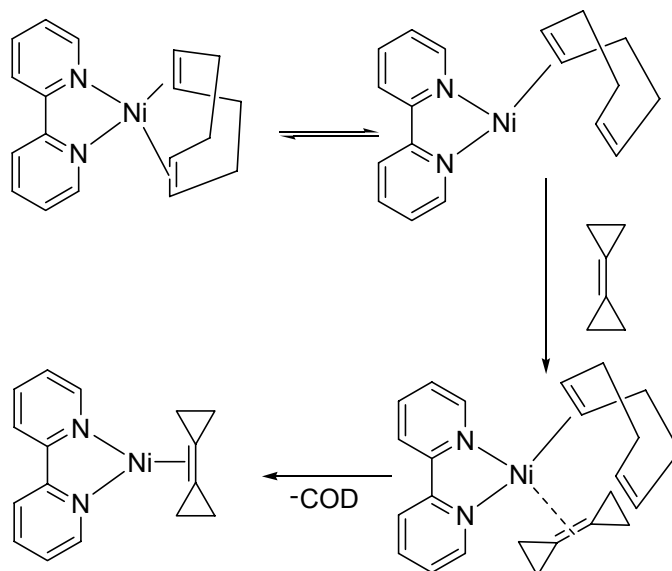


Figure 5-5: Proposed mechanism for [Ni(bipy)COD] with bcp

5.3 Results

5.3.1 [Ni(bipy)dcpa]

Due to the successful preparation and investigation of the complex [Ni(bipy)bcp] we were interested in obtaining the related [Ni(bipy)dcpa] complex and to investigate its formation mechanism.

Therefore [Ni(bipy)COD] was mixed with an excess amount of dcpa in THF obtaining pale yellow crystals suitable for crystallography study. The determined structure of [Ni(bipy)dcpa] is in line with the related [Cu(bipy)dcpa]PF₆ complex and with the previously reported complex of J. J. Eisch et al. The structure of the complex is depicted in Figure 5-6. The crystallographic data are shown in Table 5-2, bond lengths and angles are given in Table 5-3.

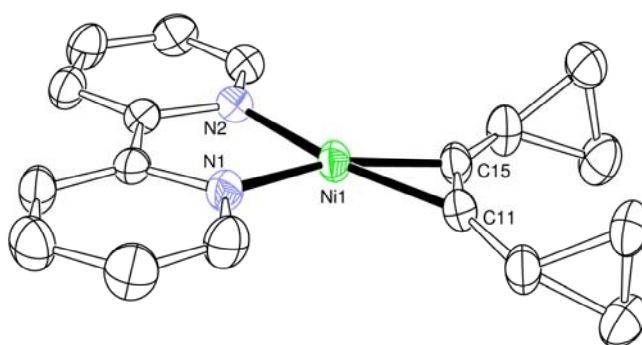


**Figure 5-6: ORTEP plot of [Ni(bipy)dcpa]
(50% probability ellipsoids) hydrogen atoms omitted for clarity**

The structure of [Ni(bipy)dcpa] shows characteristic trigonal planar Ni(0) geometry with a nickel center being coordinated by two nitrogen atoms of bipyridine and the triple bond of dicyclopropylacetylene. The essentially planar interaction of the bipyridyl ligand and the C≡C is evident (Figure 5-6). The average of Ni-C_{alkyne} distances of 1.85(2) Å is similar with σ-Ni-C bonds involving sp²-hybridized carbon centers.^[79, 237] Due to this the acetylenic C-C separation with 1.28(3) is more congruent with a C-C double bond than with the presence of a triple bond. Compared with the related copper(I) complex [Cu(bipy)dcpa]⁺ the separation of the C-C (alkyne) found in the Ni(0) complex is remarkably larger. This is in line with the fact that copper(I) is supposed to be a poorer π-back bonding metal center as Ni(0).

5.3.2 Mechanistic studies of the reaction of [Ni(bipy)COD] with dcpa

Mechanistic studies of such reactions are quite difficult due to the extreme sensitivity of dilute solutions of nickel(0) complexes towards traces of dioxygen. However, in the past the Schindler group successfully managed to overcome these difficulties by using special techniques for handling of the samples.

The formation of [Ni(bipy)dcpa] can be followed by UV-vis spectra using stopped flow techniques. Time-resolved spectra for the reaction of [Ni(bipy)COD] with dcpa are shown in Figure 5-7. Isosbestic points were observed at 390 nm and 485 nm. The reaction rate is significantly slower compared to the related reaction of [Ni(bipy)COD] with cyclopropene or bcp. However, due to the previous findings from H. Weiss it was supposed, that the reaction follows a simple rate law such as

$$\frac{d[\text{Ni}(\text{bipy})\text{COD}]}{dt} = k[\text{Ni}(\text{bipy})\text{COD}][\text{dcpa}].$$

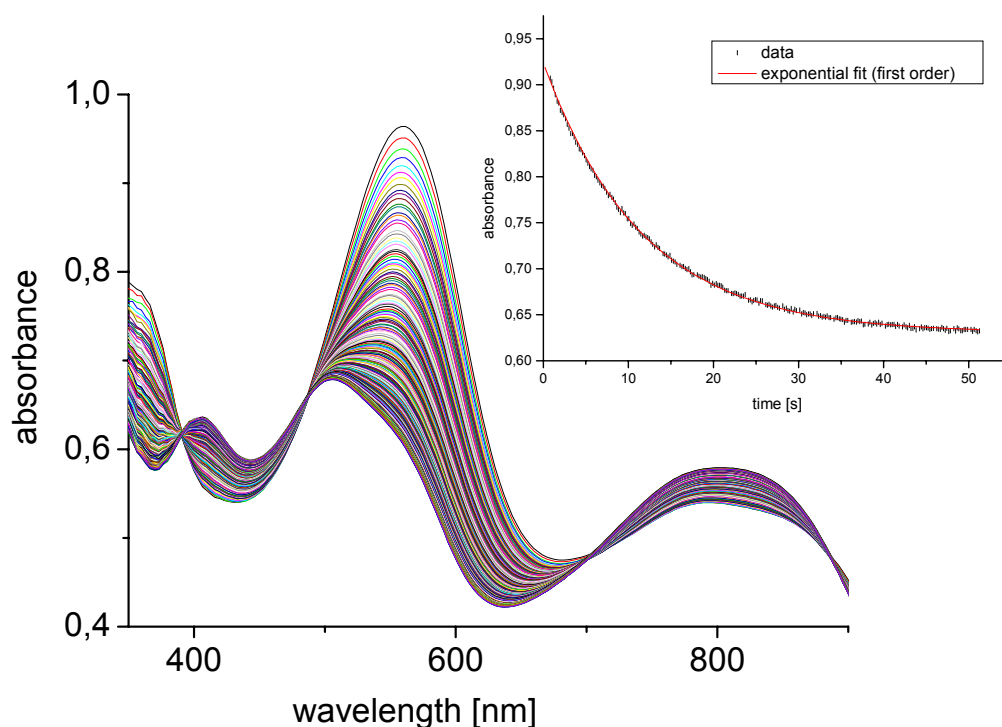


Figure 5-7: Spectral changes during reaction of [Ni(bipy)COD] with dcpa in THF

(T= 20.1 °C, [complex] = 0.25 mmol/l, [dcpa] = 30 mmol/l, t = 51.256 s)

Insert: Absorbance vs. time trace at 561nm and fit to a single one-exponential function

$$(k_{\text{obs}} = (83 \pm 6) \times 10^{-3} \text{s}^{-1})$$

However, it was not possible to obtain acceptable fittings to single one-exponential functions for all considered concentrations of dcpa over the selected temperature range. The decomposition of [Ni(bipy)COD] which arises from the labile ligand COD impeded the kinetic measurements, although an excess of COD was added to suppress this annoying side reaction. Moreover, the high temperature range (10-25°C) applied in this kinetic study supported the decomposition of [Ni(bipy)COD].

However, the reaction of [Ni(bipy)COD] with dcpa proved to be slower than observed for [Ni(bipy)COD] with bcp. This could be understandable as the substitution of COD and the coordination of the C-C triple bond of dcpa might be inhibited kinetically. The obtained dependence of the observed rate constant k_{obs} on the concentration of dcpa at different temperatures is almost linear. In contrast to the previously studied reaction of [Ni(bipy)COD] with bcp, an intercept is obtained (Figure 5-8).

This intercept may indicate that the reaction is reversible and therefore a second-order rate constant for a forward or back reaction can be assumed. In that regard and due to the difficulties that occurred during the measurements, a more detailed kinetic analysis of this reaction has not been possible.

Table 5-1: Measured reaction rates of the reaction of [Ni(bipy)COD] with dcpa in THF: [Ni(bipy)COD] = 0.25 mmol/l

dcpa [mM]	k_{obs}/s^{-1}			
	10°C	15°C	20°C	25°C
10	$(19 \pm 4) \times 10^{-3}$	$(29 \pm 7) \times 10^{-3}$	$(42 \pm 10) \times 10^{-3}$	$(54 \pm 13) \times 10^{-3}$
15	$(24. \pm 8) \times 10^{-3}$	$(35 \pm 11) \times 10^{-3}$	$(50 \pm 16) \times 10^{-3}$	
20	$(24 \pm 5) \times 10^{-3}$	$(36 \pm 8) \times 10^{-3}$	$(53 \pm 11) \times 10^{-3}$	$(62 \pm 15) \times 10^{-3}$
25	$(32 \pm 4.) \times 10^{-3}$	$(43 \pm 6) \times 10^{-3}$	$(62 \pm 8) \times 10^{-3}$	$(73 \pm 10) \times 10^{-3}$
30	$(32 \pm 2) \times 10^{-3}$	$(44 \pm 3) \times 10^{-3}$	$(84 \pm 6) \times 10^{-3}$	$(114 \pm 8) \times 10^{-3}$

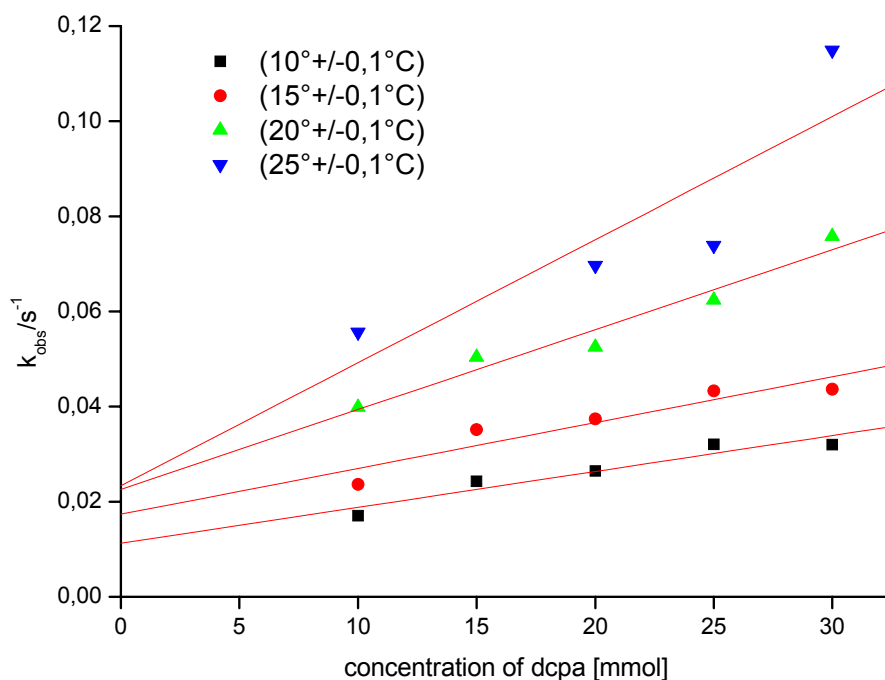


Figure 5-8: Plot of observed rate constants k_{obs} vs dcpa concentration at different temperatures: $[\text{Ni}(\text{bipy})\text{COD}] = 0.25\text{mmol/l}$

Table 5-2: Crystallographic data for $[\text{Ni}(\text{bipy})\text{dcpa}]$

Empirical formula	$\text{C}_{24} \text{H}_{24} \text{N}_{2.67} \text{Ni}_{1.33}$		
Formula weight	428.07	F(000)	672
Temperature (K)	200(2)	Crystal size (mm)	0.3 x 0.15 x 0.05
Crystal system	monoclinic.	θ range for data collected ($^\circ$)	1.94 to 28.29
Space group	P2(1)/c (no 14)	Index ranges	12 \leq h \leq 14. -13 \leq k \leq 12. -19 \leq l \leq 18
Wavelength (Å)	0.71073	Reflection collected	10000
Unit cell dimensions [$\text{Å} / ^\circ$]	a = 11.10(5) $\alpha = 90$ b = 9.83(6) $\beta = 108.8(5)$ c = 14.5(8) $\gamma = 90$	Independent refl..	3628. 0.0508
		Completeness to theta	92.3 % (theta= 28.29 $^\circ$)
		Goodness-of-fit on F^2	0.938
Z	3	R1 [$I > 2\sigma(I)$]	0.0398
Density calcd. (Mg/m^3)	1.556	wR2 [$I > 2\sigma(I)$]	0.0756
Volume [Å^3]	1495.8(14)	R1 [all data]	0.0790
Absorpt. coeff. (cm^{-1})	1.426	wR2 [all data]	0.0840

Table 5-3: Selected bond lengths (Å) and bond angles (°) for [Ni(bipy)dcpa]

Ni(1)-N(1)	1.93(2)	N(1)-Cu(1)-N(2)	82.6(3)
Ni(1)-N(2)	1.92(2)	N(3)-Cu(1)-N(4)	83.0(3)
Ni(1)-C(11)	1.85(3)	N(1)-Cu(1)-N(4)	116.6(2)
Ni(1)-C(15)	1.85(3)	N(1)-Cu(1)-N(3)	130.6(2)
C(11)-C(15)	1.28(3)	N(2)-Cu(1)-N(3)	121.0(3)
		N(4)-Cu(1)-N(2)	129.4(3)

5.4 Experimental Section

5.4.1 Materials and Reagents

Commercial reagents were used as obtained without further purification. Solvents were dried according to standard procedures. Absolute (dry) THF for kinetic measurements was either obtained commercially (Acros) or by distillation of analytical grade THF over sodium. All handling (as well as storage) of the oxygen sensitive Ni(0) compounds and materials used in the kinetic studies was carried out in a glove box (M. Braun, Germany, O₂ < 0,1 ppm, H₂O < 0,1 ppm) within argon atmosphere. The complex [Ni(bipy)COD] was previously prepared in the Schindler group and could be used without further purification.

5.4.2 Kinetic Measurements

Variable temperature stopped-flow measurements allowed the collection of time-resolved UV-vis spectra for reaction of [Ni(bipy)COD] with dcpa in THF. The solutions of the complex were prepared in a glovebox and transferred using syringes to the low-temperature stopped-flow instrument.

The reaction was studied under pseudo-first-order conditions ([Ni(bipy)COD] << [dcpa]) and the concentration of the solutions were 10 mmol/l up to 30 mmol/l (concentration is determined after mixing with solvent during measurement). Temperature was varied from 10°C up to 25°C. Time-resolved UV-vis spectra of these reactions were recorded with a home built stopped-flow unit or with a modified Hi-Tech SF-3L low-temperature stopped-flow unit (Salisbury, U.K.) equipped with a J&M TIDAS 16-500 photodiode array spectrophotometer (J&M, Aalen, Germany). Data fitting was performed using the integrated J&M software Kinspec and Origin (OriginLab Corporation, Northhampton, MA, USA). Details on such studies have been described previously.^[117] Additional informations about kinetic of inorganic reactions are given in Chapter 2.

5.4.3 X-ray Crystallography

Intensity data were collected on a Siemens SMART CCD 1000 diffractometer equipped with a low temperature system (Karlsruher Glastechnisches Werk). The X-ray crystallographic data were collected by the ω -scan technique. The collected

reflections were corrected for absorption, Lorentz and polarization effects.^[233] All structures were solved by direct methods and refined by least-squares techniques using the SHELX-97 programme package.^[234] The hydrogen atoms were positioned geometrically and all non-hydrogen atoms were refined anisotropically, if not mentioned otherwise.

5.4.4 Synthesis of the complexes

The ligand dcpa was prepared by the research group of Prof. A. de Mejere.

5.4.4.1 [Ni(bipy)(dcpa)]

To a stirred purple suspension of 3.2 mg (0.01 mmol) [Ni(bipy)COD] in 2 ml THF 106 mg (1 mmol) dcpa in 2 ml THF was added (both solutions were precooled to -20°C). The resulting solution was stirred furthermore for 2 hours. The solution was filtered of a pad of zeolite. Diffusion of n-pentane into the solution -5°C resulted in crystals suitable for X-ray structure determination.

Summary

Selective oxidations of organic substrates using a catalyst and air as an oxidant play an important role in the field of so called “green chemistry”. Nature has demonstrated that these reactions in principle are possible. Therefore, chemists have been trying for some years to model the reactivity of the according metalloenzymes using low molecular weight complexes as catalysts instead.

Thus hydroxylation reactions are important and are catalyzed for example by copper based enzymes such as the monooxygenase tyrosinase. This enzyme is responsible for the hydroxylation of monophenols to *o*-diphenols and the subsequent two-electron oxidation to *o*-quinones. However, so far a complete mechanism for this oxidation reaction could not be postulated. Therefore, to obtain a better understanding on this type of reaction, a Cu(I)bis(imine)complex [Cu₂(DAPA)]²⁺ (DAPA = 1,3-bis-[(3-(*N*-dimethyl)propyl)iminomethyl]benzene) has been synthesized and the structure of its Cu(I) complex as well as the structure of the Cu(II) product complex exhibiting a hydroxylated ligand was analyzed and characterized. The observed ligand hydroxylation reaction mediated by this complex was investigated spectroscopically (the optical absorption and vibrational spectra), kinetically and by quantum chemical DFT analysis.

The kinetic analysis of the ligand hydroxylation provided evidence for O₂-binding being the rate-limiting step in the overall reaction. The conversion into the hydroxylated Cu(II) complex was found to proceed much faster in methanol than in acetonitrile, which is due to the fact that the acetonitrile ligands of the Cu(I) precursor have to be displaced in order to bind O₂. Moreover, an inverse kinetic isotope effect (KIE) was observed for the reaction in acetonitrile while in methanol, however, no KIE was detected.

The DFT analysis of reaction of the Cu(I) precursor and O₂ demonstrated that the dominant barrier after O₂ binding is represented by the electrophilic attack of a $\mu\text{-}\eta^2\text{:}\eta^2$ peroxy intermediate on the arene ring. The reactivity of this Cu(II) peroxy intermediate proposed the presence of four pathways to the hydroxylated final product. One of the pathways studied involves the rearrangement of the $\mu\text{-}\eta^2\text{:}\eta^2$ peroxy structure to a $\mu\text{-}\eta^2\text{:}\eta^1$ peroxy intermediate that subsequently attacks the

SUMMARY

aromatic ring. However, the energetically favorable pathways identified in the DFT study involve a direct decay of the $\mu\text{-}\eta^2\text{:}\eta^2$ peroxy intermediate without rearrangement. Furthermore no stable bis($\mu\text{-oxo}$) isomer is formed in the ligand environment studied here, although its formation is expected from former studies. In contrast the energetically most favorable route provides the formation of a rather stable dienone intermediate which subsequently undergoes a second proton transfer step leading to the product formation. This scenario involves as a key intermediate the conversion of the peroxy complex to the hydroxylated product the dienone intermediate, which should eventually be detectable experimentally. (Chapter 3)

Besides the investigations on the activity of tyrosinase, efforts have been made to synthesize and characterize an oxo species in copper chemistry which is considered to be a highly reactive intermediate responsible for many oxidizing processes. However, isolation and characterization of such a species is lacking so far.

In that regard several Cu(I) complexes with nitrogen donor ligands such as bipyridine **bipy** and phenanthroline **phen** and derivatives were synthesized. To further increase the reactivity of these complexes towards dioxygen olefin ligands such as cyclooctadiene were used as co ligands to allow facile substitution reactions. The reactivity of these complexes towards air, dioxygen as well as ozone was investigated by bench top experiments and by using UV-vis spectroscopy. Therefore the reactivity of the well known complex $[\text{Cu}(\text{bipy})\text{COD}]^+$ towards dioxygen was investigated, but no formation of an adduct complex was detected. These findings are also valid for the reactivity towards dioxygen of the so far unknown complex $[\text{Cu}(\text{phen})\text{COD}]\text{PF}_6$, which was successfully characterized using X-ray diffraction methods during this work. Unfortunately, no formation of an oxo species or any other dioxygen adduct complexes was observed spectroscopically under these conditions. These findings showed that complexes such as $[\text{Cu}(\text{bipy})]^+$ or $[\text{Cu}(\text{phen})]^+$ were not capable to stabilize such sensitive and reactive intermediates. Therefore 2,9-dimethylphenanthroline **dmp** was used as ligand which is more sterically hindered. Oxidation of $[\text{Cu}(\text{dmp})_2]^+$ resulted in insertion of dioxygen and the oxidation product $[\text{Cu}_4(2\text{-methoxy-9-methyl-phenanthroline})_4]^{4+}$: one methyl group of each dmp ligand was hydroxylated. Therefore the formation of an oxo species such as Cu(II)O^- , $(\leftrightarrow \text{Cu(III)=O})$, Cu(III)O^- or $\{\text{CuO}\}^{2+}$ during the hydroxylation reaction of the

[Cu(dmp)₂]⁺ complex can be postulated. Unfortunately, it was not possible to isolate such an oxo-species or even to detect it spectroscopically in the course of the reaction (Chapter 4.4).

Phenanthroline and its derivatives are not only assumed to be suitable to stabilize dioxygen adduct complexes, its complexes are also supposed to be catalysts and templates for asymmetric synthesis. Therefore in collaboration with Prof. E. Schoffers several copper complexes with derivatives of phenanthroline were synthesized and characterized. The crystal structure of [Cu(dmpe)₂]PF₆ x 1/2 CH₃CONH₂ is reported herein. Interestingly an amide molecule can be found in every second unit cell. Its formation is assumed from a reaction of acetonitrile and traces of water. Due to this a catalytic influence of the Cu(I) center is revealed (Chapter 4.3).

However, considering “greener chemistry”, there is great interest in transition metal complexes containing unsaturated compounds and their reaction behavior. In collaboration with the research group of Prof. A. deMeijere Cu(I) and Ni(0) complexes with the unsaturated hydrocarbons bicyclopropylidene **bcp** and dicyclopropylacetylene **dcpa** were synthesized and characterized by X-ray analysis:

- [Cu(bipy)bcp]PF₆
- [Cu(bipy)dcpa]PF₆
- [Ni(bipy)dcpa]

The reported crystal structures of [Cu(bipy)dcpa]PF₆ and [Ni(bipy)dcpa] are supposed to be the first Ni(0) and Cu(I) complexes containing dcpa as ligand. (Chapters 4.2 and 5)

The behavior of the Cu(I) complexes towards dioxygen was investigated, but no formation of a dioxygen adduct complex could be detected during oxidation. When [Cu(bipy)bcp]PF₆ was exposed to air, [Cu₂(bipy)₂(OH)₂]²⁺ was obtained. No polymerization or other reaction of acetylene catalyzed by the coordinated copper center could be observed (Chapter 4.2).

The formation of [Ni(bipy)dcpa] from the reaction of [Ni(bipy)COD] and dcpa was investigated using stopped flow techniques (Chapter 5).

Furthermore, in collaboration with the research group of Prof. P. Schreiner a copper(I) complex with the adamantane derivative (tetracyclo [7.3.1.1^{4,12}.0^{2,7}]tetradeca-6,11-diene **tctd**) could be synthesized and the crystal structure of $\text{Cu}_2(\text{bipy})_2(\text{tctd})(\text{PF}_6)_2$ is reported herein. Complexes of transition metals containing such adamantane derivatives are supposed to have catalytic properties useful for several reactions in organic chemistry. In this regard also strong efforts have been made to synthesize the Ni(0) complex, but no crystals suitable for X-ray diffraction could be obtained. (Chapter 4.1)

Zusammenfassung

Die selektive Oxidation organischer Substrate durch Luftsauerstoff mit Hilfe von Katalysatoren spielt eine wichtige Rolle im Bereich "Green Chemistry". Die Natur hat uns gezeigt, dass solche Reaktionen durchaus möglich sind. Daher ist es für die chemische Forschung schon seit Jahren eine Herausforderung, die aus der Natur bekannten, meist enzymatischen Reaktionen, mit Hilfe von synthetischen Modellkomplexen nachzuahmen. Eine wichtige Rolle in diesem Zusammenhang spielen kupferhaltige Enzyme, wie zum Beispiel die Monooxygenase Tyrosinase. Dieses Enzym ist für die Hydroxylierung von o-Phenol zu Diphenol und für die anschließende Oxidation zum o-Chinon verantwortlich. Trotz intensiver Untersuchungen konnte bisher der genaue Reaktionsmechanismus für diese Umsetzung noch nicht aufgeklärt werden. Um solche Hydroxylierungsreaktionen besser zu verstehen, wurde im Rahmen dieser Arbeit ein Kupfer(I)-Bis-Imin-Komplex $[\text{Cu}_2(\text{DAPA})]^{2+}$ (DAPA = 1,3-bis-[(3-(N-dimethyl)propyl)iminomethyl]benzol synthetisiert und charakterisiert. Ebenso wurde der Kupfer(II)-Komplex dargestellt und kristallographisch charakterisiert. Die durch den Komplex vermittelte Hydroxylierung wurde spektroskopisch verfolgt und untersucht (Absorptions- und Schwingungsspektroskopie). Weiterhin wurden kinetische Untersuchungen durchgeführt und DFT-Berechnungen angefertigt.

Bei den kinetischen Messungen konnte gezeigt werden, dass die Anbindung des Sauerstoffs der geschwindigkeitsbestimmende Schritt ist. Die sich anschließende Umwandlung in den hydroxylierten Kupfer(II)-Komplex läuft dabei in Methanol bedeutend schneller ab als in Acetonitril. Dies lässt sich durch die koordinierten Acetonitrilmoleküle begründen, die der anbindende Sauerstoff ersetzen muss. Weiterhin konnte in Acetonitril ein inverser Isotopeneffekt beobachtet werden, während dies in Methanol nicht der Fall war.

Die DFT-Berechnungen für die Reaktion des Kupfer(I)-Vorläufer-Komplexes mit O_2 haben gezeigt, dass nach der Anbindung des Sauerstoffs der elektrophile Angriff des $\mu\text{-}\eta^2\text{:}\eta^2$ -Intermediats auf das aromatische Ringsystem die größte energetische Barriere während der Hydroxylierungsreaktion darstellt. Aufgrund der Reaktivität des gebildeten Peroxo-Intermediats sind vier verschiedene Reaktionswege, die zum hydroxylierten Produkt führen, möglich. Einer dieser bereits in früheren Arbeiten

untersuchten Reaktionswege geht von der Umlagerung der $\mu\text{-}\eta^2\text{:}\eta^2$ -Peroxo-Struktur in ein $\mu\text{-}\eta^2\text{:}\eta^1$ -Intermediat aus, welches dann anschließend den Aromaten angreift. Durch die DFT-Rechnungen konnte allerdings gezeigt werden, dass ein direkter Zerfall des Intermediats ohne Umlagerung energetisch günstiger ist. Auch konnte die Bildung eines bis(μ -oxo)-Isomers nicht bestätigt werden, obwohl dies in früheren Arbeiten als mögliches Intermediat vermutet wurde. Vielmehr zeigten die Berechnungen, dass die Ausbildung eines recht stabilen Dienons der energetisch günstigste Reaktionsweg ist. Dieses Dienon geht nach zweimaliger Protonenübertragung in das hydroxylierte Produkt über. Bei dieser Reaktion spielt es eine Schlüsselrolle und sollte daher auch experimentell nachweisbar sein. (Kapitel 3)

Neben Untersuchungen zur Tyrosinase-Aktivität sollte es Ziel dieser Arbeit sein, einen Kupfer-Oxo-Komplex zu erhalten und spektroskopisch bzw. kristallographisch zu charakterisieren. Diese sehr reaktiven Oxo-Intermediate sind vermutlich für viele Oxidationsprozesse verantwortlich, konnten allerdings in der Kupfer-Chemie noch nicht erfolgreich isoliert und untersucht werden.

Daher wurden im Rahmen dieser Arbeit verschiedene Kupfer(I)-Komplexe mit Stickstoff-Donorliganden wie Bipyridin oder Phenanthrolin und deren Derivate dargestellt. Um die Reaktivität dieser Komplexe gegenüber Sauerstoff zu erhöhen, wurden verschiedene Olefin-Liganden wie zum Beispiel Cyclooctadien COD an diese Komplexe angebunden. Es hat sich gezeigt, dass diese Olefin-Liganden nur schwach an das Kupfer-Zentrum koordiniert sind und somit leicht gegen Sauerstoff ausgetauscht werden können. Die Reaktivität dieser Komplexe gegenüber Luft, reinem Sauerstoff und Ozon wurde in Bench-Top-Versuchen und anschließend mit Hilfe der UV-vis-Spektroskopie untersucht. In diesem Zusammenhang wurden der in der Literatur bekannte $[\text{Cu}(\text{bipy})\text{COD}]\text{PF}_6$ Komplex synthetisiert und dessen Reaktivität gegenüber Sauerstoff untersucht. Allerdings konnte keine Ausbildung eines Sauerstoff-Addukt-Komplexes beobachtet werden. Gleiches gilt für die Reaktivität des noch nicht in der Literatur bekannten Komplexes $[\text{Cu}(\text{phen})\text{COD}]\text{PF}_6$, der im Rahmen dieser Arbeit auch erfolgreich dargestellt und kristallographisch charakterisiert werden konnte. Diese Untersuchungen zeigten, dass „einfache“ Cu(I)phen- und Cu(I)bipy-Komplexe unter diesen Bedingungen nicht in der Lage sind, reaktive Sauerstoffintermediate auszubilden und diese zu stabilisieren, was

eine Isolierung und spektroskopische Charakterisierung unmöglich macht. Aus diesem Grund wurde für weitere Untersuchungen der sterisch anspruchsvollere Ligand 2,9-Dimethylphenanthrolin dmp verwendet. Oxidation des Komplexes $[\text{Cu}(\text{dmp})_2]^+$ an Luft führte zu $[\text{Cu}_4(2\text{-methoxy-9-methyl-phenanthroline})_4]^{4+}$ als Oxidationsprodukt, wobei jeweils eine Methylgruppe des dmp-Liganden hydroxyliert worden ist. Aufgrund ähnlicher Beobachtungen in anderen Arbeiten, liegt die Vermutung nahe, dass als reaktives Intermediat ein Kupfer-Oxo-Komplex $\text{Cu}(\text{II})\text{O}^-$ ($\leftrightarrow \text{Cu}(\text{III})=\text{O}$), $\text{Cu}(\text{III})\text{O}^-$ or $\{\text{CuO}\}^{2+}$ ausgebildet wird und für die Hydroxylierung der Methylgruppen verantwortlich ist. Dennoch war es nicht möglich, diese Oxo-Spezies tatsächlich zu isolieren oder spektroskopisch zu detektieren. (Kapitel 4.4.)

Phenanthrolin und dessen Derivate sind aber nicht nur zur Stabilisierung möglicher Sauerstoff-Addukt-Komplexe geeignet, sondern es hat sich gezeigt, dass Phenanthrolin-Komplexe auch besondere katalytische Eigenschaften haben und als Template in asymmetrischen Synthesen genutzt werden können. Im Rahmen einer Zusammenarbeit mit Prof. E. Schoffers wurden daher verschiedene Kupfer-Komplexe mit Phenanthrolinderivaten erfolgreich dargestellt und charakterisiert. Dabei konnte diese interessante Beobachtung gemacht werden: Die Kristallstruktur des Komplexes $[\text{Cu}(\text{dmpe})_2]\text{PF}_6 \times 1/2 \text{CH}_3\text{CONH}_2$ weist in jeder zweiten Einheitszelle ein Acetamidmolekül auf, welches sich vermutlich katalytisch durch Hydrolyse von vorhandenem Acetonitril und Spuren von H_2O gebildet hat. Dies sollte in einer weiterführenden Arbeit näher untersucht werden (Kapitel 4.3).

Bezüglich "Green Chemistry" besteht seit Jahren großes Interesse an der Erforschung von Übergangsmetallkomplexen mit ungesättigten Liganden und deren Reaktionsverhalten. In Zusammenarbeit mit der Arbeitsgruppe von Prof. A. deMeijere (Universität Göttingen) gelang die erfolgreiche Darstellung und Charakterisierung folgender Cu(I) und Ni(0)-Komplexe mit den ungesättigten Kohlenwasserstoffen Bicyclopropylidene **bcp** und Dicyclopropylacetylene **dcpa**:

- $[\text{Cu}(\text{bipy})\text{bcp}]\text{PF}_6$
- $[\text{Cu}(\text{bipy})\text{dcpa}]\text{PF}_6$
- $[\text{Ni}(\text{bipy})\text{dcpa}]$

Die in dieser Arbeit gezeigten und beschriebenen Kristallstrukturen von $[\text{Cu}(\text{bipy})\text{dcpa}]\text{PF}_6$ und $[\text{Ni}(\text{bipy})\text{dcpa}]$ sind die ersten bekannten Cu(I) und Ni(0)-Komplexe mit dem Liganden dcpa (Kapitel 4.2 und Kapitel 5).

Das Reaktionsverhalten dieser Kupfer(I)-Komplexe gegenüber Sauerstoff wurde ebenfalls untersucht. Dabei zeigte es sich wiederum, dass aufgrund des zu geringen Stabilisierungsvermögens des bipy-Liganden kein reaktives Sauerstoff-Intermediat beobachtet werden konnte. Bei der Reaktion des Komplexes $[\text{Cu}(\text{bipy})\text{dcpa}]\text{PF}_6$ mit Luft wurde $[\text{Cu}_2(\text{bipy})_2(\text{OH})_2]^{2+}$ als Oxiaditionsprodukt erhalten. Eine eventuell erwartete katalytisch induzierte Polymerisationsreaktion des koordinierten Acetylens konnte nicht beobachtet werden. Die Kinetik der Bildung des Komplexes $[\text{Ni}(\text{bipy})\text{dcpa}]$ aus $[\text{Ni}(\text{bipy})\text{COD}]$ und dcpa wurde mit Hilfe von Stopped-Flow-Technik untersucht. (Kapitel 5)

Im Rahmen einer weiteren Zusammenarbeit mit der Arbeitsgruppe von P. Schreiner (Universität Gießen) war es möglich, ein weiteres ungewöhnliches Olefin für die Komplexierung mit Kupfer(I)-Ionen zu verwenden. Das Adamantan-Derivat (Tetracyclo[7.3.1.1^{4,12}.0^{2,7}]tetradeca-6,11-Dien **tctd**) konnte erfolgreich zu dem Komplex $\text{Cu}_2(\text{bipy})_2(\text{tctd})(\text{PF}_6)_2$ umgesetzt werden. Bei solchen Übergangsmetallkomplexen mit koordinierten Adamantan-Derivaten werden besondere katalytische Eigenschaften vermutet, die für die Organische Synthese von Nutzen sein könnten. Dies muss aber noch in weiterführenden Untersuchungen gezeigt werden. Leider gelang es im Rahmen dieser Arbeit nicht, den entsprechenden Ni(0)-Komplex zu charakterisieren, da keine für kristallographische Untersuchungen geeigneten Kristalle erhalten werden konnten. (Kapitel 4.1)

Publication

- Sander, O.; Henß, A.; Näther, C.; Würtele, C.; Holthausen, M. C.; Schindler, S.; Tucek, F.;. Aromatic Hydroxylation in a Copper Bis(imine) Complex Mediated by a μ - η^2 : η^2 Peroxo Dicopper Core: A Mechanistic Scenario *Chem. Eur. J.*, **2008**, in press.

Presentations

- Poster presentation: DFG Schwerpunkttagung in Schleiden (05/2006)
Substrate Oxidations with Iron and Copper Complexes
- Poster presentation: GDCh-Tagung in Ulm (09/2007)
Reactivity of Ni(0) complexes towards alkenes and alkynes
- Oral presentation: Koordinationschemietreffen in Gießen (02/2008)
Kupfer-Phenanthrolin-Komplexe

Curriculum Vitae

Persönliche Daten

Anja Henß, geb. Ozdoba
Frankfurter Str. 42
35392 Giessen

03.10.1978 in Jena geboren,
verheiratet
ein Kind

Ausbildungsweg und Schule

1985 - 1989	Grundschule / Jena
1989 - 1992	Gesamtschule / Jena
1992 –1999	Gymnasium / Johanneum-Gymnasium Herborn
06/1999	Abitur (Note 1,4)

Universitätsstudium

10/1999- 09/2005	Studium der Chemie an der Justus-Liebig Universität Gießen
03/2002	Vordiplom (Note „Sehr gut“)
03/2004	Diplom-Prüfung
03/2004 – 02/2005	Erziehungsjahr
02/2005 – 09/2005	Diplomarbeit „ Synthese, Charakterisierung und Reaktivität von Kupferkomplexen mit zweizähnigen Stickstoffliganden“ in der Arbeitsgruppe von Prof. Dr. Siegfried Schindler am Institut für Anorganische und Analytische Chemie
09/2005	Diplomabschluss (Note „Sehr gut“(1,1))

CURRICULUM VITAE

10/2005 – 10/2008 Promotion in der Arbeitsgruppe von Prof. Dr. Siegfried Schindler am Institut für Anorganische und Analytische Chemie; Thema: "Investigations of the reaction behavior of copper and nickel complexes with N-donor- or olefin-ligands"

Tätigkeiten

06/2001-09/2001 Praktikum bei der Unternehmensberatung „Mummert und Partner“ in Frankfurt a.M.

04/2002- 03/2004 Studentische Hilfskraft an der JLU, Betreuung von Nebenfachstudenten

12/2005 Wissenschaftliche Mitarbeiterin an der JLU, Betreuung des Anorganisch Chemischen Grundpraktikums für Chemiker und Materialwissenschaftler, Betreuung des Fortgeschrittenen Praktikums im Hauptstudium Chemie, Betreuung des Koordinationschemie-Praktikums (I/II)

Bibliography

- [1] W. Kaim, B. Schwederski, in *Bioanorganische Chemie*, Teubner Verlag, Stuttgart, **1991**, p. 204 ff.
- [2] S. J. Lippard, J. M. Berg, *Bioanorganische Chemie*, Spektrum Akademischer Verlag, **1995**.
- [3] E. A. Lewis, W. B. Tolman, *Chem. Rev.* **2004**, *104*, 1047.
- [4] L. M. Mirica, X. Ottenwaelder, T. D. P. Stack, *Chem. Rev.* **2004**, *104*, 1013.
- [5] A. F. Holleman, E. Wiberg, *Lehrbuch der Anorganischen Chemie*, Walter de Gruyter, Berlin, New York, **1995**.
- [6] W. Kaim, J. Rall, *Angew. Chem.* **1996**, *108*, 47.
- [7] K. D. Karlin, Z. Tyeklár, *Bioinorganic Chemistry of Copper*, Chapman & Hall, New York, **1993**.
- [8] M. C. Linder, in *Biochemistry of copper*, Plenum, New York, **1991**.
- [9] M. Costas, M. P. Mehn, M. P. Jensen, L. Que Jr., *Chem. Rev.* **2004**, *104*, 939.
- [10] M. Pascaly, I. Jolk, B. Krebs, *Chemie in Unserer Zeit* **1999**, *33*, 334.
- [11] E. I. Solomon, U. M. Sundaram, T. E. Machonkin, *Chem. Rev.* **1996**, *96*, 2563.
- [12] R. Ho, J. Liebman, J. Valentine, in *Active Oxygen in Chemistry* (Eds.: C. Foote, J. Valentine, A. Greenberg, J. Liebman), Chapman & Hall, **1995**, p. 2 ff.
- [13] H. Decker, T. Schweikhardt, F. Tuczek, *Angew. Chem., Int. Ed.* **2006**, *45*, 4546.
- [14] Y. Matoba, T. Kumagai, A. Yamamoto, H. Yoshitsu, M. Sugiyama, *J. Biol. Chem.* **2006**, *281*, 8961.
- [15] T. Klabunde, C. Eicken, J. C. Sacchettini, B. Krebs, *Nature Structural Biology* **1998**, *5*, 1084.
- [16] E. I. Solomon, U. M. Sundaram, T. E. Machonkin, *Chem. Rev.* **1996**, 2563.
- [17] C. Gerdemann, C. Eicken, B. Krebs, *Acc. Chem. Res.* **2002**, *35*, 183.
- [18] I. A. Koval, P. Gamez, C. Belle, K. Selmeçzib, J. Reedijk, *Chem. Soc. Rev.* **2006**, *35*, 814.
- [19] E. Kim, E. E. Chufan, K. Kamaraj, K. D. Karlin, *Chem. Rev.* **2004**, *104*, 1077.
- [20] K. D. Karlin, Y. Gultneh, *Prog. Inorg. Chem.* **1987**, 219.
- [21] S. Schindler, *Eur. J. Inorg. Chem.* **2000**, 2311.
- [22] Z. Tyeklar, K. D. Karlin, *Acc. Chem. Res.* **1989**, *22*, 241.
-

BIBLIOGRAPHY

- [23] H. Decker, R. Dillinger, F. Tuczek, *Angew. Chem.* **2000**, *112*, 1656.
- [24] E. I. Solomon, P. Chen, M. Metz, S.-K. Lee, A. E. Palmer, *Angew. Chem.* **2001**, *113*, 4702.
- [25] E. I. Solomon, R. H. Holm, **2004**, *104*, 347.
- [26] R. R. Jacobson, Z. Tyeklar, A. Farooq, K. D. Karlin, S. G. Liu, J. Zubieta, *J. Am. Chem. Soc.* **1988**, *110*, 3690.
- [27] Z. Tyeklar, R. R. Jacobson, N. N. Wei, N. Murthy, J. Zubieta, K. D. Karlin, *J. Am. Chem. Soc.* **1993**, *115*, 2677.
- [28] K. D. Karlin, M. S. Nasir, B. I. Cohen, R. W. Cruse, S. Kaderli, A. D. Zuberbühler, *J. Am. Chem. Soc.* **1994**, *116*, 1324.
- [29] K. D. Karlin, P. L. Dahlstrom, S. N. Cozzette, P. M. Scensny, J. Zubieta, *J. Am. Chem. Soc., Chem. Commun.* **1981**, 881.
- [30] K. D. Karlin, J. C. Hayes, Y. Gultneh, R. W. Cruse, J. W. McKown, J. P. Hutchinson, J. Zubieta, *J. Am. Chem. Soc.* **1984**, *106*, 2121.
- [31] M. Becker, S. Schindler, K. D. Karlin, T. K. Kaden, S. T. P. Kaderli, A. D. Zuberbühler, *Inorg. Chem.* **1999**, *38*, 1989.
- [32] E. Pidcock, S. DeBeer, H. V. Obias, B. Hedman, K. O. Hodgson, K. D. Karlin, E. I. Solomon, *J. Am. Chem. Soc.* **1999**, *121*, 1870.
- [33] K. D. Karlin, M. S. Nasir, B. I. Cohen, R. W. Cruse, S. T. P. Kaderli, A. D. Zuberbuehler, *J. Am. Chem. Soc.* **1994**, *116*.
- [34] P. L. Holland, K. R. Rodgers, W. B. Tolman, *Angew. Chem., Int. Ed.* **1999**, *38*.
- [35] C. Würtele, K. Gaoutchenova, K. Harms, M. C. Holthausen, J. Sundermeyer, S. Schindler, *Angew. Chem.* **2006**, *118*, 3951.
- [36] M. Schatz, V. Raab, S. P. Foxon, G. Brehm, S. Schneider, M. Reiher, M. C. Holthausen, J. Sundermeyer, S. Schindler, *Angew. Chem.* **2004**, *43*, 4360.
- [37] K. A. Magnus, B. Hazes, h. Ton-That, C. Bonaventura, J. Bonaventura, W. J. H. Hol, *Proteins: Struct. Funct. Genet.* **1994**, 302.
- [38] E. I. Solomon, F. Tuczek, D. E. Root, C. A. Brown, *Chem. Rev.* **1994**, *94*, 827.
- [39] M. Dekker, in *Bioinorganic Catalysis* (Eds.: J. Reedijk, E. Bouwman), New York, **1993**.
- [40] T. N. Sorell, V. A. Vankai, M. L. Garrity, *Inorg. Chem.* **1991**, *30*, 207.
- [41] T. N. Sorell, M. L. Garrity, *Inorg. Chem.* **1991**, *30*, 210.
- [42] L. Casella, M. Gullotti, M. Bartosek, G. Pallaza, E. Lauernti, *J. Chem. Soc., Chem. Commun.* **1991**, *18*, 1235.
-

BIBLIOGRAPHY

- [43] S. Mahapatra, S. T. P. Kaderli, A. Llobet, Y.-M. Neuhold, T. Palanche, J. A. Halfen, V. G. Young junior, L. Que Jr., A. D. Zuberbuehler, W. B. Tolman, *Inorg. Chem.* **1997**, *36*.
- [44] T. N. Sorell, *Tetrahedron* **1989**, *45*.
- [45] A. G. Blackman, W. B. Tolman, *Struct. Bonding* **2000**, *97*.
- [46] G. Battaini, L. Casella, M. Gullotti, E. Monzani, G. Nardin, A. Perotti, L. Randaccio, L. Santagostini, F. W. Heinemann, S. Schindler, *Inorg. Chem.* **2003**, *1197*.
- [47] H. Ma, M. Allmendinger, U. Thewalt, A. Lentz, M. Klinga, B. Rieger, *Eur. J. Inorg. Chem.* **2002**, *11*.
- [48] D. Utz, F. W. Heinemann, F. Hampel, D. T. Richens, S. Schindler, *Inorganic Chemistry* **2003**, *42*, 1430.
- [49] S. Ryan, H. Adams, D. E. Fenton, M. Becker, S. Schindler, *Inorg. Chem.* **1998**, *37*, 2134.
- [50] M. Becker, S. Schindler, R. van Eldik, *Inorg. Chem.* **1994**, *33*.
- [51] R. Menif, A. E. Martell, P. J. Squattrito, A. Clearfield, *J. Am. Chem. Soc.* **1990**, *29*.
- [52] R. Menif, A. E. Martell, *J. Chem. Soc., Chem. Commun.* **1989**, *20*.
- [53] O. J. Gelling, F. A. M. van Bolhuis, B. Feringa, *J. Chem. Soc., Chem. Commun.* **1988**, *8*, 552.
- [54] L. Casella, M. Gullotti, G. Pallaza, L. Rigoni, *J. Am. Chem. Soc.* **1988**, *110*, 4221.
- [55] L. Casella, M. Gullotti, G. Pallaza, *Biochem. Soc. Trans.* **1988**, *16*, 821.
- [56] M. G. B. Drew, J. Trocha-Grimshaw, K. P. McKillop, *Polyhedron* **1989**, *8*.
- [57] M. T. Miller, P. K. Gantzel, T. B. Karpishin, *Angew. Chem.* **1998**, *110*, 1659.
- [58] G. F. Smith, W. H. McCurdy, *Anal. Chem.* **1952**, *24*, 371.
- [59] H. Schwarz, D. Schroeder, *Pure Appl. Chem.* **2000**, *72*, 2319.
- [60] M. H. Lim, J. Rohde, A. Stubna, M. R. Bukowski, M. Costas, R. Ho, E. Münck, W. Nam, J. Que, L., *Proc. Natl. Acad. Sci. U.S.A.* **2003**, *100*.
- [61] J. Kaizer, E. J. Klinker, N. Y. Oh, J. Rohde, W. J. Song, A. Stubna, J. Kim, E. Münck, W. Nam, L. Que Jr., *J. Am. Chem. Soc.* **2004**, *126*.
- [62] J. Rohde, J. In, M. H. Lim, W. W. Brennessel, M. R. Bukowski, A. Stubna, E. Münck, W. Nam, L. Que Jr., *SCIENCE* **2003**, *299*, 1037.
-

BIBLIOGRAPHY

- [63] D. Schroeder, M. C. Holthausen, H. Schwarz, *J. Phys. Chem.* **2004**, *108*, 14407.
- [64] J. S. Thompson, R. L. Harlow, F. J. Whitney, *J. Am. Chem. Soc.* **1983**, *105*, 3522.
- [65] J. S. Thompson, R. M. Swiatek, *Inorg. Chem.* **1985**, *24*, 110.
- [66] J. S. Thompson, F. J. Whitney, *J. Am. Chem. Soc.* **1983**, *105*, 5488.
- [67] J. S. Thompson, F. J. Whitney, *Inorg. Chem.* **1984**, *24*, 2813.
- [68] M. Munakata, S. Kitagawa, H. Shimono, H. Masuda, *Inorg. Chem.* **1991**, *30*, 2610.
- [69] P. Jolly, G. Wilke, in *The organic chemistry of nickel, Vol. 1 and 2*, Academic Press, New York, London.
- [70] S. I. Ikeda, *Angew. Chem.* **2003**, *115*, 5276.
- [71] Y. Tamaru, in *Modern organonickel chemistry, Vol. 1*, Wiley-VCH, Weinheim, **2005**, p. 327.
- [72] W. Geibel, G. Wilke, R. Goddard, C. Krueger, R. Mynott, *J. Organometal. Chem.* **1978**, *160*.
- [73] W. Reppe, O. Schichting, K. Klager, T. Toepel, *Ann.* **1948**, *560*, 1.
- [74] W. Reppe, W. J. Sweckendiek, *Ann.* **1948**, *560*.
- [75] G. Wilke, *Pure Appl. Chem.* **1978**, *50*.
- [76] W. Gausing, G. Wilke, *Angew. Chem.* **1978**, *90*.
- [77] B. Bodanovic, M. Kroener, G. Wilke, *Ann.* **1966**, *699*.
- [78] G. Wilke, *Angew. Chem.* **1960**, *72*.
- [79] J. J. Eisch, X. Ma, K. I. Han, J. N. Gitua, C. Krueger, *Eur. J. Inorg. Chem.* **2001**, *77*.
- [80] G. Schiffer, G. Oenbrink, in *Ullmann's Encyclopedia of Industrial Chemistry*, Wiley-VCH, **2002**.
- [81] P. W. Jolly, in *Comprehensive Organometallic Chemistry* (Eds.: F. G. Wilkinson, A. Stone, E. Abel), Pergamon, New York, **1982**, p. 671.
- [82] G. Wilke, *Angew. Chem.* **1963**, *75*.
- [83] G. Wilke, *J. Organometal. Chem.* **1980**, *200*.
- [84] G. Wilke, *Angew. Chem.* **1988**, *100*.
- [85] G. Wilke, A. Eckerle, in *Applied Homogeneous Catalysis with Organometallic Complexes* (Eds.: B. Cornils, W. A. Herrmann), Wiley-VCH, Weinheim, **1996**.
- [86] S. Tobisch, T. Ziegler, *J. Am. Chem. Soc.* **2002**, *124*.
-

BIBLIOGRAPHY

- [87] M. T. Kieber-Emmons, C. G. Riordan, *Acc. Chem. Res.* **2007**, *40*, 618.
- [88] V. Leclere, P. Boiron, R. Blondeau, *Curr. Microbiol.* **1999**, *39*, 365.
- [89] H.-D. Youn, E.-J. Kim, J.-H. Roe, Y. C. Hah, S.-O. Kang, *Biochem. J.* **1996**, *318*, 889.
- [90] H.-D. Youn, H. Youn, J.-W. Lee, Y.-I. Yim, J. K. Lee, Y. C. Hah, S.-O. Kang, *Arch. Biochem. Biophys.* **1996**, *334*, 341.
- [91] B. Palenik, B. Brahamsha, F. W. Larimer, M. Land, L. Hauser, P. Chain, J. Lamerdin, W. Regala, E. E. Allen, J. McCarren, I. Paulsen, A. Dufresne, F. Partensky, E. A. Webb, J. Waterbury, *Nature* **2003**, *424*, 1037.
- [92] Y. Dai, P. C. Wensink, R. H. Abeles, *J. Biol. Chem.* , *274*, 1193.
- [93] Y. Dai, T. C. Pochapsky, R. H. Abeles, *Biochemistry* **2001**, *40*, 6379.
- [94] J. Polster, *Reaktionskinetische Auswertung spektroskopischer Messdaten*, Vieweg, Braunschweig/ Wiesbaden, **1995**.
- [95] R. B. Jordan, *Mechanismen anorganischer und metallorganischer Reaktionen*, Teubner Studienbücher Chemie, Stuttgart, **1994**.
- [96] J. H. Espenson, *Chemical Kinetics and Reaction Mechanisms*, McGraw-Hill, New York, **1995**.
- [97] R. G. Wilkins, *Kinetics and Mechanism of Reactions of Transition Metal Complexes*, 2 ed., VCH: Weinheim, **1991**.
- [98] A. Sanchez-Ferrer, J. N. Rodríguez-López, F. García-Cánovas, F. García-Carmona, *Biochimica et Biophysica Acta* **1995**, *210*, 1.
- [99] C. Eicken, C. Gerdemann, B. Krebs, in *Handbook of Metalloproteins* (Eds.: A. Messerschmidt, R. Huber, T. Poulos, K. Wieghardt), J. Wiley & Sons, **2001**, p. 1319.
- [100] M. Trémolières, J. B. Bieth, *Phytochem.* **1984**, *23*, 501.
- [101] H. Decker, in *Encyclopedia of Inorganic Chemistry Vol. 2*, 2 ed. (Ed.: R. B. King), Wiley, New York, **2006**, p. 1159.
- [102] K. E. van Holde, K. I. Miller, H. Decker, *Journal of Biological Chemistry* **2001**, *276*, 15563.
- [103] S. P. Foxon, D. Utz, J. Astner, S. Schindler, F. Thaler, F. W. Heinemann, G. Liehr, J. Mukherjee, V. Balamurugan, D. Ghosh, R. Mukherjee, *Dalton Transactions* **2004**, 2321.
- [104] G. Ghosh, R. Mukherjee, *Inorg. Chem.* **1998**, *37*, 6597.
- [105] L. Li, A. A. N. Sarjeant, K. D. Karlin, *Inorganic Chemistry* **2006**, *45*, 7160.
-

BIBLIOGRAPHY

- [106] P. E. M. Siegbahn, *Journal of Biological Inorganic Chemistry* **2003**, *8*, 567.
- [107] P. E. M. Siegbahn, M. Wirstam, *Journal of the American Chemical Society* **2001**, *123*, 11819.
- [108] S. Itoh, M. Taki, H. Nakao, P. L. Holland, W. B. Tolman, L. Que, S. Fukuzumi, *Angewandte Chemie-International Edition* **2000**, *39*, 398.
- [109] E. Pidcock, H. V. Obias, C. X. Zhang, K. D. Karlin, E. I. Solomon, *Journal of the American Chemical Society* **1998**, *120*, 7841.
- [110] A. Company, S. Palavicini, I. Garcia-Bosch, R. Mas-Balleste, L. Que, E. V. Rybak-Akimova, L. Casella, X. Ribas, M. Costas, *Chemistry-a European Journal* **2008**, *14*, 3535.
- [111] L. M. Mirica, D. J. Rudd, M. A. Vance, E. I. Solomon, K. O. Hodgson, B. Hedman, T. D. P. Stack, *Journal of the American Chemical Society* **2006**, *128*, 2654.
- [112] L. M. Mirica, M. Vance, D. J. Rudd, B. Hedman, K. O. Hodgson, E. I. Solomon, T. D. P. Stack, *Science* **2005**, *308*, 1890.
- [113] P. Amudha, P. Akilan, M. Kandaswamy, *Polyhedron* **1999**, *18*, 1355.
- [114] B. Feringa, in *Bioinorganic Chemistry of Copper* (Ed.: K. Karlin, Tyeklar, Z.), Chapman & Hall, **1993**, p. 306.
- [115] G. J. Kubas, B. Monzyk, A. L. Crumbliss, *Inorg. Synth.* **1979**, *19*, 90.
- [116] S. V. Kryatov, E. V. Rybak-Akimova, S. Schindler, *Chemical Reviews* **2005**, *105*, 2175.
- [117] M. Weitzer, M. Schatz, F. Hampel, F. W. Heinemann, S. Schindler, *J. Chem. Soc., Dalton Trans.* **2002**, 686.
- [118] A. D. Becke, *Phys. Rev. A* **1988**, *38*, 3098.
- [119] A. D. Becke, *J. Chem. Phys.* **1993**, *98*, 5648.
- [120] C. Lee, W. Yang, R. G. Parr, *Phys. Rev. B* **1988**, *37*, 785.
- [121] P. J. Stephens, F. J. Devlin, C. F. Chabalowski, M. J. Frisch, *Journal of Physical Chemistry* **1994**, *98*, 11623.
- [122] F. Neese, 2.5.00 ed., Universität Bonn (Germany), **2006**, pp. An ab initio.
- [123] A. Schaefer, H. Horn, R. Ahlrichs, *J. Chem. Phys.* **1992**, *97*, 2571.
- [124] F. Neese, *Journal of Computational Chemistry* **2003**, *24*, 1740.
- [125] F. Neese, G. Olbrich, *Chemical Physics Letters* **2002**, *362*, 170.
- [126] K. Eichkorn, O. Treutler, H. Ohm, M. Haser, R. Ahlrichs, *Chemical Physics Letters* **1995**, *240*, 283.
-

- [127] K. Eichkorn, F. Weigend, O. Treutler, R. Ahlrichs, *Theoretical Chemistry Accounts* **1997**, *97*, 119.
- [128] R. A. Kendall, H. A. Fruchtl, *Theoretical Chemistry Accounts* **1997**, *97*, 158.
- [129] A. Klamt, G. Schürmann, *J. Chem. Soc. Perkin Trans. 2* **1993**, 799.
- [130] A. Klamt, (Eds.: N. L. N. L. Allinger, T. T. Clark, J. Gasteiger, P. Kollmann, H. F. Schaefer, P. v. R. Schleyer, P. R. Schreiner), Wiley, Chichester, **1998**, p. 604.
- [131] *We successfully repeated some of the transition state searches with identical results (to numerical accuracy) with the extended geometry optimization routines implemented in the most recent ORCA Version 2.6.35, that was made available to us by the Bonn developer group after this project was about to be finished.*
- [132] M. J. Frisch, G. W. Trucks, H. B. Schlegel, G. E. Scuseria, M. A. Robb, J. R. Cheeseman, J. J. A. Montgomery, T. Vreven, K. N. Kudin, J. C. Burant, J. M. Millam, S. S. Iyengar, J. Tomasi, V. Barone, B. Mennucci, M. Cossi, G. Scalmani, N. Rega, G. A. Petersson, H. Nakatsuji, M. Hada, M. Ehara, K. Toyota, R. Fukuda, J. Hasegawa, M. Ishida, T. Nakajima, Y. Honda, O. Kitao, H. Nakai, M. Klene, X. Li, J. E. Knox, H. P. Hratchian, J. B. Cross, C. Adamo, J. Jaramillo, R. Gomperts, E. Stratmann, O. Yazyev, A. J. Austin, R. Cammi, C. Pomelli, J. W. Ochterski, P. Y. Ayala, K. Morokuma, G. A. Voth, P. Salvador, J. J. Dannenberg, V. G. Zakrzewski, S. Dapprich, A. D. Daniels, M. C. Strain, O. Farkas, D. K. Malick, A. D. Rabuck, K. Raghavachari, J. B. Foresman, Q. Ortiz, A. G. Cui, S. Baboul, J. Clifford, J. V. Cioslowski, B. B. Stefanov, G. Liu, A. Liashenko, P. Piskorz, I. Komaromi, R. L. Martin, D. J. Fox, T. Keith, M. A. Al-Laham, C. Y. Peng, A. Nanayakkara, M. P. Challacombe, M. W. Gill, B. Johnson, W. Chen, M. W. Wong, C. Gonzalez, J. A. Pople, Gaussian, Inc Pittsburgh, PA, **2003**.
- [133] L. Noodleman, T. Lovell, W. G. Han, J. Li, F. Himo, *Chemical Reviews* **2004**, *104*, 459.
- [134] L. Noodleman, *J. Chem. Phys.* **1981**, *74*, 5737.
- [135] L. Noodleman, E. J. Baerends, *J. Am. Chem. Soc.* **1984**, *106*, 2316.
- [136] L. Noodleman, D. A. Case, *Adv. Inorg. Chem.* **1992**, *38*, 423.
- [137] L. Noodleman, E. R. Davidson, *Chem. Phys.* **1986**, *109*, 131.
-

BIBLIOGRAPHY

- [138] L. Noodleman, J. Li, X.-G. Zhao, W. H. Richardson, *Density-functional Methods in Chemistry and Materials*, Wiley, New York, **1997**.
- [139] T. Soda, Y. Kitagawa, T. Onishi, Y. Takano, Y. Shigeta, H. Nagao, Y. Yoshioka, K. Yamaguchi, *Chemical Physics Letters* **2000**, 319, 223.
- [140] K. Yamaguchi, Y. Takahara, T. Fueno, *Applied Quantum Chemistry*, Reidel, Dordrecht, **1986**.
- [141] F. Neese, *Journal of Physics and Chemistry of Solids* **2004**, 65, 781.
- [142] F. Bernardi, A. Bottoni, R. Casadio, P. Fariselli, A. Rigo, *Inorganic Chemistry* **1996**, 35, 5207.
- [143] J. Cano, E. Ruiz, P. Alemany, F. Lloret, S. Alvarez, *Journal of the Chemical Society-Dalton Transactions* **1999**, 1669.
- [144] I. Ciofini, C. A. Daul, *Coordination Chemistry Reviews* **2003**, 238, 187.
- [145] C. Desplanches, E. Ruiz, A. Rodriguez-Forteza, S. Alvarez, *Journal of the American Chemical Society* **2002**, 124, 5197.
- [146] F. Illas, I. D. R. Moreira, J. M. Bofill, M. Filatov, *Theoretical Chemistry Accounts* **2006**, 116, 587.
- [147] I. D. R. Moreira, R. Costa, M. Filatov, F. Illas, *Journal of Chemical Theory and Computation* **2007**, 3, 764.
- [148] A. Rodriguez-Forteza, P. Alemany, S. Alvarez, E. Ruiz, *Inorganic Chemistry* **2002**, 41, 3769.
- [149] E. Ruiz, J. Cano, S. Alvarez, P. Alemany, *Journal of the American Chemical Society* **1998**, 120, 11122.
- [150] T. Saito, Y. Kitagawa, M. Shoji, Y. Nakanishi, M. Ito, T. Kawakami, M. Okumura, K. Yamaguchi, *Chemical Physics Letters* **2008**, 456, 76.
- [151] A. Bencini, D. Gatteschi, *J. Am. Chem. Soc.* **1986**, 108, 5763.
- [152] M. C. Holthausen, *Journal of Computational Chemistry* **2005**, 26, 1505.
- [153] D. Schroder, S. Shaik, H. Schwarz, *Accounts of Chemical Research* **2000**, 33, 139.
- [154] H. Schwarz, *International Journal of Mass Spectrometry* **2004**, 237, 75.
- [155] S. Shaik, D. Danovich, A. Fiedler, D. Schroder, H. Schwarz, *Helvetica Chimica Acta* **1995**, 78, 1393.
- [156] J. N. Harvey, *Physical Chemistry Chemical Physics* **2007**, 9, 331.
- [157] J. B. Perdew, *Phys. Rev. B* **1986**, 33, 8822.

BIBLIOGRAPHY

- [158] W. Koch, M. Holthausen, *A Chemist's Guide to Density Functional Theory*, 2 ed., Wiley-VCH, Weinheim, **2001**.
- [159] S. Mandal, R. Mukherjee, *Inorganica Chimica Acta* **2006**, 359, 4019.
- [160] K. D. Karlin, Y. Gultneh, J. P. Hutchinson, J. Zubieta, *J. Am. Chem. Soc.* **1982**, 104, 5240.
- [161] A. Company, L. Gomez, R. Mas-Balleste, I. V. Korendovych, X. Ribas, A. Poater, T. Parella, X. Fontrodona, J. Benet-Buchholz, M. Sola, L. Que, E. V. Rybak-Akimova, M. Costas, *Inorganic Chemistry* **2007**, 46, 4997.
- [162] L. Casella, M. Gullotti, G. Pallanza, L. Rigoni, *J. Am. Chem. Soc.* **1988**, 110, 4221.
- [163] J. W. Pyrz, K. D. Karlin, T. N. Sorrell, G. C. Vogel, J. Que, L., *Inorg. Chem.* **1984**, 23, 4581.
- [164] S. Mahapatra, J. A. Halfen, W. B. Tolman, *Journal of the American Chemical Society* **1996**, 118, 11575.
- [165] P. Chen, D. E. Root, C. Campochiaro, K. Fujisawa, E. I. Solomon, *Journal of the American Chemical Society* **2003**, 125, 466.
- [166] C. J. Cramer, W. B. Tolman, K. H. Theopold, A. L. Rheingold, *Proceedings of the National Academy of Sciences of the United States of America* **2003**, 100, 3635.
- [167] B. F. Gherman, C. J. Cramer, *Inorganic Chemistry* **2004**, 43, 7281.
- [168] M. Metz, E. I. Solomon, *Journal of the American Chemical Society* **2001**, 123, 4938.
- [169] E. I. Solomon, P. Chen, M. Metz, S. K. Lee, A. E. Palmer, *Angewandte Chemie-International Edition* **2001**, 40, 4570.
- [170] Y. Takano, K. Yamaguchi, *International Journal of Quantum Chemistry* **2007**, 107, 3103.
- [171] N. Kitajima, K. Fujisawa, Y. Moro-Oka, K. Toriumi, *J. Am. Chem. Soc.* **1989**, 111, 8975.
- [172] M. J. Henson, M. A. Vance, C. X. Zhang, H. C. Liang, K. D. Karlin, E. I. Solomon, *Journal of the American Chemical Society* **2003**, 125, 5186.
- [173] V. Mahadevan, M. J. Henson, E. I. Solomon, T. D. P. Stack, *Journal of the American Chemical Society* **2000**, 122, 10249.
- [174] V. Mahadevan, Z. G. Hou, A. P. Cole, D. E. Root, T. K. Lal, E. I. Solomon, T. D. P. Stack, *Journal of the American Chemical Society* **1997**, 119, 11996.
-

- [175] T. D. P. Stack, *Dalton Transactions* **2003**, 1881.
- [176] M. Taki, S. Teramae, S. Nagatomo, Y. Tachi, T. Kitagawa, S. Itoh, S. Fukuzumi, *Journal of the American Chemical Society* **2002**, *124*, 6367.
- [177] W. B. Tolman, *Accounts of Chemical Research* **1997**, *30*, 227.
- [178] H. V. Obias, Y. Lin, N. N. Murthy, E. Pidcock, E. I. Solomon, M. Ralle, N. J. Blackburn, Y.-M. Neuhold, A. D. Zuberbühler, K. D. Karlin, *J. Am. Chem. Soc.* **1998**, *120*, 12960.
- [179] P. Spuhler, M. C. Holthausen, *Angewandte Chemie-International Edition* **2003**, *42*, 5961.
- [180] R. Berger, *Angew. Chem., Int. Ed.* **2004**, *43*, 398.
- [181] R. T. Skodje, D. G. Truhlar, *J. Phys. Chem.* **1981**, *85*, 624.
- [182] X. Ottenwaelder, D. J. Rudd, M. C. Corbett, K. O. Hodgson, B. Hedman, T. D. P. Stack, *Journal of the American Chemical Society* **2006**, *128*, 9268.
- [183] S. S. Yi, E. L. Reichert, M. C. Holthausen, W. Koch, J. C. Weisshaar, *Chemistry-a European Journal* **2000**, *6*, 2232.
- [184] M. S. Nasir, B. I. Cohen, K. D. Karlin, *J. Am. Chem. Soc.* **1992**, *114*, 2482.
- [185] R. S. Himmelwright, N. C. Eickman, C. D. LuBien, E. I. Solomon, K. Lerch, *J. Am. Chem. Soc.* **1980**, *102*, 7339.
- [186] A. Tepper, L. Bubacco, G. W. Canters, *Journal of the American Chemical Society* **2005**, *127*, 567.
- [187] H. Decker, F. Tuczek, *Trends in Biochemical Sciences (TIBS)* **2000**, *25*, 392.
- [188] L. Santagostini, M. Gullotti, E. Monzani, L. Casella, R. Dillinger, F. Tuczek, *Chemistry-a European Journal* **2000**, *6*, 519.
- [189] O. J. Gelling, B. Feringa, *J. Am. Chem. Soc.* **1990**, *112*.
- [190] N. A. Fokina, B. A. Tkachenko, A. Merz, M. Serafin, J. E. P. Dahl, R. M. K. Carlson, A. A. Fokin, P. R. Schreiner, *European Journal of Organic Chemistry* **2007**, 4738.
- [191] H. Schwertfeger, A. A. Fokin, P. R. Schreiner, *Angewandte Chemie-International Edition* **2008**, *47*, 1022.
- [192] H. Masuda, N. Yamamoto, T. Taga, K. Machida, S. Kitagawa, M. Munakata, *J. Organomet. Chem.* **1987**, *322*, 121.
- [193] I. Emme, T. Labahn, A. de Meijere, *Eur. J. Inorg. Chem.* **2006**, 399.
- [194] I. Emme, S. Redlich, T. Labahn, J. Magull, A. de Meijere, *Angew. Chem. Int. Ed.* **2002**, *41*, 786.
-

BIBLIOGRAPHY

- [195] J. Foerstner, S. Kozhushkov, P. Binger, P. Wedemann, M. Noltemeyer, A. de Meijere, H. Butenschon, *Chem. Commun. (Cambridge)* **1998**, 239.
- [196] A. de Meijere, S. Redlich, D. Frank, J. Magull, A. Hofmeister, H. Menzel, B. König, J. Svoboda, *Angew. Chem. Int. Ed.* **2007**, *46*, 4574.
- [197] L. Römmling, *Diplomarbeit unveröffentlichte Ergebnisse* **2005**.
- [198] M. Munakata, S. Kitagawa, S. Kosome, A. Asahara, *Inorg. Chem.* **1986**, *25*, 2622.
- [199] M. Dakkouri, V. Typke, R. J. Bitschenauer, *Mol. Struct.* **1995**, *355*, 239.
- [200] M. Schatz, V. Raab, S. P. Foxon, G. Brehm, S. Schneider, M. Reiher, M. C. Holthausen, J. Sundermeyer, S. Schindler, *Angewandte Chemie-International Edition* **2004**, *43*, 4360.
- [201] L. Q. Hatcher, K. D. Karlin, *J. Biol. Inorg. Chem.* **2004**, *9*, 669.
- [202] J. Reedijk, E. Bouwman, in *Bioinorganic catalysis*, second ed., **1999**, p. 606 pp.
- [203] S. Herres, U. Flörke, G. Henkel, *Acta Cryst.* **2004**, *C60*, m659.
- [204] S. Herres, A. J. Heuwing, U. Flörke, J. Schneider, G. Henkel, *Inorg. Chim. Acta* **2005**, *358*, 1089.
- [205] B. Cornils, W. A. Herrmann, *Applied Homogeneous Catalysis with Organometallic Compounds*, Wiley-VCH, Weinheim, **2000**.
- [206] S. Bhaduri, D. Mukesh, *Homogeneous Catalysis- Mechanisms and Industrial Applications*, Wiley-Interscience, New York, **2000**.
- [207] S. Murahashi, G. Davies, *Transition Metal Catalysed Reactions*, Blackwell Science, Oxford, **1999**.
- [208] L. Horner, H. Siegel, H. Blüthe, *Angew. Chem. Int. Ed. Engl.* **1968**, *7*, 942.
- [209] L. Horner, H. Siegel, H. Blüthe, *Angew. Chem.* **1968**, *80*, 1034.
- [210] W. S. Knowles, M. J. Sabacky, *Chem. Commun.* **1968**, 1445.
- [211] T. P. Dang, H. B. Kagan, *J. Chem. Soc.* **1971**, 481.
- [212] H. B. Kagan, T. P. Dang, *J. Am. Chem. Soc.* **1972**, *94*, 6429.
- [213] H. Takaya, T. Ohta, R. Noyori, (Ed.: I. Ojima), VCH Publishers Inc., New York, **1993**, pp. 1.
- [214] K. M. Pietrusiewicz, M. Zablocka, *Chem. Rev.* **1994**, *94*, 1375.
- [215] H. B. Kagan, in *Comprehensive Asymmetric Catalysis* (Eds.: E. N. Jacobsen, A. Pfaltz, H. Yamamoto), Springer, New York, **1999**, p. chapter 2.
- [216] E. Schoffers, *Eur. J. Org. Chem.* **2003**, 1145.
-

- [217] E. Schoffers, S. D. Tran, K. Mace, *Heterocycles* **2003**, *60*, 769.
- [218] A. Henß, *Diplomarbeit unveröffentlichte Ergebnisse* **2005**.
- [219] J. A. Blake, P. Hubberstey, W. S. Li, D. J. Quinlan, C. E. Russell, C. L. Sampson, *J. Chem. SOC., Dalton Trans.* **1999**, 4261.
- [220] M. J. J. Cunningham C. T., Cunningham K. L. H., M. D. R. Fanwick P.W., *Inorg. Chem.* **2000**, 3638.
- [221] S. Goldstein, G. Czapski, *J. Am. Chem. SOC.* **1983**, *105*, 7276.
- [222] S. Goldstein, G. Czapski, *Inorg. Chem.* **1985**, *24*, 1087.
- [223] R. Haenaelaenen, M. Ahlgren, U. Turpeinen, T. Raikas, *Cryst. Struct. Commun.* **1979**, *8*, 75.
- [224] P. J. Burke, D. R. McMillin, W. R. Robinson, *Inorg. Chem.* **1980**, *19*, 1211.
- [225] P. C. Healy, I. M. Engelhardt, V. A. Patrick, A. H. White, *J. Am. Chem. Soc., Daltons Trans.* **1985**, 2541.
- [226] C. Krueger, J. C. Sekutowski, H. H., K.-G. R. J., *Organomet. Chem.* **1977**, *141*, 141.
- [227] M. Munakata, M. Maekawa, S. Kitagawa, S. Matsuyama, H. Masuda, *Inorg. Chem.* **1989**, *28*, 4300.
- [228] B. A. Gandhi, O. Green, J. N. Burstyn, *Inorg. Chem.* **2007**, *42*, 3816.
- [229] D. Maiti, D.-H. Lee, K. Gaoutchenova, C. Würtele, M. C. Holthausen, A. A. Narducci Sarjeant, J. Sundermeyer, S. Schindler, K. D. Karlin, *Angew. Chem.* **2008**, *120*, 88.
- [230] C. J. Cramer, W. B. Tolman, *Accounts of Chemical Research* **2007**, *40*, 601.
- [231] A. Decker, E. I. Solomon, *Curr. Opin. Chem. Biol.* **2005**, *9*, 152.
- [232] C. A. Grapperhaus, B. Mienert, E. Bill, T. Weyhermüller, K. Wieghardt, *Inorg. Chem.* **2000**, *39*, 5306.
- [233] in *SADABS* (Ed.: 2.26), Bruker AXS, Inc., Madison, WI, USA, **2002**.
- [234] G. M. Sheldrick, in *SHELX-97*, University Göttingen, **1997**.
- [235] H. Weiss, F. Hampel, W. Donaubaue, M. A. Grundl, J. W. Bats, A. S. K. Hashmi, S. Schindler, *Organometallics* **2001**, *20*, 1713.
- [236] C. Geyer, S. Schindler, *Organometallics* **1998**, *17*, 4400.
- [237] W. Keim, F. H. Kowaldt, R. Goddard, C. Krüger, *Angew. Chem.* **1978**, *90*, 493.